# Measurement of $\sigma(p\bar{p} \to t\bar{t}X)$ in $\tau + jets$ channel using 5.0 fb$^{-1}$ of data

Dhiman Chakraborty (NIU), Phillip Gutierrez (Oklahoma), Diego Menezes (NIU)

(Dated: May 18, 2011)

This note presents a new measurement of $p\bar{p} \to t\bar{t}X$ production at $\sqrt{s} = 1.96$ TeV using 4951.86 pb$^{-1}$ of data collected with the DØ detector between 2002 and 2010. We focus on the final state where the $W$ boson from one of the top quarks decays into a $\tau$ lepton and its associated neutrino, while the other W boson decays into a quark-antiquark pair. We aim to select those events in which the $\tau$ lepton subsequently decays hadronically, meaning to one or three charged hadrons, zero or more neutral hadrons and a tau neutrino. We use a neural network b-tagging algorithm as well as a topological neural network to enhance signal over the background. For a top quark mass of 172.5 GeV the preliminary result for the measured cross section is:

$$\sigma(t\bar{t}) = 8.46\ ^{+1.06}_{-1.04}\ (\text{stat})\ ^{+0.92}_{-0.88}\ (\text{syst})\ \pm 0.3\ (\text{lumi})\ \text{pb}.$$

**Contents**

# I. INTRODUCTION

Since its discovery at the Fermilab TEVATRON collider in 1995, the top quark has been one of the most important topics in High Energy Physics. The study of its production rate and properties allows us to perform precision tests of standard model (SM) predictions as well as represents a chance of observing possible deviations from such predictions. Amongst all subsequent top decays, the process $t \to Wb \to \tau\nu_\tau b$ represents one of the most important tools for probing beyond-SM physics. For instance, the MSSM (Minimal Supersymmetric Standard Model) [1] predicts the existence of the decay $t \to H^+b$ if $m_{H^+_-} < m_t - m_b$. As the Higgs-fermion coupling is proportional to the latter's mass, the subsequent decay of a charged Higgs boson into a $\tau$ lepton is much more favored than its decays into $e$'s and $\mu$'s. Therefore, for high values of tan $\beta$ (the ratio of the vacuum expectation values of the two Higgs doublets) the charged Higgs preferentially decays to $\tau\nu_\tau$, which increases the branching ratio (BR) of $t \to \tau\nu_\tau b$ relative to the SM prediction. Thus, any non-standard flavor- and mass-dependent could produce a significant effect on the $\tau$ production channel. In this respect, the work presented here represents an important test of the SM predictions as well as one step further on the investigation of non-SM processes.

In this analysis we study the process when the $W$ boson from one of the top quarks decays into a $\tau$ lepton and its associated neutrino, while the other $W$ boson decays into a quark-antiquark pair. The $\tau$ is the heaviest lepton and its prompt decay into other particles and the probability of being faked by electrons, muons and jets makes its reconstruction and identification much more difficult than other top decays.

Here we focus on events where the $\tau$ decays hadronically, meaning to one or three charged hadrons, zero or more neutral hadrons and a tau neutrino. This implies that our signal consists of a final state with four or more jets. Figures 1 and 2 show respectively the Feynman diagram that decribes the process $t\bar{t} \to \tau + jets$ and the pie chart of top decay. In Section II we discuss or signal and main backgrounds.

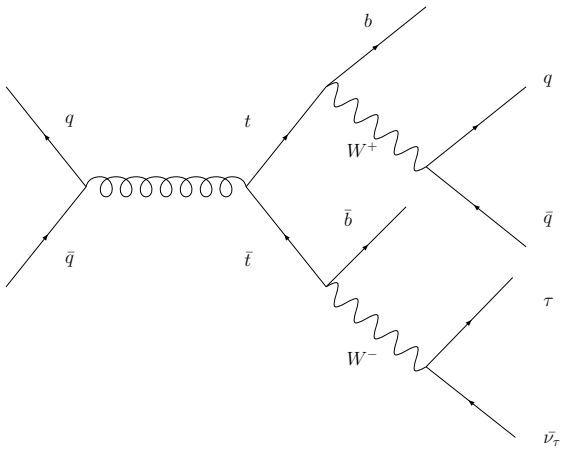


FIG. 1: Feynman diagram for $t\bar{t} \to \tau + jets$ .

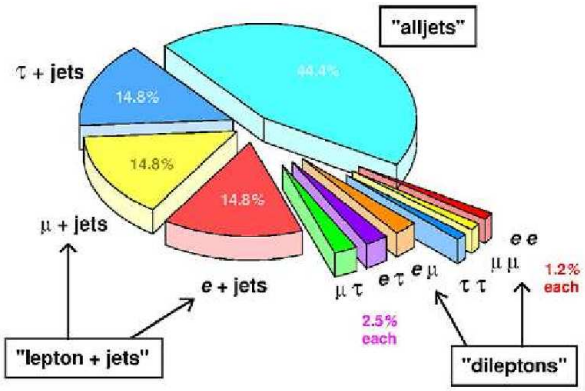


FIG. 2: Top quark decay pie chart.

The present work is the third measurement of the $t\bar{t}$ cross section in the $\tau + jets$ channel performed with the DØ detector. Previous results [2, 3] used using p14 RunI and p17 RunIIa Data and are summarized in Table I (only statistical uncertainties are shown).

| Data set ($pb^{-1}$) | cross section ($pb$) |
|---|---|
| p14 (349.0) | $5.05\ ^{+4.31}_{-3.46}$ |
| p17 (974.2) | $6.90\ ^{+1.20}_{-1.20}$ |

TABLE I: Previous $t\bar{t}$ cross section measurements in the $\tau + jets$ channel

The main improvements upon previous p17 analysis are listed below:

- 5 times more data (RunIIb1, RunIIb2 and RunIIb3).
- Trigger used: we use a new set of multijet triggers that represents a gaim of 10% in the final efficiency.
- Use of vertex confirmed jets.
- Tau energy scale added to the analysis.
- Improved neural net (NN) optimization.
- New set of p20 b-tag TRF's.

## II. DATASET

### A. Data Sample

For this analysis the framework used was vjets_cafe v04-00-08 (Release p21.18.00) and the data set consisted of 3JET skim produced by the commom samples group [4] and recorded between August 2002 and May 2010 (runs 151817 - 258547).

- CSG_CAF_3JET_PASS2_p21.10.00
- CSG_CAF_3JET_PASS4_p21.10.00_p20.12.00
- CSG_CAF_3JET_PASS4_p21.10.00_p20.12.01
- CSG_CAF_3JET_PASS4_p21.10.00_p20.12.02
- CSG_CAF_3JET_PASS4_p21.10.00_p20.12.04
- CSG_CAF_3JET_PASS4_p21.12.00_p20.12.05_allfix
- CSG_CAF_3JET_PASS4_p21.10.00_p20.16.07_fix
- CSG_CAF_3JET_PASS4_p21.12.00_p20.16.07_summer2010

In this analysis we chose the three jets trigger JT2_3JT15L_IP_VX.

This particular trigger was chosen based on our needs of looking for events with multiple jets and the fact that it represents a gain of 20% efficiency on signal selection if compared to previous p17 analysis. Since the efficiencies for such trigger are not currently part of caf_trigger package, in this analysis we benefit from the trigger modelling provided by the *hbb* group [5] for the $\phi b \rightarrow b\bar{b}b$ analysis. Trigger weight distributions for all MC samples used in the analysis as a function of the number of b-tagged jets are found in Appendix A and Table II summarizes their mean values:

| Process | 0 tags | 1 tag | 2 tags | 3 or more tags |
|---|---|---|---|---|
| $t\bar{t} \rightarrow \tau + jets$ | 0.7923 | 0.8620 | 0.8953 | 0.9039 |
| $t\bar{t} \rightarrow e + jets$ | 0.7902 | 0.8599 | 0.8933 | 0.9020 |
| $t\bar{t} \rightarrow \mu + jets$ | 0.7942 | 0.8639 | 0.8973 | 0.9058 |
| $t\bar{t} \rightarrow l + l$ | 0.7274 | 0.7915 | 0.8223 | 0.8302 |
| $Wjj + jets \rightarrow l\nu + jj + jets$ | 0.5821 | 0.6337 | 0.6586 | 0.6652 |
| $Wbb + jets \rightarrow l\nu + bb + jets$ | 0.5948 | 0.6475 | 0.6729 | 0.6796 |
| $Wcc + jets \rightarrow l\nu + cc + jets$ | 0.5912 | 0.6435 | 0.6687 | 0.6754 |
| $Zjj + jets \rightarrow ee + jj + jets$ | 0.6769 | 0.7363 | 0.7646 | 0.7719 |
| $Zbb + jets \rightarrow ee + bb + jets$ | 0.4331 | 0.4712 | 0.4895 | 0.4943 |
| $Zcc + jets \rightarrow ee + cc + jets$ | 0.6167 | 0.6746 | 0.7035 | 0.7127 |
| $Zjj + jets \rightarrow \mu\mu + jj + jets$ | 0.6641 | 0.7233 | 0.7520 | 0.7598 |
| $Zbb + jets \rightarrow \mu\mu + bb + jets$ | 0.6057 | 0.6598 | 0.6860 | 0.6931 |
| $Zcc + jets \rightarrow \mu\mu + cc + jets$ | 0.5817 | 0.6335 | 0.6585 | 0.6653 |
| $Zjj + jets \rightarrow \tau\tau + jj + jets$ | 0.5712 | 0.6220 | 0.6465 | 0.6530 |
| $Zbb + jets \rightarrow \tau\tau + bb + jets$ | 0.6049 | 0.6586 | 0.6845 | 0.6914 |
| $Zcc + jets \rightarrow \tau\tau + cc + jets$ | 0.5889 | 0.6410 | 0.6661 | 0.6727 |
| $Zjj + jets \rightarrow \nu\nu + jj + jets$ | 0.5739 | 0.6241 | 0.6480 | 0.6541 |
| $Zbb + jets \rightarrow \nu\nu + bb + jets$ | 0.6012 | 0.6539 | 0.6790 | 0.6854 |
| $Zcc + jets \rightarrow \nu\nu + cc + jets$ | 0.6360 | 0.6914 | 0.7177 | 0.7242 |

TABLE II: Mean values of the trigger weight for all MC samples.

For this trigger we also measured the luminosity of our data sample. Table III shows the results for both v15 and v16 trigger versions.

| Trigger version | Trigger name | Delivered $\mathcal{L}$ ($pb^{-1}$) | Recorded $\mathcal{L}$ ($pb^{-1}$) | Reconstructed $\mathcal{L}$ ($pb^{-1}$) |
|---|---|---|---|---|
| V15.0 - V15.99 | JT2_3JT15L_IP_VX | 1682.08 | 1544.71 | 1385.99 |
| V16.0 - V16.99 | JT2_3JT15L_IP_VX | 4059.92 | 3887.95 | 3565.86 |
| T O T A L | | 5742.00 | 5432.66 | 4951.85 |

TABLE III: The results of luminosity calculation for the Run2b 3JET data skim for different D0 trigger list versions

### B. Backgrounds

In this analysis the largest background sources are QCD ("fake $\tau$"), which is estimated from data and $W/Z$+jets, which are simulated Monte Carlo samples. Other backgrounds that were not included in this analysis due to their small contribution are single top and diboson production. A list of backgrounds sources is found in Section III of [3]. In the following sections we describe both signal and background simulation.

### C. Monte Carlo Samples

We use p20 certified MC samples as produced by CSG and caffed with p21.11.00 (version3) [6]. All $W/Z$ and $t\bar{t}$ were generated with ALPGEN v2.11 [7] interfaced with Pythia v6.409 [8] for production of parton-level showers and hadronization. EvtGen [9] is used to model b hadrons decays and TAUOLA [10] used to model tau leptons decays.

ALPGEN is a leading order (LL) generator. In order to correct it to match with next-to-leading order (NLO) cross sections we apply *correction factors* and then provide a correct normalization. These correction factors were taken from `vjets_cafe` framework and are described in Ref.[11]. There are two kinds of correction factors: *k-factors*, which are the result of the ratio between NLO and LL cross sections ($\sigma_{NLO}/\sigma_{LL}$) and *heavy flavor factors*, which are in turn the ratio between k-factors for $HF + 0lp(incl)$ and $2lp(incl)$ process from MCFM [12]. Here $HF$ denotes $Z + bb$, $Z + cc$, $W + bb$ or $W + cc$ and $lp$ stands for *light parton*. Heavy flavor factors are applied on the top of k-factors in order to provide the correct normalization for process where heavy quarks are present. For $Z$ production, samples are split into $Z$ + light jets, $Z + bb$ and $Z + cc$. $Z$ + light parton cross sections are multiplied by a k-factor of 1.3, while $Z + bb$ and $Z + cc$ are multiplied by additional heavy flavor factors of 1.52 and 1.67 respectively. $W$ + jets samples are also split the same way: $W$ + light jets, $W + bb$ and $W + cc$. In $W$ + light jets case a k-factor of 1.3 is applied while an additional heavy flavor factor of 1.47 is applied to both $W + bb$ and $W + cc$ samples.

Table IV summarizes the correction factors applied.

| Process | k-factor |
|---|---|
| W + light partons | 1.3 |
| W + bb | 1.3×1.47 |
| W + cc | 1.3×1.47 |
| Z + light partons | 1.3 |
| Z + bb | 1.3×1.52 |
| Z + cc | 1.3×1.67 |

TABLE IV: k-factors for MC.

All MC samples used in this analysis are shown in Table V with theirs respective cross sections and number of events. The cross sections shown are the averages of the cross-sections of each set of MC process generated and are calculated from /caf_mc_util/mc_sample_info/MC.list

| Sample | $\sigma(pb)$ | # of Events |
|---|---|---|
| $t+t+0lp-l\nu+2b+2lpc$_excl_$m172$ | 1.392196 | 793267 |
| $t+t+1lp-l\nu+2b+3lpc$_excl_$m172$ | .576927 | 456317 |
| $t+t+2lp-l\nu+2b+4lpc$_incl_$m172$ | .281831 | 277912 |
| $\mathrm{W}+0lp\rightarrow lnu+0lp$_excl | 4530.269741 | 47070044 |
| $\mathrm{W}+1lp\rightarrow lnu+1lp$_excl | 1283.094130 | 20683540 |
| $\mathrm{W}+2lp\rightarrow lnu+2lp$_excl | 306.073315 | 19686862 |
| $\mathrm{W}+3lp\rightarrow lnu+3lp$_excl | 73.494491 | 4269023 |
| $\mathrm{W}+4lp\rightarrow lnu+4lp$_excl | 16.958254 | 3084707 |
| $\mathrm{W}+5lp\rightarrow lnu+5lp$_incl | 5.218917 | 2565942 |
| $\mathrm{W}+2b+0lp\rightarrow l\nu+2b+0lp$_excl | 9.315458 | 1120570 |
| $\mathrm{W}+2b+1lp\rightarrow l\nu+2b+1lp$_excl | 4.288365 | 812095 |
| $\mathrm{W}+2b+2lp\rightarrow l\nu+2b+2lp$_excl | 1.554786 | 563315 |
| $\mathrm{W}+2b+3lp\rightarrow l\nu+2b+3lp$_incl | 0.716175 | 464475 |
| $\mathrm{W}+2b+0lp\rightarrow l\nu+2c+0lp$_excl | 24.404153 | 934253 |
| $\mathrm{W}+2b+1lp\rightarrow l\nu+2c+1lp$_excl | 13.486806 | 738709 |
| $\mathrm{W}+2b+2lp\rightarrow l\nu+2c+2lp$_excl | 5.459005 | 554236 |
| $\mathrm{W}+2b+3lp\rightarrow l\nu+2c+3lp$_incl | 2.526973 | 469900 |
| $\gamma\mathrm{Z}+0lp\rightarrow ee+0lp$_excl_75_130 | 132.086811 | 1212214 |
| $\gamma\mathrm{Z}+1lp\rightarrow ee+1lp$_excl_75_130 | 40.060963 | 599588 |
| $\gamma\mathrm{Z}+2lp\rightarrow ee+2lp$_excl_75_130 | 9.981935 | 298494 |
| $\gamma\mathrm{Z}+3lp\rightarrow ee+3lp$_incl_75_130 | 3.297072 | 150267 |
| $\gamma\mathrm{Z}+2b+0lp\rightarrow ee+2b+0lp$_excl_75_130 | 0.400826 | 200121 |
| $\gamma\mathrm{Z}+2b+1lp\rightarrow ee+2b+1lp$_excl_75_130 | 0.173438 | 97474 |
| $\gamma\mathrm{Z}+2b+2lp\rightarrow ee+2b+2lp$_incl_75_130 | 0.107248 | 48269 |
| $\gamma\mathrm{Z}+2c+0lp\rightarrow ee+2c+0lp$_excl_75_130 | 0.900923 | 182485 |
| $\gamma\mathrm{Z}+2c+1lp\rightarrow ee+2c+1lp$_excl_75_130 | 0.506337 | 89293 |
| $\gamma\mathrm{Z}+2b+2lp\rightarrow ee+2b+2lp$_incl_75_130 | 0.285871 | 47357 |
| $\gamma\mathrm{Z}+0lp\rightarrow \mu\mu+0lp$_excl_75_130 | 133.850906 | 1553222 |
| $\gamma\mathrm{Z}+1lp\rightarrow \mu\mu+1lp$_excl_75_130 | 41.677185 | 639392 |
| $\gamma\mathrm{Z}+2lp\rightarrow \mu\mu+2lp$_excl_75_130 | 9.822132 | 446737 |
| $\gamma\mathrm{Z}+3lp\rightarrow \mu\mu+3lp$_incl_75_130 | 3.195801 | 172628 |
| $\gamma\mathrm{Z}+2b+0lp\rightarrow \mu\mu+2b+0lp$_excl_75_130 | 0.424239 | 210139 |
| $\gamma\mathrm{Z}+2b+1lp\rightarrow \mu\mu+2b+1lp$_excl_75_130 | 0.195271 | 101055 |
| $\gamma\mathrm{Z}+2b+2lp\rightarrow \mu\mu+2b+2lp$_incl_75_130 | 0.099004 | 49600 |
| $\gamma\mathrm{Z}+2c+0lp\rightarrow \mu\mu+2c+0lp$_excl_75_130 | 0.932203 | 193928 |
| $\gamma\mathrm{Z}+2c+1lp\rightarrow \mu\mu+2c+1lp$_excl_75_130 | 0.548182 | 92744 |
| $\gamma\mathrm{Z}+2b+2lp\rightarrow \mu\mu+2b+2lp$_incl_75_130 | 0.280795 | 51277 |
| $\gamma\mathrm{Z}+0lp\rightarrow \tau\tau+0lp$_excl_75_130 | 131.564780 | 1556389 |
| $\gamma\mathrm{Z}+1lp\rightarrow \tau\tau+1lp$_excl_75_130 | 40.300291 | 595169 |
| $\gamma\mathrm{Z}+2lp\rightarrow \tau\tau+2lp$_excl_75_130 | 10.072067 | 305312 |
| $\gamma\mathrm{Z}+3lp\rightarrow \tau\tau+3lp$_excl_75_130 | 3.089442 | 205365 |
| $\gamma\mathrm{Z}+2b+0lp\rightarrow \tau\tau+2b+0lp$_excl_75_130 | 0.423679 | 196943 |
| $\gamma\mathrm{Z}+2b+1lp\rightarrow \tau\tau+2b+1lp$_excl_75_130 | 0.196527 | 103105 |
| $\gamma\mathrm{Z}+2b+2lp\rightarrow \tau\tau+2b+2lp$_incl_75_130 | 0.103561 | 48476 |
| $\gamma\mathrm{Z}+2c+0lp\rightarrow \tau\tau+2c+0lp$_excl_75_130 | 0.898135 | 260243 |
| $\gamma\mathrm{Z}+2c+1lp\rightarrow \tau\tau+2c+1lp$_excl_75_130 | 0.487548 | 100802 |
| $\gamma\mathrm{Z}+2b+2lp\rightarrow \tau\tau+2b+2lp$_incl_75_130 | 0.297808 | 50711 |
| $\gamma\mathrm{Z}+0lp\rightarrow \nu\nu+0lp$_excl | 806.552968 | 2368495 |
| $\gamma\mathrm{Z}+1lp\rightarrow \nu\nu+1lp$_excl | 244.651772 | 2591505 |
| $\gamma\mathrm{Z}+2lp\rightarrow \nu\nu+2lp$_excl | 61.014112 | 657110 |
| $\gamma\mathrm{Z}+3lp\rightarrow \nu\nu+3lp$_excl | 14.091090 | 194705 |
| $\gamma\mathrm{Z}+4lp\rightarrow \nu\nu+4lp$_excl | 3.277295 | 100158 |
| $\gamma\mathrm{Z}+5lp\rightarrow \nu\nu+5lp$_incl | 0.936465 | 49660 |
| $\gamma\mathrm{Z}+2b+0lp\rightarrow \nu\nu+2b+0lp$_excl | 2.562976 | 375572 |
| $\gamma\mathrm{Z}+2b+1lp\rightarrow \nu\nu+2b+1lp$_excl | 1.143703 | 180558 |
| $\gamma\mathrm{Z}+2b+2lp\rightarrow \nu\nu+2b+2lp$_incl | 0.617265 | 91588 |
| $\gamma\mathrm{Z}+2c+0lp\rightarrow \nu\nu+2c+0lp$_excl | 5.634504 | 376456 |
| $\gamma\mathrm{Z}+2c+1lp\rightarrow \nu\nu+2c+1lp$_excl | 3.002712 | 199012 |
| $\gamma\mathrm{Z}+2b+2lp\rightarrow \nu\nu+2b+2lp$_incl | 1.635746 | 96147 |

TABLE V: MC Samples. Here $l$ stands for the three lepton flavor ($e$, $\mu$ and $\tau$). $\tau$ decays are not restricted.

### D. MC samples corrections

Standard DØ corrections are applied to MC in order to obtain a better MC-data agreement [13].
**Trigger efficiency**: an additional scale factor (weight) is applied to MC to account for the trigger efficiency in data. Further details are given in Section III.
**Luminosity reweighting**: in order to reproduce luminosity effects from real data, simulated samples are overlaid to Zero Bias data Due to a difference in intantaneous luminosity between the overlay and real data, the luminosity profile of all MC samples is reweighted to match the luminosity profile in data [14].
**Primary vertex reweighting**: $z$ vertex distributions are different between data and MC.This difference is corrected by reweighting MC $z$ vertex distributions using the reweight processor from the `caf_mc_util` package [15].
**$W$ and $Z$ $p_T$ reweighting**: for both $W$ + jets and $Z$ + jets, the $p_T$ distribution from MC samples is reweighted to match the equivalent distribution in data, accordingly to the standard way [16].
**b fragmentation**: the systematics on the reweight of the b-fragmentation function from the default in Pythia to the value tuned to reproduce collider data was assumed to be the symmetrized difference between the AOD and SLD tunes [17].
**Jet Shifting Smearing and Removing (JSSR)**: due to differences in energy scale, resolution, reconstruction and identification between data and MC, MC jets are shifted, smeared and possibly removed using standard JSSR processor [18]. In this analysis shifting is turned off to signal $t\bar{t}$ and on to $W/Z$ + jets samples.
**Tau Energy Scale (TES)**: due to the analysis sensitivity to any difference between data and MC in the energy scale of taus decaying hadronically we apply a $E/p$ correction to this energy scale as described in [19].

## III. TRIGGER PARAMETRIZATION

As aforementioned the trigger used in this analysis is JT2_3JT15L_IP_VX. In both v15 and v16 trigger versions, this trigger has 4 terms at level 2. Currently, only three of these, the L2 $H_T$, missing $E_T$ ($\not\!\!E_T$) and sphericity based branches have been modelled by the *hbb* group [5]. Therefore these are the ones used in this analysis. The missing term is the acoplanarity term, namely, L2JET(1,20,2.4) L2HT(35,6) MJT(20,10) L2ACOP(168.75), which is the same in both v15 and v15 trigger lists.

Table VI shows the L1, L2 and L3 requirements of the trigger.

In its work, the *hbb* group has parametrized the trigger in three instantaneous luminosity ($10^{32}$)regions: low ($L_{int} < 77$ ), medium ( $77 \leq L_{int} < 124$ ) and high ( $L_{int} \geq 124$ ). The final goal is to measure the total trigger efficiency for our events. In order to do so we take into account both the trigger probabilities and the b-tag probabilities. Thus, the trigger probabilities for 0, 1, 2 and 3 or more b-tagged jets are then multiplied by the probabilities of 0, 1, 2 and 3 or more jets being tagged, which are themselves got from TRF's, as described in section IV D.

The trigger efficiency is computed as a probability (*TrigWeight*) which we associate to each MC event with:

$$P = P_{t0} * P_{b0} + P_{t1} * P_{b1} + P_{t2} * P_{b2} + P_{t\geq 3} * P_{b\geq 3} \tag{1}$$

where $P_{ti}$ is the trigger probability for the event if it has $i$ b-tags and $P_{bi}$ is in turn the probability of having $i$ b-tags in the event offline reconstruction.

What follows is a brief description of how the trigger probabilities at each level were calculated. Single-object turn-on curves were determined using muon triggered events from the TOPJETTRIG skim. Some turn-on curves are found in Appendix B. A more complete description can be found in [5].

| Level | v15 |
|---|---|
| L1 | CSWJT(3,8,3.2)CSWJT(2,15,2.4)CSWJT(1,30,2.4) |
| L2 | L2JET(3,6) L2HT(75,6) SPHER(0.1) OR<br>L2JET(1,30,2.6) L2JET(2,15,2.6) L2JET(3,8) L2HT(75,6) MJT(10,10) OR<br>L2JET(1,30,2.6) L2JET(2,15,2.6) L2JET(3,8) L2HT(100,6) |
| L3 | L3JET(3,15,3.6) L3JET(2,25,3.6) $\lvert z_{PV}\rvert < 35$ cm BTAG(0.4) |
| Name | JT2_3JT15L_IP_VX |

| Level | v16 |
|---|---|
| L1 | CSWJT(3,8,3.2)CSWJT(2,15,2.4)CSWJT(1,30,2.4) |
| L2 | L2JET(3,6) L2HT(75,6) SPHER(0.1) STTIP(1,5.5,3) OR<br>L2JET(1,30,2.6) L2JET(2,15,2.6) L2JET(3,8) L2HT(75,6) MJT(20,10) OR<br>L2JET(1,30,2.4) L2JET(2,15,2.4) L2JET(3,8,2.4) L2HT(75,6) STTIP(1,5.5,3) |
| L3 | L3JET(3,15,3.6) JT(2,25,3.6) $\lvert z_{PV}\rvert < 35$ cm BTAG(0.4) |
| Name | JT2_3JT15L_IP_VX |

TABLE VI: Level-by-level description of trigger JT2_3JT15L_IP_VX. The CSWJT(x,y,z) term corresponds to x L1 jets above y GeV and within $|\eta| <$ z. The JT(x,y,z) term corresponds to x jets reconstructed at L2 or L3 with $p_T > y$ GeV and $|\eta| <$ z. The HT(x,y) term is used only at L2 and requires that the sum of the transverse momenta of L2 jets with $p_T > y$ GeV is above x GeV. The SPHER(0.1) term requires the event sphericity calculated from L2 jets to be greater than 0.1. The MJT(x,y) term corresponds to a missing transverse energy > x GeV calculated from jets with $E_T >$ y GeV. The STTIP(1,5.5,3) term requires one L2STT track with an impact parameter significance greater than or equal to three and a $\chi^2 < 5.5$. The $|z_{PV}| < 35$ cm term requires the primary vertex reconstructed at L3 to be within 35 cm of the center of the detector and the BTAG(0.4) term is used only at L3 and corresponds to a cut of 0.4 on the probability for the event to not contain a $b$-quark.

### A. Level 1

Level 1 consists of jet terms only: 1 jet with $E_T > 30$ GeV and $|\eta| < 2.4$, a second jet with $E_T > 15$ GeV and $|\eta| < 2.4$ and a third jet with $E_T > 8$ GeV and $|\eta| < 3.2$. The total L1 probability is given by

$$\begin{aligned} P(L1) = &[P(\geq 3\text{jets}) + P(=2\text{jets}) * P(\geq 1\text{noise jet}) + P(=1\text{jet}) * P(\geq 2\text{noise jets}) + P(=0\text{jets}) * P(\geq 3\text{noise jets})] \\ &* [P(\geq 2\text{jets}) + P(=1\text{jet}) * P(\geq 1\text{noise jet}) + P(=0\text{jets}) * P(\geq 2\text{noise jets})] \\ &* [P(\geq 1\text{jet}) + P(=0\text{jets}) * P(\geq 1\text{noise jet})] \end{aligned} \tag{2}$$

where $P(\geq xjets)$ is the probability of having $x$ or more jets present in the event and $P(= xjets)$ is the probability of having exactly $x$ jets in the event. The term *noise jets* refers to all those L1 jets that didn't match to an offline jet within $\Delta R < 0.5$. In the equation above the first line corresponds to the term CSWJT(3,8,$|\eta| < 3.2$), the second to the term CSWJT(2,15,$|\eta| < 2.4$) and the third to the term CSWJT(1,30,$|\eta| < 2.4$). L1 jets that matched offline ones had their turn-on curves parametrized as functions of offline jet $pT$'s. The number of noise jets per event was parametrized as a function of offline $H_T$. All L1 turn-on curves are found in Appendix B 1.

### B. Level 2

Level 2 part of this trigger consists of an OR of three terms (here classified as *top*, *hbb* and *mjt*), each with a variation for v15 and v16:

**v15 top:** 3 jets with $p_T$ >8 GeV, 2 with $p_T$ >15 GeV, 1 with $p_T$ >30 GeV and $H_T$ >100 GeV

**v16 top:** 3 jets with $p_T$ >8 GeV, 2 with $p_T$ >15 GeV, 1 with $p_T$ >30 GeV, $H_T$ >75 GeV and STT IP with IPSIG $\geq 3$ and $\chi^2 < 5.5$.

**v15 hbb:** 3 jets with $p_T$ >6 GeV, $H_T$ >75 GeV and sphericity > 0.1

**v16 hbb:** 3 jets with $p_T$ >6 GeV, $H_T$ >75 GeV, sphericity > 0.1 and STT IP with IPSIG $\geq 3$ and $\chi^2 < 5.5$.

**v15 mjt:** 3 jets with $p_T$ >8 GeV, 2 jets with $p_T$ >15 GeV, 1 jet with $p_T$ >30 GeV, $H_T$ >75 GeV and $\not\!\!E_T$ > 10 GeV.

**v16 mjt:** 3 jets with $p_T$ >8 GeV, 2 jets with $p_T$ >15 GeV, 1 jet with $p_T$ >30 GeV, $H_T$ >75 GeV and $\not\!\!E_T$ > 20 GeV.

For this level the net trigger probability is

$$\begin{aligned} P(L2) &= P(hbb \cup mht \cup top) \\ &= P(top) + P(hbb) + P(mht) - P(top \cap hbb) - P(top \cap mht) - P(hbb \cap mht) + P(hbb \cap mht \cap top) \end{aligned} \tag{3}$$

where P(x) corresponds to the probability of either L2, the mht, hbb or the top term firing.
**Level 2 jet terms**: from Table VI we see that for v15 trigger version, L2 jets terms are actually subsets of L1. As here conditional probability is used, it means that the probability of L2 jet terms firing if L1 terms fired is unity. However in v16 the Pt requirement of jets in the first trigger term was loosened from 8 to 6 GeV and $\eta$ requirement on 8 GeV jets in the third trigger term was tightened from $|\eta| < 3.2$ to $|\eta| < 2.4$. As in the L1 case, all L2 jets matching offline ones had their turn-on curves parametrized as functions of offline jet $p_T$'s, except for noise jets, whose number in each event which paratrized as funcions of offline $H_t$. Turn-on curves for these cases are found in Appendix B 2.
**Level 2 $H_T$ term**: this term consists of a cut of $H_T > 75$ GeV for v15 and $H_T >$ 100 GeV for v16). Correspondent turn-on curves are shown in Appendix B 3.
**Level 2 $\not\!\!E_T$ term**: the correspondent $\not\!\!E_T$ cuts are > 10 GeV and > 20 GeV for v15 and v16 respectively. Their turn-on are shown in Appendix B 4.
**L2 Sphericity Term**: this term requires a sphericity cut of > 0.1. Corresponding turn-on curves are shown in Appendix B 5.
**L2 STT**: the L2STTIP efficiency was measured for events in v16 which have passed the rest of the L1, L2 (L2top OR L2hbb) and L3 (except L3 b-tag) trigger requirements and the offline three to five jet selection. The efficiency was measured versus the invariant mass of the two leading jets, separately for 0, 1, 2 and 3 offline tight NN b-tagged events, in the three different luminosity regions. Appendix B 6 shows the STTIP(1,5.5,3) efficiency versus the leading invariant di-jet mass in the low, medium and high luminosity range for different number of offline b-tags.

### C. Level 3

L3 consists of a jet part and a b-tag one. For the jet part of L3, turn-on curves were determined for events passing both L1 and L2 requirements. Corresponding probability is given the equation below

$$\begin{aligned} P(L3) = &[P(\geq 3\text{jets}) + P(=2\text{jets}) * P(\geq 1\text{noise jet}) + P(=1\text{jet}) * P(\geq 2\text{noise jets}) + P(=0\text{jets}) * P(\geq 3\text{noise jets})] \\ &* [P(\geq 2\text{jets}) + P(=1\text{jet}) * P(\geq 1\text{noise jet}) + P(=0\text{jets}) * P(\geq 2\text{noise jets})] \end{aligned} \tag{4}$$

In the equation above the first line corresponds to the term JT(3,15,$|\eta| < 3.6$), the second to the term JT(2,25,$|\eta| < 3.6$). Here was applied the same treatment to L3 jets matching offline ones and to noise jets as in L1 and L2 jet terms. Corresponding turn-on curves are shown in Appendix B 1.

Efficiencies for the b-tag part of L3 were measured in two different ways depending whether the trigger list was v15 or v16. In the v15 case events were recorded with the JT2_4JT20 and JT2_3JT12L_MM3_V triggers, since their L1 and L2 conditions were exactly the same. Events were further required to pass the rest of L3 conditions of JT2_3JT15L_IP_VX and the offline event selection. In the v16 case efficiencies were measured in a similar fashion, but using trigger JT4_3JT15L_VX (which has no L2STT or L3BTAG requirements). Events were then required to have fired one of the three L2 branches of JT2_3JT15L_IP_VX and to pass the offline three to five jet selection. All turn-on curves for both trigger lists are found in Appendix B 8.

## IV. OBJECT IDENTIFICATION

In this section we describe the main objects used in this study: $\not\!\!E_T$ , jets and hadronic tau candidates.

### A. Taus

Taus are reconstructed in the DØ detector from energy in the calorimeter and one or more tracks.The tau reconstruction algorithm uses a cone of $\Delta R = \sqrt{\delta\eta^2 + \delta\phi^2} < 0.5$ and an inner cone of $\Delta R < 0.3$ is used to calculate tau isolation variables.

For us, the most important discriminating variables for $\tau$-leptons are [20]:

- Profile - $\frac{E_T^1+E_T^2}{\sum_i E_T^i}$, where $E_T^i$ is the $E_T$ of the $i^{\text{th}}$ highest $E_T$ tower in the cluster.
- Isolation, defined as $\frac{E(0.5)-E(0.3)}{E(0.3)}$, where $E(R)$ is the energy contained in a $y, \phi$ of radius $R$ around the calorimeter cluster centroid.
- Track isolation, defined as scalar sum of the $p'_T$ of non-$\tau$ tracks in a $\eta, \phi$ cone of 0.5 around the calorimeter cluster centroid divided by similar sum for tracks associated with $\tau$.

Such variables are chosen based on the possible tau decays:

- electron or muon ($\tau \to e\nu_e\nu_\tau$ or $\tau \to \mu\nu_\mu\nu_\tau$), BR = 35% .
- single charged hadron and no neutral hadrons ($\tau \to \pi^-\nu_\tau$), BR =12% .
- single charged hadron + $\geq 1$ neutral hadron (i.e., $\tau \to \rho^-\nu_\tau \to (\pi^0 + \pi^-)\nu_\tau$) , BR = 38% .
- 3 charged hadrons + $\geq 0$ neutral hadrons, BR = 15% (so-called "3-prong" decays).

which leads us classificate reconstructed taus into three different types depending on the number of tracks and electromagnetic (EM) clusters [21]:

1. **Type1**: calorimeter cluster, one matched charged track and no associated EM subcluster. Mainly $\tau \to \pi^-\nu_\tau$.
2. **Type2**: calorimeter cluster, one matched charged track and one or more associated EM subclusters. Mainly $\tau \to \rho^-\nu_\tau \to \pi^0\pi^-\nu_\tau$.
3. **Type3**: calorimeter cluster, two or more matched charged tracks and with or without EM subcluster. Mainly $\tau \to \pi^-\pi^-\pi^+(\pi^0)\nu_\tau$.

In order to provide an optimal tau identification,three Neural Networks (NNs) are trained to identify the three types of the taus (1,2 and 3).

The output of these NNs provides a set of three variables (`nnout` = 1,2,3) to be used to select the tau in the event. The types roughly correspond to the $\tau$ lepton decay modes. High values of NN correspond to the physical taus, while low ones should indicate jets misidentified as taus (fakes).

### B. Jets

Jets are identified using the RunII cone algorithm [22] with cone size of $\Delta R < 0.5$. The jet algorithm T42 [23] is ran before jet reconstruction to remove isolated small energy deposits due to noise. DØ standard jet quality cuts [24] include L1 Trigger information, calorimeter electromagnetic fraction and coarse hadronic fraction.

Jets used in this analysis are required to have at least two primary vertex tracks associated to them (vertex confirmed jets). It implies that although a calorimeter cluster is still reconstructed as a jet, it will be discarded if it has less than 2 associated PV tracks. In order to correct the energies of reconstructed jets in data and MC back to parton-level energies, we apply certified jet energy scale correction (JES)[25]. Additionally, jets containing a muon with $\Delta R(\mu, jet) < 0.5$ from a $b$-quark decay are corrected to take into account the momentum carried away by the muon and the neutrino [26].

### C. $\not\!\!E_T$

Presence of neutrinos in an event causes an imbalance of energy in the transverse plane ($\not\!\!E_T$ ). This quantity is calculated from the transverse energies of all calorimeter cells that pass the T42 algorithm, except those of the coarse hadronic layers due to high noise level. However, they are included in the case that they are clustered within a reconstructed jet. This raw $\not\!\!E_T$ is corrected for the energies of other objects like photons, electrons, taus and jets. As muons deposit only a small portion of their energy in the calorimeter, their momenta is subtracted from the $\not\!\!E_T$ vector.

### D. The Neural Network b-tagging Algorithm

Being QCD and $W$ + jets the main sources of backgrounds in this analysis, requiring the presence of at least one jet coming from a $b$-quark is a very powerful method of background rejection. The $b$-tagging algorithm used in this measurement is a Neural Network (NN) tagging algorithm developed by the b-ID group [27], which combines 7 characteristic variables of SVT, JLIP and CSIP tagging algorithms into the NN discriminant. As in the previous analysis we have chosen the operating point TIGHT, which is equivalent to requiring the NN discriminant output to be greater than 0.775. Both the average efficiency and fake rate are comparable between this p20 version of the algorithm and the version used in p17 [28].

*a. b-tagging efficiency* In data we apply the b-tagging algorithm directly to jets selected in our sample. In MC such "direct tag" is not done. Instead we have to apply a certain efficiency to MC samples. This inclusive b-decay efficiency ($\epsilon_b$) is measured in data and it is the product of the probability to tag a b-jet in an MC sample ($\epsilon_b^{MC}$) containing inclusive decays of the b quark times a scale factor. This data/MC scale factor is given by the ratio of data semileptonic efficiency ($\epsilon_{b\to\mu}^{DATA}$) and a MC semileptonic efficiency ($\epsilon_{b\to\mu}^{MC}$). This scale factor, that measures the effect on the tagging rate caused by the differences in tracking between data and MC, is then used to properly scale the MC-derived efficiency. It is assumed that such factor could be applied to any MC tagging efficiency [27].

*b. c-tagging efficiency* It is assumed that the same procedure adopted in the b-jet case is also valid for c-jets, namely, a c-jet scale factor $(\epsilon_{b\to\mu}^{DATA})/(\epsilon_{b\to\mu}^{MC})$ multiplies the probability to tag a c-jet in an MC sample ($\epsilon_b^{MC}$) to get the c-tagging efficiency.

*c. Light jet tagging efficiency* The $b$-tag fake rate from light quarks is computed by measuring the negative tag rate as defined in [29]. The method uses fits of b-, c- and light jets tagging rates to binned data combined with sample composition estimated from data. Binned NN output ($NN_{out}$) distributions for b, c and light jets is fitted to data distribution using b- and c-jet efficiencies provided by standard bID TRF's.

*d. Taggability* $b$-tag algorithm can't be applied to any jet, but only the ones that contain tracks. Such jets are called "taggable" and are defined by matching within $\Delta R < 0.5$ to a track jet, composed of at least two tracks. Just like b-tagging, taggability is different in data and MC, due to imperfect simulation of tracking system. To account for this, taggability rate functions are applied to MC events. Such functions are parametrized in terms of jet $p_T$, jet $\eta$ and primary vertex $z$. They were derived on the single top loose data samples, where the isolation quality of the lepton is loose.The validity of these functions is tested by comparing observed and predicted taggability to tight samples. The results show a good agreement as described in [30].

## V. ANALYSIS OUTLINE

Up to this point we have presented the data sample used in this analysis (Section II A) the Monte Carlo samples and corrections applied to them (Sections II C and II D), the trigger used and its simulation (Section III) and the object ID method (Section IV). Now we describe the next steps of the analysis towards the final crosse section measurement:

- Preselection (section VI): at least 4 jets, at least one $\tau$ with NN>0.3 and $p_T > 10$ GeV/$c$, 15 GeV $\leq \not\!\!E_T \leq 500$ GeV and $\not\!\!E_T$ significance >4.0.
- $\tau$- and b-ID cuts (section VII): at least one good $\tau$ lepton candidate and at least one tight NN b-tag are required.
- Topological NN (section VIII B): a feed-forward NN's is trained in order to provide signal-background separation. The NN was optimized by testing different sets of topological variables as its inputs and by applying different $\not\!\!E_T$ significance cuts.
- Topological Variables (section IX): section showing final analysis plots of topological variables of interest.
- Cross Section (section X) The signal fraction determination is combined with integrated luminosity measurement to calculate the cross section. Systematic uncertainties are determined by fluctuating the significant components up and down by one standard deviation one at a time, propagating it through the entire procedure.

## VI. PRESELECTION

The preselection is the first step of the analysis. The cuts presented here were chosen in order to provide the best background reduction and enhance the $t\bar{t}$ content at this point. The cuts are the similar to those used in the p17 analysis [3] except that for this time we opted to optimize the value of $\not\!\!E_T$ significance along with the sets of variables we used as inputs to NN training (Section VIII). Cuts shown below were applied to samples shown in Table V as well as to data as shown in Section II A.

- At least 4 jets with $p_T > 15$ GeV and $\eta$ <2.5, with leading (in $p_T$) jet $p_T > 35$ GeV and second and third jets have $p_T > 25$ GeV
- at least one $\tau$ with NN>0.3 and $p_T > 10$ GeV
- 15 GeV $\leq \not\!\!E_T \leq 500$ GeV
- $\not\!\!E_T$ significance $\geq 4.0$
- No isolated electron or muon. This is done in order to ensure orthogonality with other DØ measurements ([31] and [32]) - events that pass the lepton preselection cuts from these measurements were vetoed. Also events that pass the all-jets analysis preselection cuts (described in the alljet analysis note [33]) are rejected here.

Among all preselection cuts one of them requires a more detailed description at this point since it represents an improvement upon the old p17 analysis: $\not\!\!E_T$ significance. Missing transverse energy significance is a measure of the likelihood of $\not\!\!E_T$ arising from physical sources. It is computed from calculated resolutions of physical objects (jets, electrons, muons and unclustered energy) [3, 34]. Initially no $\not\!\!E_T$ significance was applied neither on MC nor on data. In this analysis we decided to optimize the $\not\!\!E_T$ significance cut along with the NN optimization itself. After finishing the $\not\!\!E_T$ significance optimization part we went back and applied the optimized cut along with the non-optimized NNelec cut only to MC. The entire optimization procedure is described in Section VIII C.

In data, initially the sample contained approximately 650 million events and the number of preselected events (once again, without $\not\!\!E_T$ significance applied) is approximately 2.8 million events.

Another relevant aspect of the preselection is the usage of Particle Selector (only applied to MC samples). In this step we aimed to select a particular $t\bar{t}$ final state, namely, we split $W$ decay into $W \to e/\mu/\tau$ and tracked separate efficiencies for each of these processes. In this step we selected hadronic decays of tau, and

at the same events where tau decays into electrons and muons were put into $e + jets$ and $\mu + jets$ samples. As in p17, we decided to do not split the dilepton sample in different lepton flavors.

Before proceeding to the next step, it is important to describe the result of the preselection in terms of its efficiencies since all the rest of analysis strongly depends on the cuts applied at this level. As previously described, $t\bar{t}$ were generated by ALPGEN. In ALPGEN, different process with different numbers of partons have different cross-sections and number of events. This fact must be taken into account when calculating the efficiencies, namely, efficiencies must be properly scaled to the luminosity (4951.85 $\text{pb}^{-1}$) of the sample. Tables VI and III show the number beforementioned for $t\bar{t} \rightarrow$ lepton + jets and $t\bar{t} \rightarrow$ dilepton respectively.

| Process | # of events | cross-section (pb) | alpgen weight |
|---|---|---|---|
| 0 light parton | 777068 | 1.4 | 0.00892 |
| 1 light parton | 457782 | 0.577 | 0.00624 |
| $\geq$ 2 light partons | 321166 | 0.267 | 0.00412 |

TABLE VII: $t\bar{t} \rightarrow$ lepton + jets ALPGEN weights.

| Process | # of events | cross-section (pb) | alpgen weight |
|---|---|---|---|
| 0 light parton | 749642 | 0.352 | 0.00233 |
| 1 light parton | 452177 | 0.142 | 0.00156 |
| $\geq$ 2 light partons | 281453 | 0.068 | 0.00119 |

TABLE VIII: $t\bar{t} \rightarrow$ dilepton ALPGEN weights.

Tables IX, X, XI and XII show cut flows for all preselection cuts applied to different $t\bar{t}$ decays (only statistical uncertainties are shown).

| Selection | Events | Relative | Cumulative |
|---|---|---|---|
| Initial | 11164 | | |
| Particle selector | 2412 | $21.60 \pm 0.03$ % | $21.60 \pm 0.03$ % |
| Duplicate events removal | 2411 | $99.98 \pm 0.01$ % | $21.60 \pm 0.03$ % |
| Event quality | 2315 | $96.00 \pm 0.04$ % | $20.74 \pm 0.03$ % |
| Jet selection | 1307 | $59.45 \pm 0.09$ % | $11.70 \pm 0.03$ % |
| Vertex selection | 1296 | $99.18 \pm 0.02$ % | $11.61 \pm 0.03$ % |
| Electron veto | 1282 | $98.93 \pm 0.01$ % | $11.49 \pm 0.03$ % |
| Muon veto | 1282 | $99.93 \pm 0.01$ % | $11.48 \pm 0.03$ % |
| MET selection | 1218 | $95.05 \pm 0.05$ % | $10.91 \pm 0.02$ % |
| MET significance | 772 | $63.39 \pm 0.12$ % | $6.92 \pm 0.02$ % |
| NN tau cut | 394 | $53.51 \pm 0.15$ % | $3.70 \pm 0.02$ % |

TABLE IX: Preselection $t\bar{t} \rightarrow \tau + jets$ cut flow

| Selection | Events | Relative | Cumulative |
|---|---|---|---|
| Initial | 11164 | | |
| Particle selector | 4385 | $39.28 \pm 0.04$ % | $39.28 \pm 0.04$ % |
| Duplicate event removal | 4383 | $99.96 \pm 0.01$ % | $39.26 \pm 0.04$ % |
| Event quality | 4207 | $95.97 \pm 0.03$ % | $37.68 \pm 0.04$ % |
| Jet selection | 1923 | $45.71 \pm 0.07$ % | $17.22 \pm 0.03$ % |
| Vertex selection | 1907 | $99.20 \pm 0.02$ % | $17.08 \pm 0.03$ % |
| Electron veto | 1048 | $54.94 \pm 0.10$ % | $9.39 \pm 0.02$ % |
| Muon veto | 1047 | $99.95 \pm 0.01$ % | $9.38 \pm 0.02$ % |
| MET selection | 1002 | $95.64 \pm 0.05$ % | $8.97 \pm 0.02$ % |
| MET significance | 669 | $66.74 \pm 0.13$ % | $5.99 \pm 0.02$ % |
| NN tau cut | 395 | $59.12 \pm 0.16$ % | $3.54 \pm 0.02$ % |

TABLE X: Preselection $t\bar{t} \to e + jets$ cut flow

| Selection | Events | Relative | Cumulative |
|---|---|---|---|
| Initial | 11164 | | |
| Particle selector | 4367 | $39.12 \pm 0.04$ % | $39.12 \pm 0.04$ % |
| Duplicate event removal | 4366 | $99.96 \pm 0.04$ % | $39.10 \pm 0.04$ % |
| Event quality | 4189 | $95.95 \pm 0.03$ % | $37.52 \pm 0.04$ % |
| Jet selection | 1990 | $47.52 \pm 0.07$ % | $17.83 \pm 0.03$ % |
| Vertex selection | 1975 | $99.23 \pm 0.02$ % | $17.69 \pm 0.03$ % |
| Electron veto | 1967 | $99.59 \pm 0.01$ % | $17.62 \pm 0.03$ % |
| Muon veto | 1170 | $59.48 \pm 0.09$ % | $10.48 \pm 0.02$ % |
| MET selection | 1127 | $96.31 \pm 0.04$ % | $10.09 \pm 0.02$ % |
| MET significance | 812 | $72.06 \pm 0.11$ % | $7.27 \pm 0.02$ % |
| NN tau cut | 186 | $22.95 \pm 0.13$ % | $1.67 \pm 0.01$ % |

TABLE XI: Preselection $t\bar{t} \to \mu + jets$ cut flow

| Selection | Events | Relative | Cumulative |
|---|---|---|---|
| Initial | 2799 | | |
| Particle selector | 2799 | $100.00 \pm 0.00$ % | $100.00 \pm 0.00$ % |
| Duplicate event removal | 2799 | $100.00 \pm 0.00$ % | $100.00 \pm 0.00$ % |
| Event quality | 2685 | $95.92 \pm 0.02$ % | $95.92 \pm 0.02$ % |
| Jet selection | 145 | $5.41 \pm 0.02$ % | $5.19 \pm 0.02$ % |
| Vertex selection | 144 | $99.32 \pm 0.03$ % | $5.16 \pm 0.02$ % |
| Electron veto | 110 | $76.14 \pm 0.13$ % | $3.93 \pm 0.01$ % |
| Muon veto | 83 | $75.08 \pm 0.16$ % | $2.95 \pm 0.01$ % |
| MET selection | 80 | $96.45 \pm 0.08$ % | $2.84 \pm 0.01$ % |
| MET significance | 60 | $75.32 \pm 0.19$ % | $2.14 \pm 0.01$ % |
| NN tau cut | 38 | $63.21 \pm 0.24$ % | $1.35 \pm 0.01$ % |

TABLE XII: Preselection $t\bar{t} \to l + l$ cut flow

## VII. $b$ AND $\tau$ SELECTIONS

In the next step we applied the requirements of tight $\tau$- and $b$-tagging. Table XIII shows the selection criteria that we applied to data and MC. The b-tag operating point used was TIGHT, which corresponds to NNbtag $> 0.775$. We chose the $\tau$ with the highest $NN_\tau$ as *the* $\tau$ candidate. At this stage of the analysis we separated the events dataset we deal with into parts, according to which type of $\tau$ the candidate with highest NN belongs. This was done primarily to separate the type 3 tau events (which are expected to have much higher fake rate and thus weaker $t\bar{t}$ cross section result) from the type 2 events. The separate measurement channels were later combined to get the final result (Section X). In principle, types 1 and 2 should be separated as well but as there exists a considerable cross-migration between them [20] and type 1 is a small fraction of the total (10% of type 1, 54.5% of type 2 and 35.5% of type 3), they were taken togetther in this analysis. The topological NN used to enhance the signal content is described in section VIII B .

At this point, we used these ID algorithms to define 3 mutually exclusive and exhastive subsamples out of the original preselected data sample:

- The "non-$b$ veto" or "signal" sample - the $\tau$ candidate has $NN_\tau > 0.90$ ($NN_\tau$ denotes the NN cut commonly applied to all taus) for taus types 1 and 2 and $NN(\tau) > 0.95$ for taus type 3, and at least one NN b-tag (as in Table XIII). These $NN(\tau)$ cuts were chosen based on previous studies involving hadronic decays of taus [19, 37]. This is the sample used to extract the cross section. Jets matched to $\tau$ candidates are not $b$-tagged, althought they still count as jets.

- The "$\tau$ veto sample" or "loose-tight $\tau$ sample" - Same selection, but with $0.3 < NN_\tau < 0.7$ for all taus. $\tau$ NN lower cut of 0.3 instead of 0.0 was chosen to bias their jet properties closer to those of tight tau candidates, in particular, so they have narrow showers. The upper cut is at 0.7 and not 0.95 or 0.90 to reduce signal contamination. In this sample, 1400000 events were used for NN training for taus type 1 and 2 and 600000 events were used in the case of type 3 taus. In both cases, the rest of the samples served as QCD template.

- The "$b$ veto" sample - Require exactly 0 tight $b$-tags. This is the control sample used to verify the validity of the QCD modelling method. The b veto requirement implies this sample is almost purely background.

Along with the $NN_\tau$ cut described above, we also applied the cut NNelec $> 0.9$ only to type 2 taus since these are more likely to be faked by electrons. The cut NNelec $> 0.9$ was chosen in order to match the lowest cut of $NN_\tau > 0.9$ applied to type 2 taus (Section VII).

As both b and $\tau$ ID is the step immediately after the preselection, the number of events available is 2800000 million events. As explained above 1400000 events were used for taus type 1 and 2 NN training and 600000 for type 3 taus NN training. Thus, there are 1400000 events available in each sample for the measurement in the case of types 1 and 2 and 2200000 in the case of type 3. Details on NN training are given in Section VIII B.

The QCD modelling method used here is the same as used in p17 and is described in Section IXA of [3].

The final number of events in each channel for both signal and $b$ veto samples is shown on Tables XIV, XV, XVI and XVII (only statistical uncertainties are shown).

As important as determining the subsamples to be used in this analysis, a determination as precise as possible of both signal and electroweak contamination in the "loose-tight $\tau$ sample" had be done in order to know whether this sample is totally QCD dominated or not. Numbers showing the composition of such sample are shown on Tables XVIII and XIX with their respective statistical uncertainties. From the $t\bar{t}$ content in each case we are able estimate the signal contamination in the loose-tight sample. Such contaminations are 5.4% and 3.0% for taus type 1 and 2 and type 3 respectively when a cross section of 7.46 pb is assumed (Section II C). Likewise we see that electroweak contaminations are 2.2% and 0.9%. As this is the sample used to model the QCD background both signal and electroweak contaminations were taken into account when measuring the cross section in Section X.

| data | taggingMC |
|---|---|
| $\geq 1$ $\tau$ with $\|\eta\| < 2.5$ and $p_T > 20$ GeV | $\geq 1$ $\tau$ with $\|\eta\| < 2.5$ and $p_T > 20$ GeV |
| $\geq 1$ NN b-tag | $mcweight \cdot TrigWeight \cdot bTagProb \cdot lumiReWeight \cdot PVzReWeight \cdot bFragWeight \cdot WZPtReweight$ |
| $\geq 4$ jets with $\|\eta\| < 2.5$ and $p_T > 20$ GeV | $\geq 4$ jets with $\|\eta\| < 2.5$ and $p_T > 20$ GeV |

TABLE XIII: $b$-tagging and $\tau$ ID. In the MC, we use the $b$-tagging certified parameterization rather than actual $b$-tagging, that is, we applied the $b$-tagging weight. We also used the triggering weight as computed by the trigger efficiency parameterization as well as luminosity profile and $PV_Z$ reweighting weights. $mcweight$ is the MC normalization factors (to luminosity), which are different for MC samples with different parton multiplicities in ALPGEN MC samples.

| Sample | # events |
|---|---|
| data | 386 |
| $t\bar{t} \rightarrow \tau + jets$ | 48.03 ± 0.53 |
| $t\bar{t} \rightarrow e + jets$ | 25.57 ± 0.36 |
| $t\bar{t} \rightarrow \mu + jets$ | 3.21 ± 0.14 |
| $t\bar{t} \rightarrow l + l$ | 4.01 ± 0.07 |
| $Wbb + jets \rightarrow l\nu + bb + jets$ | 7.48 ± 0.30 |
| $Wcc + jets \rightarrow l\nu + cc + jets$ | 4.68 ± 0.17 |
| $Wjj + jets \rightarrow l\nu + jj + jets$ | 5.66 ± 0.11 |
| $Zbb + jets \rightarrow \tau\tau + bb + jets$ | 0.93 ± 0.08 |
| $Zcc + jets \rightarrow \tau\tau + cc + jets$ | 0.51 ± 0.04 |
| $Zjj + jets \rightarrow \tau\tau + jj + jets$ | 1.07 ± 0.10 |
| $Zbb + jets \rightarrow ee + bb + jets$ | 0.03 ± 0.01 |
| $Zcc + jets \rightarrow ee + cc + jets$ | 0.00 ± 0.00 |
| $Zjj + jets \rightarrow ee + jj + jets$ | 0.02 ± 0.01 |
| $Zbb + jets \rightarrow \mu\mu + bb + jets$ | 0.07 ± 0.02 |
| $Zcc + jets \rightarrow \mu\mu + cc + jets$ | 0.02 ± 0.01 |
| $Zjj + jets \rightarrow \mu\mu + jj + jets$ | 0.01 ± 0.01 |
| $Zbb + jets \rightarrow \nu\nu + bb + jets$ | 0.08 ± 0.03 |
| $Zcc + jets \rightarrow \nu\nu + cc + jets$ | 0.00 ± 0.00 |
| $Zjj + jets \rightarrow \nu\nu + jj + jets$ | 0.04 ± 0.01 |

TABLE XIV: Final number of events in each channel for taus types 1 and 2 $\tau$ after b-tagging, $\tau$ ID and trigger in the signal sample when the assumed cross section is 7.46 pb. An estimate of QCD background is not included.

| Sample | # of events |
|---|---|
| data | 459 |
| $t\bar{t} \rightarrow \tau + jets$ | 25.88 ± 0.39 |
| $t\bar{t} \rightarrow e + jets$ | 4.35 ± 0.16 |
| $t\bar{t} \rightarrow \mu + jets$ | 3.43 ± 0.14 |
| $t\bar{t} \rightarrow l + l$ | 2.80 ± 0.06 |
| $Wbb + jets \rightarrow l\nu + bb + jets$ | 3.92 ± 0.17 |
| $Wcc + jets \rightarrow l\nu + cc + jets$ | 3.26 ± 0.15 |
| $Wjj + jets \rightarrow l\nu + jj + jets$ | 4.08 ± 0.11 |
| $Zbb + jets \rightarrow \tau\tau + bb + jets$ | 0.74 ± 0.07 |
| $Zcc + jets \rightarrow \tau\tau + cc + jets$ | 0.41 ± 0.03 |
| $Zjj + jets \rightarrow \tau\tau + jj + jets$ | 0.80 ± 0.10 |
| $Zbb + jets \rightarrow ee + bb + jets$ | 0.00 ± 0.00 |
| $Zcc + jets \rightarrow ee + cc + jets$ | 0.01 ± 0.01 |
| $Zjj + jets \rightarrow ee + jj + jets$ | 0.01 ± 0.01 |
| $Zbb + jets \rightarrow \mu\mu + bb + jets$ | 0.04 ± 0.02 |
| $Zcc + jets \rightarrow \mu\mu + cc + jets$ | 0.01 ± 0.01 |
| $Zjj + jets \rightarrow \mu\mu + jj + jets$ | 0.00 ± 0.00 |
| $Zbb + jets \rightarrow \nu\nu + bb + jets$ | 0.12 ± 0.04 |
| $Zcc + jets \rightarrow \nu\nu + cc + jets$ | 0.19 ± 0.04 |
| $Zjj + jets \rightarrow \nu\nu + jj + jets$ | 0.06 ± 0.01 |

TABLE XV: Final number of events in each channel for taus type 3 $\tau$ After b-tagging, $\tau$ ID and trigger in the signal sample when the assumed cross section is 7.46 pb. An estimate of QCD background is not included.

| Sample | # of events |
|---|---|
| data | 2494 |
| $t\bar{t} \to \tau + jets$ | 33.57 ± 0.34 |
| $t\bar{t} \to e + jets$ | 15.67 ± 0.23 |
| $t\bar{t} \to \mu + jets$ | 2.30 ± 0.09 |
| $t\bar{t} \to l + l$ | 2.69 ± 0.04 |
| $Wbb + jets \to l\nu + bb + jets$ | 9.29 ± 0.27 |
| $Wcc + jets \to l\nu + cc + jets$ | 31.63 ± 0.90 |
| $Wjj + jets \to l\nu + jj + jets$ | 169.95 ± 2.68 |
| $Zbb + jets \to \tau\tau + bb + jets$ | 1.30 ± 0.11 |
| $Zcc + jets \to \tau\tau + cc + jets$ | 3.15 ± 0.20 |
| $Zjj + jets \to \tau\tau + jj + jets$ | 16.86 ± 1.14 |
| $Zbb + jets \to ee + bb + jets$ | 0.02 ± 0.01 |
| $Zcc + jets \to ee + cc + jets$ | 0.00 ± 0.00 |
| $Zjj + jets \to ee + jj + jets$ | 0.74 ± 0.33 |
| $Zbb + jets \to \mu\mu + bb + jets$ | 0.08 ± 0.02 |
| $Zcc + jets \to \mu\mu + cc + jets$ | 0.07 ± 0.03 |
| $Zjj + jets \to \mu\mu + jj + jets$ | 0.38 ± 0.22 |
| $Zbb + jets \to \nu\nu + bb + jets$ | 0.10 ± 0.03 |
| $Zcc + jets \to \nu\nu + cc + jets$ | 0.00 ± 0.00 |
| $Zjj + jets \to \nu\nu + jj + jets$ | 1.36 ± 0.49 |

TABLE XVI: $b$-veto data set composition for types 1 and 2 $\tau$ when the assumed cross section is 7.46 pb.

| Sample | # of events |
|---|---|
| data | 3688 |
| $t\bar{t} \to \tau + jets$ | 19.85 ± 0.27 |
| $t\bar{t} \to e + jets$ | 3.53 ± 0.13 |
| $t\bar{t} \to \mu + jets$ | 2.80 ± 0.10 |
| $t\bar{t} \to l + l$ | 1.81 ± 0.03 |
| $Wbb + jets \to l\nu + bb + jets$ | 5.26 ± 0.19 |
| $Wcc + jets \to l\nu + cc + jets$ | 22.43 ± 0.80 |
| $Wjj + jets \to l\nu + jj + jets$ | 126.41 ± 2.60 |
| $Zbb + jets \to \tau\tau + bb + jets$ | 0.92 ± 0.09 |
| $Zcc + jets \to \tau\tau + cc + jets$ | 2.86 ± 0.20 |
| $Zjj + jets \to \tau\tau + jj + jets$ | 14.53 ± 1.15 |
| $Zbb + jets \to ee + bb + jets$ | 0.00 ± 0.00 |
| $Zcc + jets \to ee + cc + jets$ | 0.08 ± 0.04 |
| $Zjj + jets \to ee + jj + jets$ | 0.31 ± 0.18 |
| $Zbb + jets \to \mu\mu + bb + jets$ | 0.04 ± 0.02 |
| $Zcc + jets \to \mu\mu + cc + jets$ | 0.05 ± 0.02 |
| $Zjj + jets \to \mu\mu + jj + jets$ | 0.05 ± 0.04 |
| $Zbb + jets \to \nu\nu + bb + jets$ | 0.16 ± 0.05 |
| $Zcc + jets \to \nu\nu + cc + jets$ | 0.83 ± 0.15 |
| $Zjj + jets \to \nu\nu + jj + jets$ | 2.31 ± 0.46 |

TABLE XVII: $b$-veto data set composition for type 3 $\tau$ when the assumed cross section is 7.46 pb.

| Sample | # of events |
|---|---|
| data | 1217 |
| $t\bar{t} \to \tau + jets$ | 32.94 ± 0.48 |
| $t\bar{t} \to e + jets$ | 17.02 ± 0.34 |
| $t\bar{t} \to \mu + jets$ | 14.37 ± 0.32 |
| $t\bar{t} \to l + l$ | 2.43 ± 0.06 |
| $Wbb + jets \to l\nu + bb + jets$ | 6.33 ± 0.23 |
| $Wcc + jets \to l\nu + cc + jets$ | 4.63 ± 0.19 |
| $Wjj + jets \to l\nu + jj + jets$ | 11.34 ± 0.26 |
| $Zbb + jets \to \tau\tau + bb + jets$ | 0.50 ± 0.06 |
| $Zcc + jets \to \tau\tau + cc + jets$ | 0.58 ± 0.06 |
| $Zjj + jets \to \tau\tau + jj + jets$ | 1.10 ± 0.13 |
| $Zbb + jets \to ee + bb + jets$ | 0.01 ± 0.01 |
| $Zcc + jets \to ee + cc + jets$ | 0.01 ± 0.01 |
| $Zjj + jets \to ee + jj + jets$ | 0.00 ± 0.00 |
| $Zbb + jets \to \mu\mu + bb + jets$ | 0.03 ± 0.01 |
| $Zcc + jets \to \mu\mu + cc + jets$ | 0.04 ± 0.01 |
| $Zjj + jets \to \mu\mu + jj + jets$ | 0.02 ± 0.01 |
| $Zbb + jets \to \nu\nu + bb + jets$ | 1.07 ± 0.17 |
| $Zcc + jets \to \nu\nu + cc + jets$ | 0.57 ± 0.10 |
| $Zjj + jets \to \nu\nu + jj + jets$ | 0.36 ± 0.04 |

TABLE XVIII: loose-tight data set composition for types 1 and 2 $\tau$ when the assumed cross section is 7.46 pb.

| Sample | # of events |
|---|---|
| data | 4733 |
| $t\bar{t} \to \tau + jets$ | 51.16 ± 0.57 |
| $t\bar{t} \to e + jets$ | 40.02 ± 0.50 |
| $t\bar{t} \to \mu + jets$ | 48.00 ± 0.56 |
| $t\bar{t} \to l + l$ | 2.16 ± 0.05 |
| $Wbb + jets \to l\nu + bb + jets$ | 8.95 ± 0.27 |
| $Wcc + jets \to l\nu + cc + jets$ | 7.80 ± 0.23 |
| $Wjj + jets \to l\nu + jj + jets$ | 16.32 ± 0.30 |
| $Zbb + jets \to \tau\tau + bb + jets$ | 0.52 ± 0.05 |
| $Zcc + jets \to \tau\tau + cc + jets$ | 0.46 ± 0.04 |
| $Zjj + jets \to \tau\tau + jj + jets$ | 1.16 ± 0.12 |
| $Zbb + jets \to ee + bb + jets$ | 0.00 ± 0.00 |
| $Zcc + jets \to ee + cc + jets$ | 0.00 ± 0.00 |
| $Zjj + jets \to ee + jj + jets$ | 0.01 ± 0.01 |
| $Zbb + jets \to \mu\mu + bb + jets$ | 0.06 ± 0.01 |
| $Zcc + jets \to \mu\mu + cc + jets$ | 0.07 ± 0.01 |
| $Zjj + jets \to \mu\mu + jj + jets$ | 0.11 ± 0.02 |
| $Zbb + jets \to \nu\nu + bb + jets$ | 2.49 ± 0.24 |
| $Zcc + jets \to \nu\nu + cc + jets$ | 1.90 ± 0.14 |
| $Zjj + jets \to \nu\nu + jj + jets$ | 1.28 ± 0.08 |

TABLE XIX: loose-tight data set composition for type 3 $\tau$ when the assumed cross section is 7.46 pb.

# VIII. NEURAL NETWORK ANALYSIS

## A. Variables for NN training

Following the same procedure as in the previous analysis, we determine the content of signal and background in the preselected sample, increase signal/background rate and from this, measure the cross-section. The procedure adopted in the p17 analysis was feed a set of topological variables into an artificial neural network in order to provide the best possible separation between signal and background. As before, the criteria for choosing such variables were: power of discrimination and $\tau$-uncorrelated variables. The set is presented below:

- $H_T$ - the scalar sum of all jet's $p_T$ (here and below including $\tau$ lepton candidates).
- $\not\!\!E_T$ ***significance*** - As being the variable that provides the best signal-background separation we decided to optimize it.
- ***Aplanarity*** [35] - the normalized momentum tensor is defined as

$$\mathcal{M} = \frac{\sum_o p_i^o p_j^o}{\sum_o |\overrightarrow{p^o}|} \tag{5}$$

  where $\overrightarrow{p^0}$ is the momentum-vector of a reconstructed object $o$ and $i$ and $j$ are cartesian coordinates. From the diagonalization of $\mathcal{M}$ we find three eigenvalues $\lambda_1 \geq \lambda_2 \geq \lambda_3$ with the constraint $\lambda_1+\lambda_2+\lambda_3 = 1$. The aplanarity A is given by $\mathcal{A} = \frac{3}{2}\lambda_3$ and measures the flatness of an event. Hence, it is defined in the range $0 \leq \mathcal{M} \leq 0.5$. Large values of $\mathcal{A}$ correspond to more spherical events, like $t\bar{t}$ events for instance, since they are typical of decays of heavy objects. On the other hand, both QCD and $W+$jets events are more planar since jets in these events are primarily due to initial state radiation.
- ***Sphericity*** [35] - being defined as $\mathcal{S} = \frac{3}{2}(\lambda_2 + \lambda_3)$, and having a range $0 \leq \mathcal{S} \leq 1.0$, sphericity is a measure of the summed $p_\perp^2$ with respect to the event axis. In this sense a 2-jets event corresponds to $\mathcal{S} \approx 0$ and an isotropic event $\mathcal{S} \approx 1$. $t\bar{t}$ events are very isotropic as they are typical of the decays of heavy objects and both QCD and $W+$jets events are less isotropic due to the fact that jets in these events come primarily from initial state radiation.
- ***Top and*** $W$ ***mass likelihood*** - a $\chi^2$-like variable. $L \equiv \left(\frac{M_{3j}-m_t}{\sigma_t}\right)^2 + \left(\frac{M_{2j}-M_W}{\sigma_W}\right)^2$, where $m_t, M_W, \sigma_t, \sigma_W$ are top and W masses (172.4 GeV and 81.02 GeV respectively) and resolution values (19.4 GeV and 8.28 GeV respectively). $M_{3j}$ and $M_{2j}$ are invariant masses composed of the jet combinations. We choose combination that minimizes $L$.
- ***Centrality***, defined as $\frac{H_T}{H_E}$ , where $H_E$ is sum of energies of the jets.
- $\cos(\theta*)$ - The angle between the beam axis and the highest-$p_T$ jet in the rest frame of all the jets in the event.
- $\sqrt(s)$ - The invariant mass of all jets and $\tau$s in the event.

The chosen variables are in the end a consequence of the method employed in this analysis: use events from the QCD-enriched loose-tight sample to model QCD events in the signal-rich sample, and use a b-tag veto sample as an independent control sample to check the validity of such background modeling.

## B. Topological NN

For training the Neural Network we used the Multilayer Perceptron algorithm, as described in [38]. As explained before in Section VII, the first 1400000 events in the "loose-tight" sample were used as background for NN training for taus types 1 and 2, and the first 600000 of the same sample for NN training for type 3 taus. This means that different tau types are being treated separately in the topological NN. In both cases

1/3 of the Alpgen sample of $t\bar{t} \rightarrow \tau + jets$ was used for NN training and 2/3 of it for the measurement. When doing the measurement later on (Section X) we pick the tau with the highest $NN(\tau)$ in the signal sample as the tau cadidate at same time that taus in the loose-tight sample are picked at random since all of them are regarded as fake taus by being below the cut $NN(\tau) = 0.7$. By doing this we expect to avoid any bias when selecting real taus for the measurement. Figures 3 and 4 show the effect of each of the chosen the topological event NN input variables on the final output.

Figures 5 and 6 show the NN output as a result of the training described above. It is evident from both pictures that high values of NN correspond to the signal-enriched region.

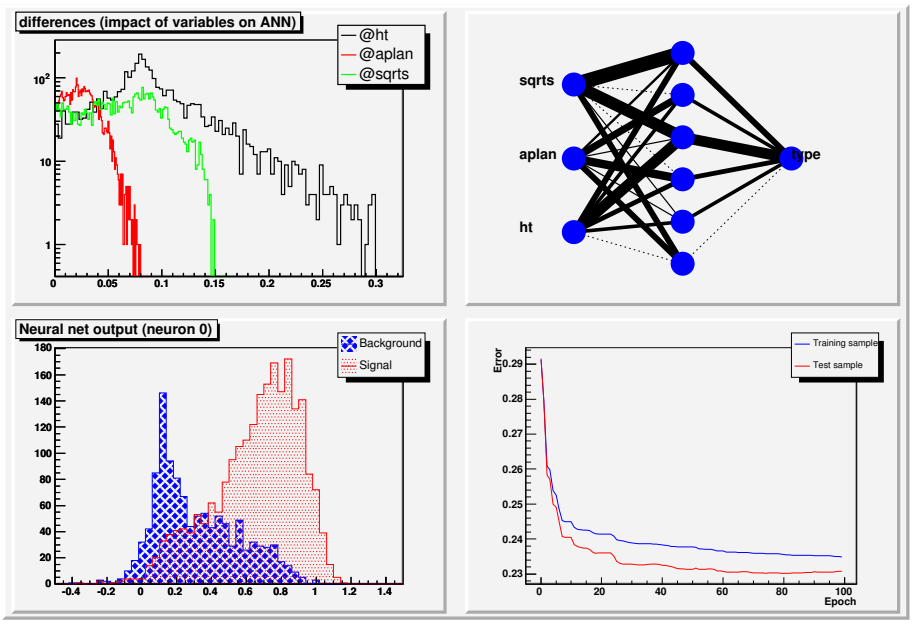


FIG. 3: Training of topological Neural Network output for type 1 and 2 $\tau$ channel. Upper left: relative impact of each of the input variables; upper right: topological structure; lower right: final signal-background separation of the method; lower left: convergence curves.

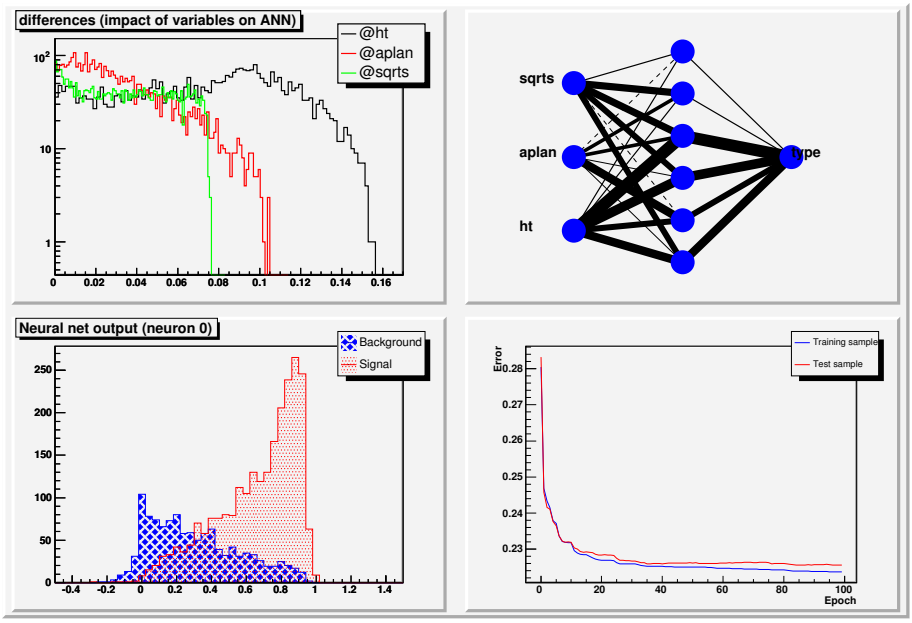


FIG. 4: Training of topological Neural Network output for type 3 $\tau$ channel. Upper left: relative impact of each of the input variables; upper right: topological structure; lower right: final signal-background separation of the method; lower left: convergence curves.

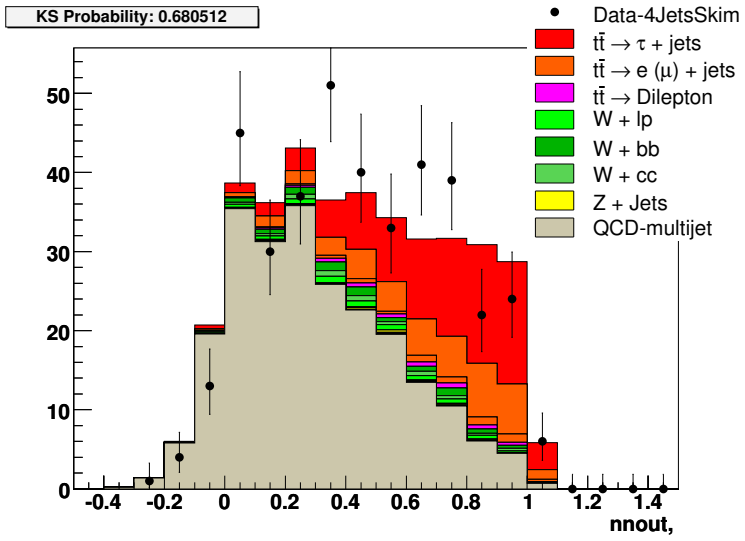


FIG. 5: The topological Neural Network output for type 1 and 2 $\tau$ channel

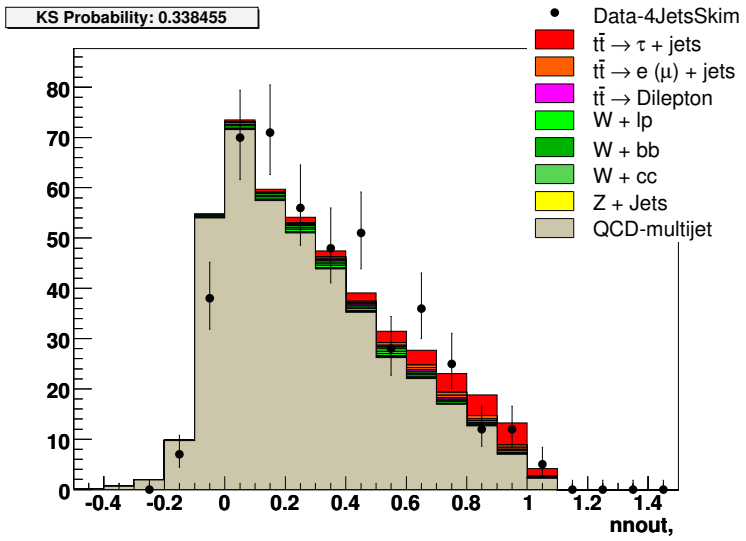


FIG. 6: The topological Neural Network output for type 3 $\tau$ channel

### C. NN optimization

One difference between this present analysis and the previous p17 is that we performed a NN optimization along with a $\not\!\!E_T$ significance optimization. Previously a cut of $> 3.0$ was applied to $\not\!\!E_T$ significance at the preselection stage and then it was included as one of the variables for NN training. This time as we chose to optimize it, since it is still a good variable to provide signal-background discrimination (Figure 7). It is important to stress out that after the optimization we performed the analysis with the optimized $\not\!\!E_T$ significance cut applied when doing both $\tau$ and b ID (Section VII), therefore after the preselection where no $\not\!\!E_T$ significance cut was applied. We then went back anp reprocessed (preselected) all MC samples with the optimized cut. Both results, with $\not\!\!E_T$ significance applied during and after preselectio were identical. We then chose to present this analyis with this cut applied at the preselection level in order to have a consistent cut flow throughout the analysis(Section VI).

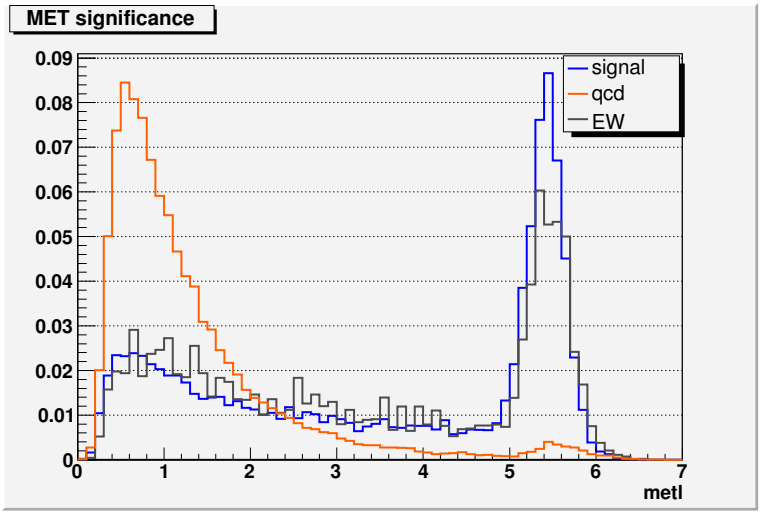


FIG. 7: $\not\!\!E_T$ significance distribution for signal and backgrounds.

Below we describe how we split this part of the analysis into two parts:

1. **Set optimization:** We applied an arbitrary cut on $\not{E}_T$ significance of $\geq 4.0$ and varied the set of varibles going into NN training
2. $\not{E}_T$ **significance optimization:** After chosing the best set based on the lowest RMS, we then varied the $\not{E}_T$ significance cut

For this part of the analysis we present the sets of variables that were taken into account to perform the NN traning

- ***Set I*** : $H_T$, aplan (aplanarity), sqrts ($\sqrt{s}$)
- ***Set II*** : $H_T$, aplan, cent (centrality)
- ***Set III*** : $H_T$, aplan, spher (spherecity)
- ***Set IV*** : $H_T$, cent, spher
- ***Set V*** : aplan, cent, spher
- ***Set VI*** : $H_T$, aplan, sqrts, spher
- ***Set VII*** : $H_T$, aplan, sqrts, cent
- ***Set VIII*** : $H_T$, aplan, sqrts, costhetastar ($cos(\theta^*)$
- ***Set IX*** : $H_T$, aplan, sqrts, cent, spher
- ***Set X*** : $H_T$, aplan, sqrts, cent, costhetastar
- ***Set XI*** : $H_T$, aplan, sqrts, spher, costhetastar
- ***Set XII*** : metl, $H_T$, aplan, sqrts
- ***Set XIII*** : metl, $H_T$, aplan, cent
- ***Set XIV*** : metl, $H_T$, aplan, spher
- ***Set XV*** : metl, $H_T$, cent, spher
- ***Set XVI*** : metl, $H_T$, aplan
- ***Set XVII*** : metl, $H_T$, sqrts
- ***Set XVIII*** : metl, aplan, sqrts
- ***Set XIX*** : metl, $H_T$, cent
- ***Set XX*** : metl, $H_T$, aplan, sqrts, cent
- ***Set XXI*** : metl, $H_T$, aplan, cent, spher
- ***Set XXII*** : metl, $H_T$, aplan, sqrts, spher
- ***Set XXIII*** : metl, $H_T$, aplan, sqrts, costhetastar
- ***Set XXIV*** : metl, sqrts, cent, spher, costhetastar
- ***Set XXV*** : metl, $H_T$, cent, spher, costhetastar
- ***Set XXVI*** : metl, aplan, cent, spher, costhetastar
- ***Set XXVII*** : metl, $H_T$, aplan, cent, costhetastar
- ***Set XXVIII*** : $H_T$, aplan, topmassl
- ***Set XXIX*** : $H_T$, aplan, sqrts, topmassl

- ***Set XXX*** : $H_T$, aplan, sqrts, cent, topmassl
- ***Set XXXI*** : $H_T$, aplan, sqrts, costhetastar, topmassl
- ***Set XXXII*** : metl, $H_T$, topmassl, aplan, sqrts
- ***Set XXXIII*** : metl, spher, costhetastar, aplan, cent

The criteria used for making a decision on which variable should be used follow:

- No more than 5 variables to keep NN simple and stable. More variables leads to instabilities (different result after each retraining) and require larger training samples.
- We do not want to use highly correlated variables in same NN.
- We want to use variables with high discriminating power.

In order to make the decision about which of these 11 choices is the optimal we created an ensemble of 20000 pseudo-datasets each containing events randomly (according to a Poisson distribution) picked from QCD, EW and $t\bar{t}$ templates. Each of these datasets was treated like real data, meaning applying all the cuts and doing the shape fit of event topological NN. QCD templates for fit were made from the same "loose-tight $\tau$ sample" from which the QCD component of the "data" was drawn. The figure of merit chosen is given by Equation 6 below:

$$f = \frac{(N_{fit} - N_{true})}{N_{true}} \tag{6}$$

where $N_{fit}$ is the number of $t\bar{t}$ pairs given by the fit and $N_{true}$ is the number of $t\bar{t}$ pairs from the Poisson distribution. In both Set and $\not\!\!E_T$ significance optimization, the lowest RMS was used to caracterize which configuration is the best in each case.

The plots showing results concerning the set optimizations are found in Appendix E and are summarized in Table XX below, where each RMS and mean are shown. For NN training is standard to choose the number of hidden nodes as being twice the number the number of variables used for the training. The parenthesis after each set ID show the number of hidden nodes in NN training.

From Table XX we see that Set I has the lowest RMS, thus we chose it as the set to be used in $\not\!\!E_T$ significance optimization part, whose results are shown in Appendix F and then summarized in Table XXI below

Combined results from Tables XX and XXI show that the best configuration found was Set I with $\not\!\!E_T$ significance $\geq 4.0$. Therefore, this was the configuration used to perform the cross-section measurement.Figure 8 shows the variation of the RMS as function of the $\not\!\!E_T$ significance we applied.

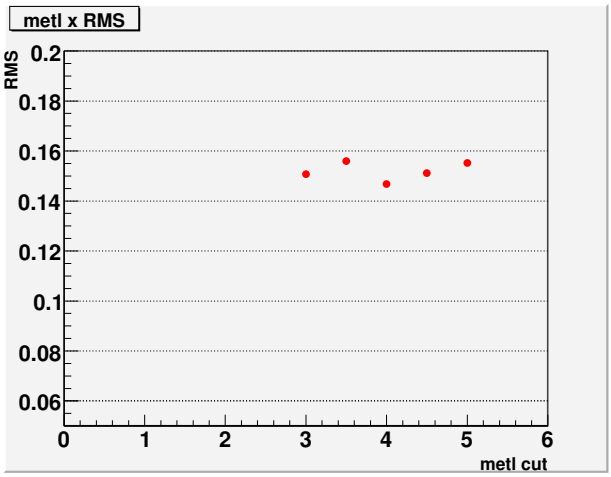


FIG. 8: Plot of RMS as a function the $\not\!\!E_T$ significance applied

| Set of variables | RMS | mean |
|---|---|---|
| Set1(6) | 0.1642 | 0.0265 |
| Set2(6) | 0.1840 | 0.0054 |
| Set3(6) | 0.1923 | 0.0060 |
| Set4(6) | 0.1978 | 0.0175 |
| Set5(6) | 0.2385 | 0.0022 |
| Set6(8) | 0.1687 | 0.0115 |
| Set7(8) | 0.1667 | 0.0134 |
| Set8(10) | 0.1668 | 0.0162 |
| Set9(10) | 0.1721 | 0.0102 |
| Set10(10) | 0.1722 | 0.0210 |
| Se11(10) | 0.1716 | 0.0180 |
| Set12(8) | 0.1662 | 0.0039 |
| Set13(8) | 0.1819 | 0.0018 |
| Set14(8) | 0.1879 | 0.0019 |
| Set15(8) | 0.1884 | -0.0004 |
| Set16(6) | 0.1912 | 0.0034 |
| Set17(6) | 0.1768 | 0.0074 |
| Set18(6) | 0.2216 | -0.0030 |
| Set19(6) | 0.1921 | 0.0015 |
| Set20(10) | 0.1620 | 0.0262 |
| Set21(10) | 0.1753 | 0.0010 |
| Set22(10) | 0.1646 | 0.0086 |
| Set23(10) | 0.1683 | 0.0132 |
| Set24(10) | 0.2053 | 0.0122 |
| Set25(10) | 0.1906 | 0.0038 |
| Set26(10) | 0.2130 | 0.0028 |
| Set27(10) | 0.1859 | 0.0004 |
| Set28(6) | 0.1910 | -0.0022 |
| Set29(8) | 0.1587 | 0.0214 |
| Set30(10) | 0.1546 | 0.0148 |
| Set31(10) | 0.1543 | 0.0203 |
| Set32(10) | 0.1468 | 0.0172 |
| Set33(10) | 0.2201 | 0.0081 |

TABLE XX: Results for set optimization part whit $\not{E}_T$ significance $> 4.0$ applied to all sets. The number in parenthesis refers to number of hidden nodes in each case.

| Set of variables | $\not{E}_T$ significance cut | RMS | mean |
|---|---|---|---|
| Set32(10) | 3.0 | 0.1507 | 0.0157 |
| Set32(10) | 3.5 | 0.1559 | 0.0189 |
| Set32(10) | 4.0 | 0.1468 | 0.0172 |
| Set32(10) | 4.5 | 0.1511 | 0.0153 |
| Set32(10) | 5.0 | 0.1552 | 0.0205 |

TABLE XXI: Results for $\not{E}_T$ significance optimization part when varying the $\not{E}_T$ significance cut The number in parenthesis refers to number of hidden nodes in each case.

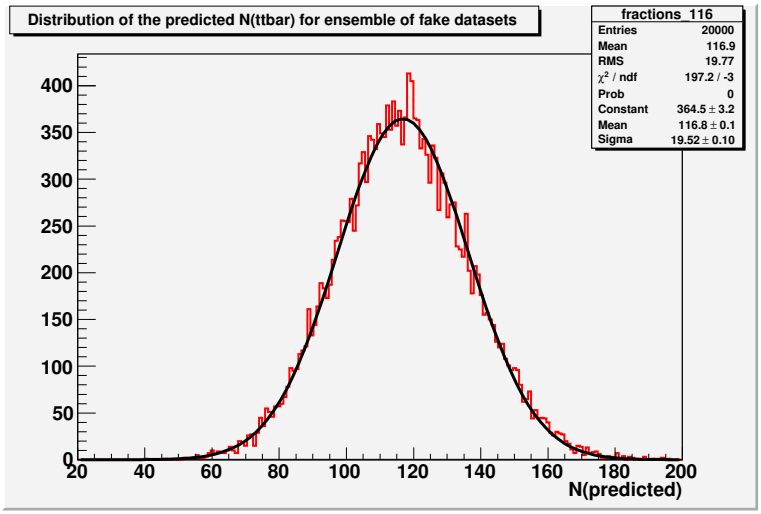


FIG. 9: Distribution of the output "measurement" for an ensemble with 116.9 $t\bar{t}$ events.

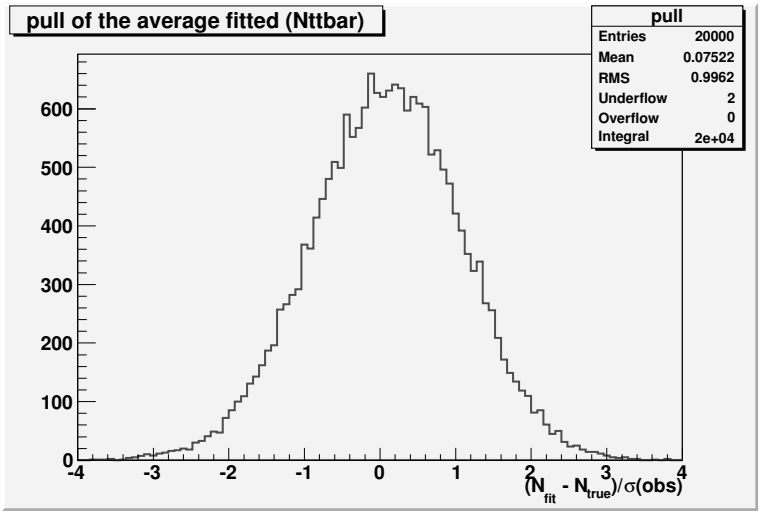


FIG. 10: The ensemble test's pull.

In order to check the validity of our emsemble tests procedure, it is instructive to plot both the distribution of the predicted number of $t\bar{t}$ and what is called "pull", defined in Equation 7 below:

$$p = \frac{(N_{fit} - N_{true})}{\sigma_{fit}} \tag{7}$$

where $\sigma_{fit}$ is the error on the number of $t\bar{t}$ pairs given by the fit.

Figures 9 and 10 show both beforementioned distributions.

From Figure 9 we see a good agreement between the number of $t\bar{t}$ pairs initially set in the ensemble and the measured value. And Figure 10 shows a nice gaussian curve, that indicates a good behaviour of the fit uncertainties in the ensembles.

# IX. TOPOLOGICAL VARIABLES

In this section we show plots of the topological variables used in this analysis in order to check the agreement between data and Monte Carlo in all cases. Plots are separated in two kinds: signal sample and b-veto control plots.

## A. Signal sample plots

As stated in Section VII the signal sample is the one we used to perform the measurement. The cuts here consist of $NN(\tau) > 0.90$ for taus types 1 and 2, $NN(\tau) > 0.95$ for taus type 3, and at least one NN b-tag. This sample contains a good amount of $t\bar{t}$ (19.7% for types 1 and 2 and 8.6% for type 3) as shown in Tables XIV and XV. Next we show the plots of the topological variables for this sample. The error bars represent the statistical uncertainties only.

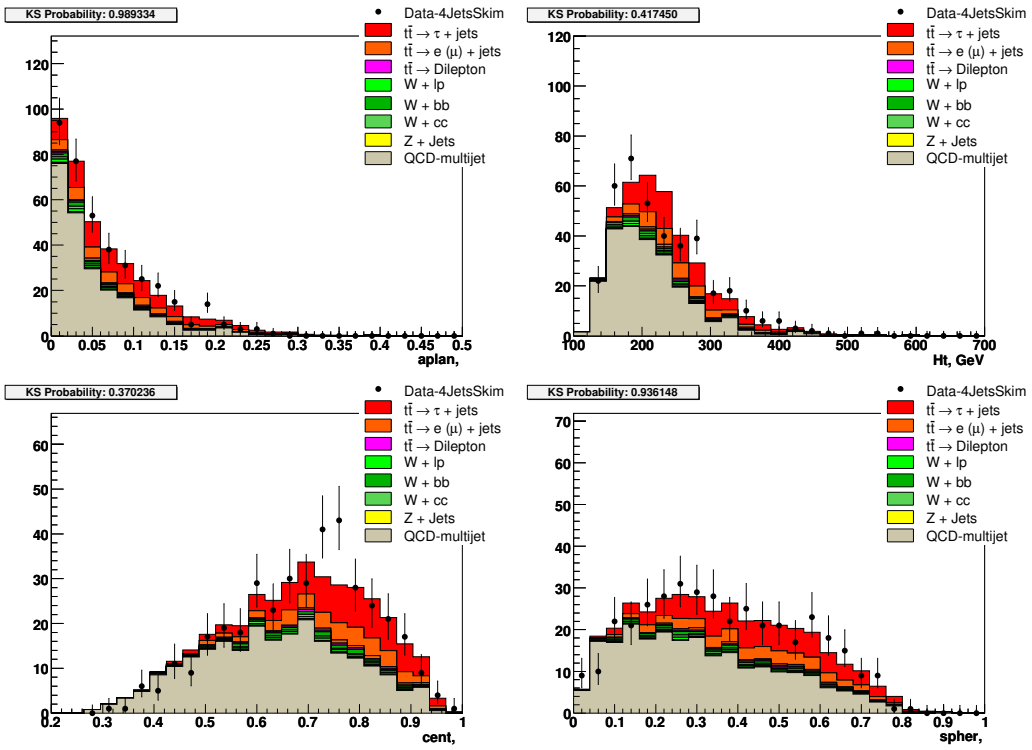


FIG. 11: The topological variables in the signal sample ($\tau$ types 1 and 2). The Kolmogorov-Smirnov (KS) probabilities are shown, indicating the level of agreement.

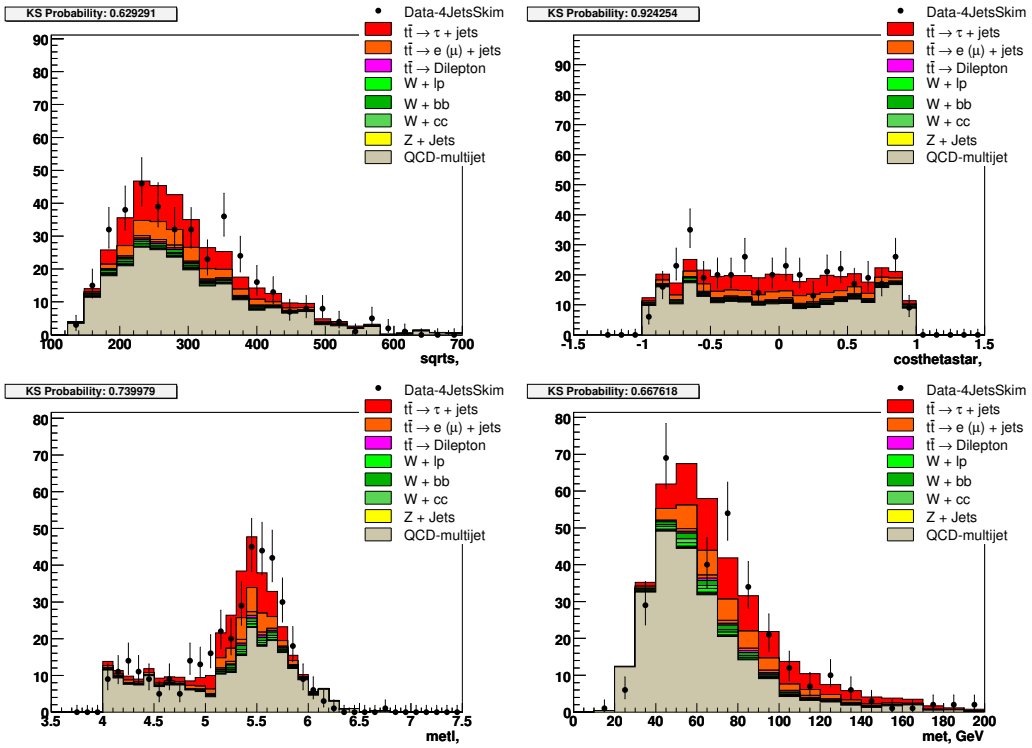


FIG. 12: The topological variables in the signal sample ($\tau$ types 1 and 2). The Kolmogorov-Smirnov (KS) probabilities are shown, indicating the level of agreement.

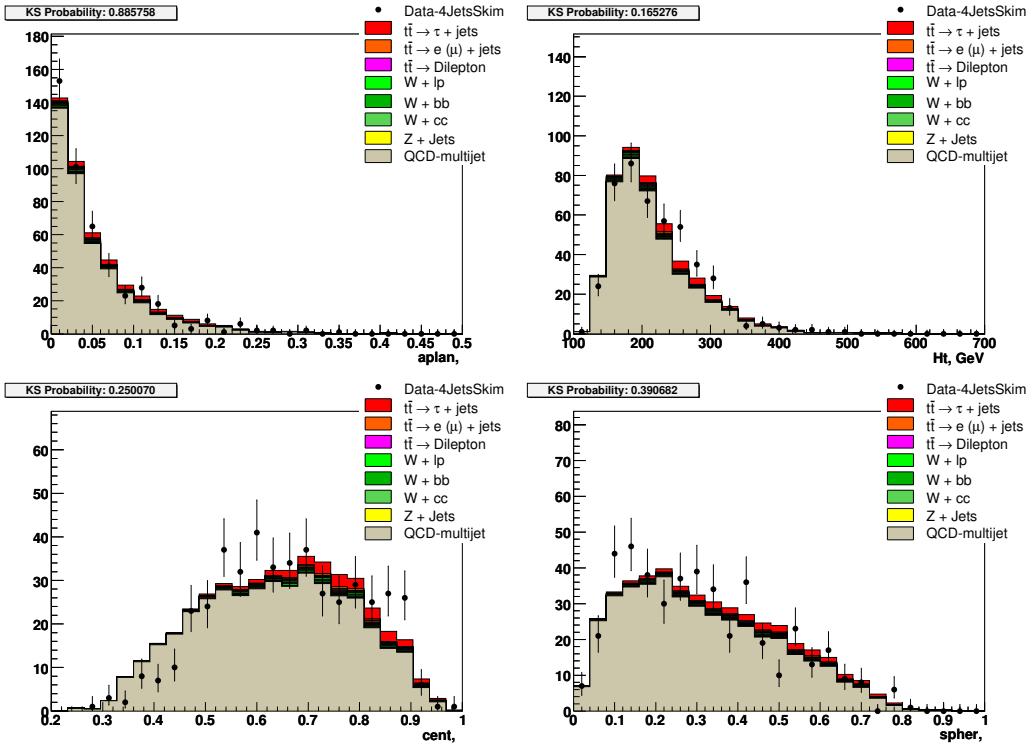


FIG. 13: The topological variables in the signal sample ($\tau$ types 3). The Kolmogorov-Smirnov (KS) probabilities are shown, indicating the level of agreement.

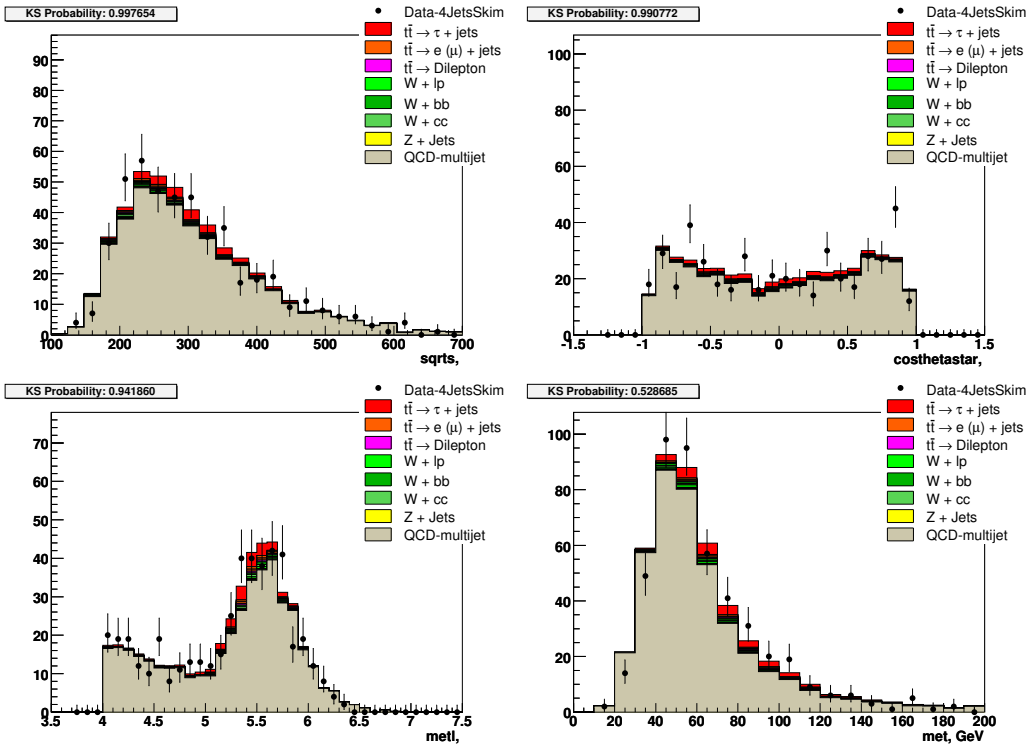


FIG. 14: The topological variables in the signal sample ($\tau$ types 3). The Kolmogorov-Smirnov (KS) probabilities are shown, indicating the level of agreement.

## B. b-veto control sample plots

The b-veto sample is the one used to test our QCD modelling VII. As it requires no NN b-tags it is QCD-dominated and has a tiny amount of $t\bar{t}$ (1.9% for types 1 and 2 and 0.7% for type 3) as shown in Tables XVI and XVII. It consists of an ideal sample to make sure that the QCD modelling works and can be used in the measurement. Next we show the plots of the topological variables for this sample. The error bars represent the statistical uncertainties only.

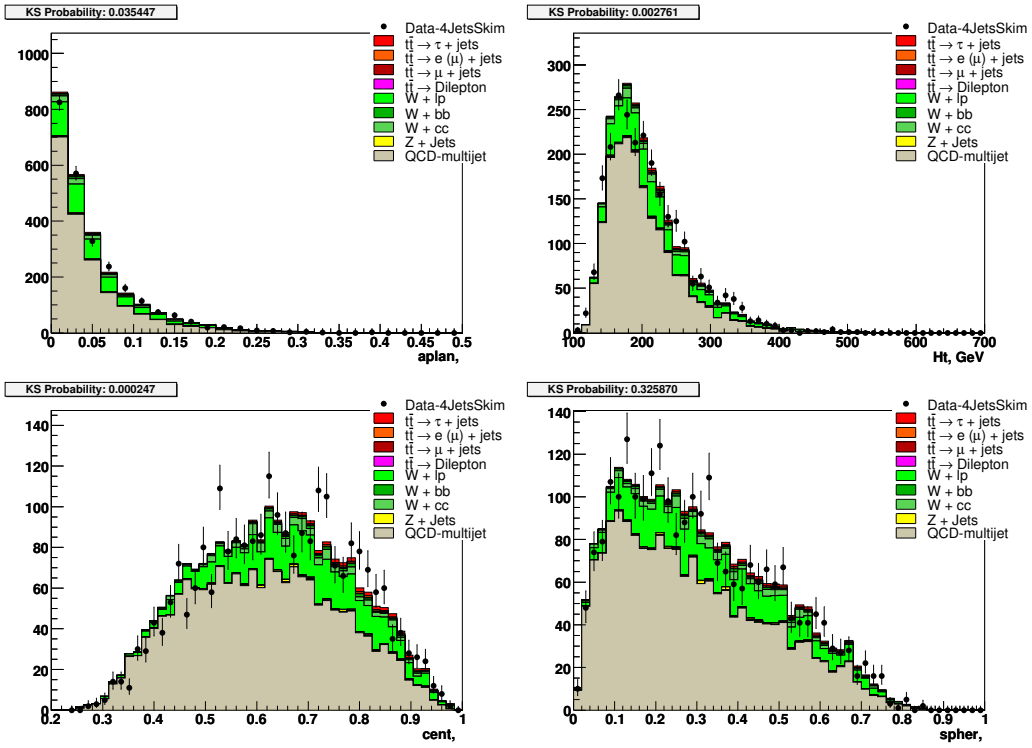


FIG. 15: The topological variables in the b-veto control sample ($\tau$ types 1 and 2). The Kolmogorov-Smirnov (KS) probabilities are shown, indicating how good the agreement is.

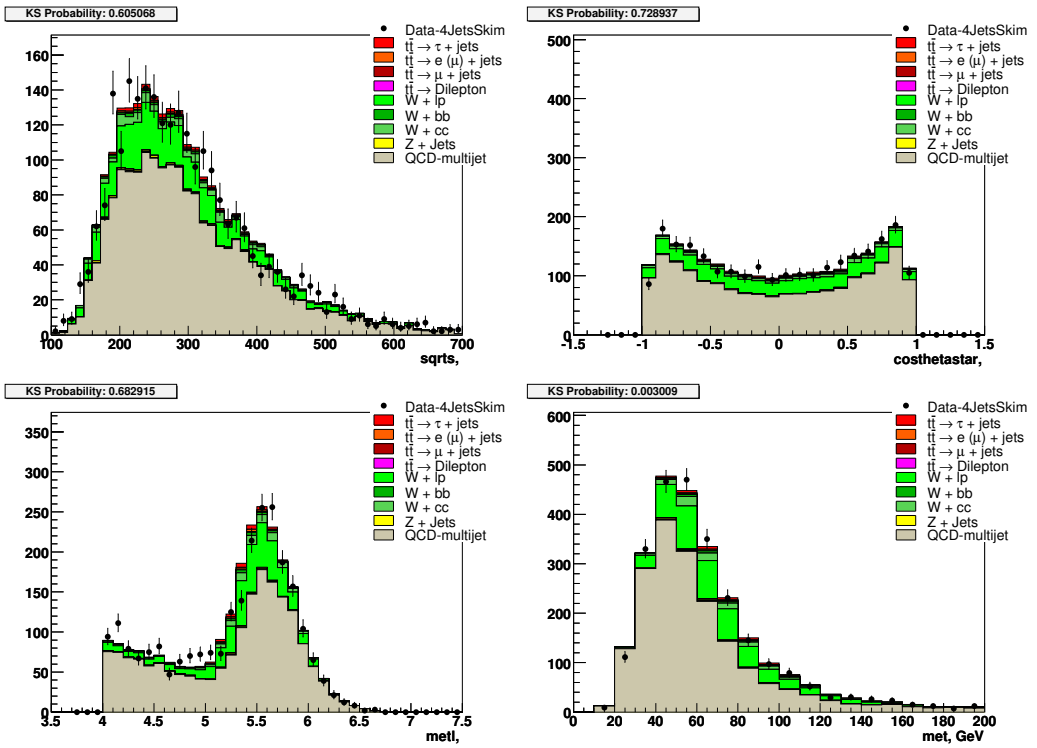


FIG. 16: The topological variables in the b-veto control sample ($\tau$ types 1 and 2). The Kolmogorov-Smirnov (KS) probabilities are shown, indicating how good the agreement is.

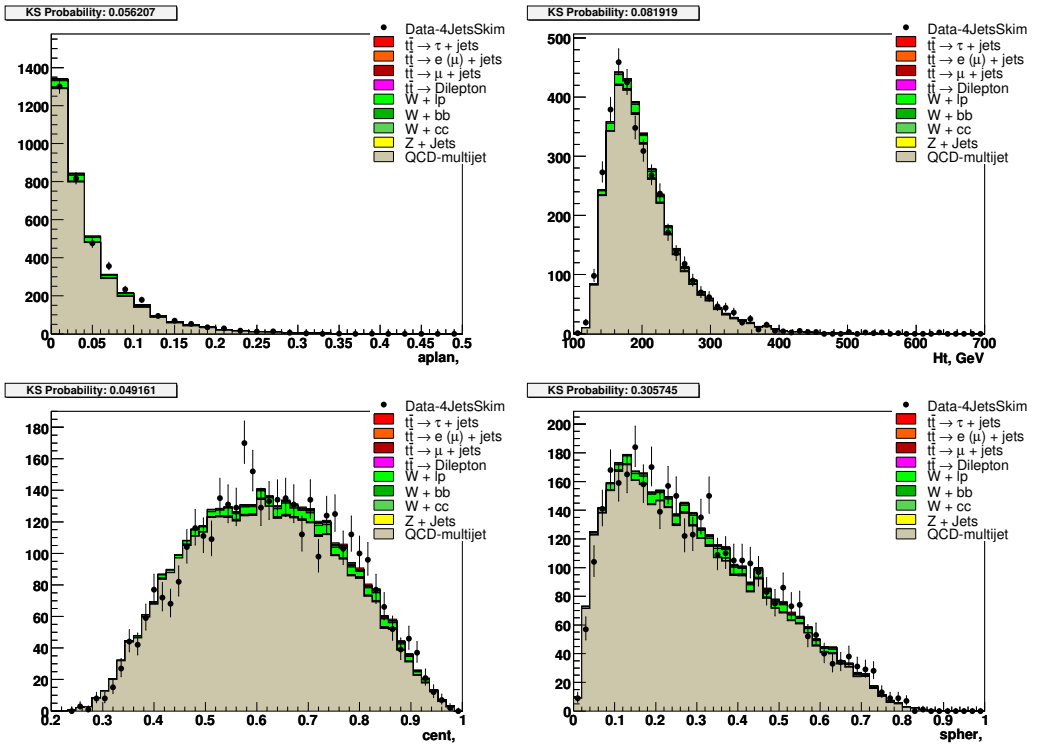


FIG. 17: The topological variables in the b-veto control sample ($\tau$ types 3). The Kolmogorov-Smirnov (KS) probabilities are shown, indicating how good the agreement is.

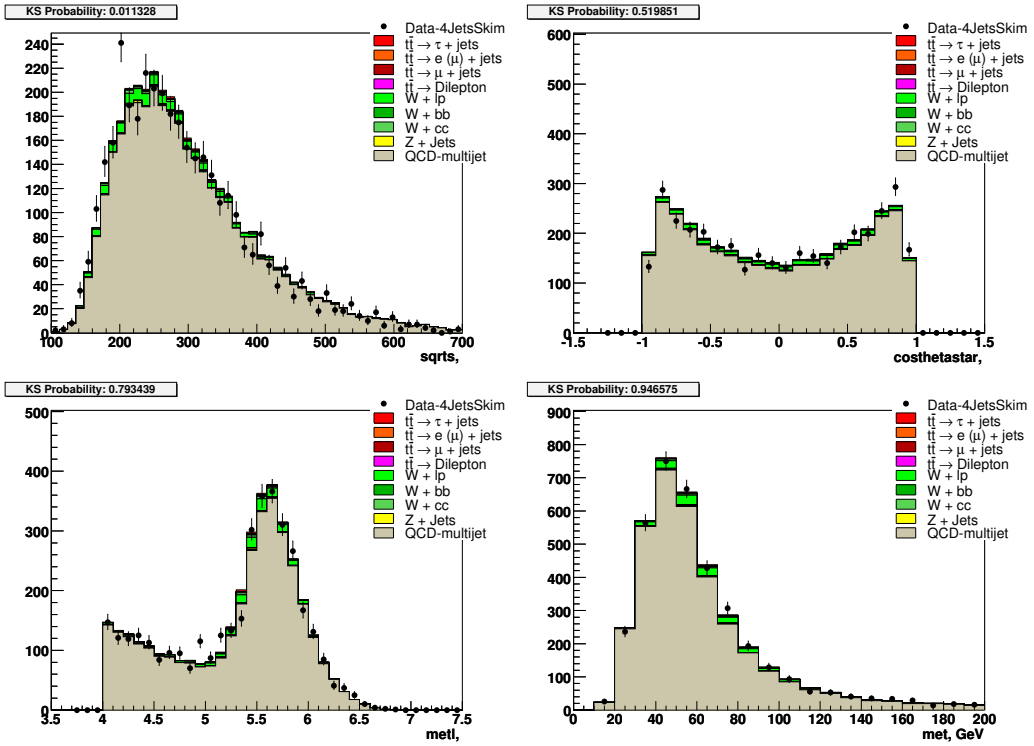


FIG. 18: The topological variables in the b-veto control sample ($\tau$ types 3). The Kolmogorov-Smirnov (KS) probabilities are shown, indicating how good the agreement is.

## X. CROSS SECTION

Having presented the preselection yelds on Section VI we now show the results of the efficiencies for $\tau$ ID, b-tagging and trigger for all $t\bar{t}$ channels

| Selection | Relative(%) | Cumulative(%) |
|---|---|---|
| $\tau$ ID | $22.20 \pm 0.24$ | $22.20 \pm 0.24$ |
| Trigger | $84.54 \pm 0.55$ | $18.77 \pm 0.22$ |
| b-tagging | $61.82 \pm 0.55$ | $11.61 \pm 0.16$ |

TABLE XXII: $t\bar{t} \rightarrow \tau + jets$ final cut flow for taus types 1 and 2

| Selection | Relative(%) | Cumulative(%) |
|---|---|---|
| $\tau$ ID | $12.37 \pm 0.21$ | $12.37 \pm 0.21$ |
| Trigger | $84.79 \pm 0.75$ | $10.49 \pm 0.19$ |
| b-tagging | $59.63 \pm 0.75$ | $6.26 \pm 0.13$ |

TABLE XXIII: $t\bar{t} \rightarrow \tau + jets$ final cut flow for taus type 3

| Selection | Relative(%) | Cumulative(%) |
|---|---|---|
| $\tau$ ID | $10.81 \pm 0.20$ | $10.81 \pm 0.20$ |
| Trigger | $83.40 \pm 0.81$ | $9.02 \pm 0.18$ |
| b-tagging | $61.30 \pm 0.82$ | $5.52 \pm 0.12$ |

TABLE XXIV: $t\bar{t} \rightarrow e + jets$ final cut flow for taus types 1 and 2

| Selection | Relative(%) | Cumulative(%) |
|---|---|---|
| $\tau$ ID | $2.25 \pm 0.11$ | $2.25 \pm 0.11$ |
| Trigger | $83.62 \pm 1.77$ | $1.88 \pm 0.09$ |
| b-tagging | $58.26 \pm 1.76$ | $1.10 \pm 0.06$ |

TABLE XXV: $t\bar{t} \rightarrow e + jets$ final cut flow for taus type 3

| Selection | Relative(%) | Cumulative(%) |
|---|---|---|
| $\tau$ ID | $3.38 \pm 0.19$ | $3.38 \pm 0.19$ |
| Trigger | $84.44 \pm 2.13$ | $2.86 \pm 0.17$ |
| b-tagging | $61.25 \pm 2.16$ | $1.75 \pm 0.11$ |

TABLE XXVI: $t\bar{t} \rightarrow \mu + jets$ final cut flow for taus types 1 and 2.

| Selection | Relative(%) | Cumulative(%) |
|---|---|---|
| $\tau$ ID | $3.88 \pm 0.21$ | $3.88 \pm 0.21$ |
| Trigger | $82.79 \pm 2.04$ | $3.21 \pm 0.18$ |
| b-tagging | $58.11 \pm 2.05$ | $1.87 \pm 0.11$ |

TABLE XXVII: $t\bar{t} \rightarrow \mu + jets$ final cut flow for taus type 3

| Selection | Relative(%) | Cumulative(%) |
|---|---|---|
| $\tau$ ID | $21.18 \pm 0.37$ | $21.18 \pm 0.37$ |
| Trigger | $79.56 \pm 0.90$ | $16.85 \pm 0.34$ |
| b-tagging | $62.83 \pm 0.92$ | $10.59 \pm 0.25$ |

TABLE XXVIII: $t\bar{t} \rightarrow dilepton$ final cut flow for taus types 1 and 2

| Selection | Relative(%) | Cumulative(%) |
|---|---|---|
| $\tau$ ID | $14.73 \pm 0.34$ | $14.73 \pm 0.34$ |
| Trigger | $78.78 \pm 1.08$ | $11.60 \pm 0.30$ |
| b-tagging | $63.62 \pm 1.11$ | $7.38 \pm 0.22$ |

TABLE XXIX: $t\bar{t} \rightarrow$ *dilepton* final cut flow for taus type 3.

After having computed all efficiencies it is worthy to summarize all of them (in %) for the different tau types:

| Channel | Preselection | $\tau$ ID | Trigger | b-tag |
|---|---|---|---|---|
| $t\bar{t} \rightarrow \tau + jets$ | $3.70 \pm 0.02$ | $22.20 \pm 0.24$ | $18.77 \pm 0.22$ | $11.61 \pm 0.16$ |
| $t\bar{t} \rightarrow e + jets$ | $3.54 \pm 0.02$ | $10.80 \pm 0.20$ | $9.02 \pm 0.18$ | $5.53 \pm 0.12$ |
| $t\bar{t} \rightarrow \mu + jets$ | $1.67 \pm 0.01$ | $3.38 \pm 0.19$ | $2.86 \pm 0.17$ | $1.75 \pm 0.11$ |
| $t\bar{t} \rightarrow dilepton$ | $1.36 \pm 0.01$ | $21.18 \pm 0.37$ | $16.85 \pm 0.34$ | $10.59 \pm 0.25$ |

TABLE XXX: Summary of all selections for taus type 1 & 2.

| Channel | Preselection | $\tau$ ID | Trigger | b-tag |
|---|---|---|---|---|
| $t\bar{t} \rightarrow \tau + jets$ | $3.70 \pm 0.02$ | $12.37 \pm 0.21$ | $10.49 \pm 0.19$ | $6.26 \pm 0.13$ |
| $t\bar{t} \rightarrow e + jets$ | $3.54 \pm 0.02$ | $2.25 \pm 0.11$ | $1.88 \pm 0.09$ | $1.10 \pm 0.06$ |
| $t\bar{t} \rightarrow \mu + jets$ | $1.67 \pm 0.01$ | $3.88 \pm 0.21$ | $3.21 \pm 0.18$ | $1.87 \pm 0.11$ |
| $t\bar{t} \rightarrow dilepton$ | $1.36 \pm 0.01$ | $14.73 \pm 0.34$ | $11.60 \pm 0.30$ | $7.38 \pm 0.22$ |

TABLE XXXI: Summary of all selections for taus type 3.

Table below summarizes the number of events in each channel after final selection.

TABLE XXXII: Final number of events in the two analysis channels.

| | $\tau$ type I,II | $\tau$ type I,II (fitted) | $\tau$ type III | $\tau$ type III (fitted) |
|---|---|---|---|---|
| data | 386 | | 459 | |
| $t\bar{t} \rightarrow \tau + jets$ | 72.04 ± 0.53 | | 38.82 ± 0.39 | |
| $t\bar{t} \rightarrow e + jets$ | 38.35 ± 0.36 | | 6.52 ± 0.16 | |
| $t\bar{t} \rightarrow \mu + jets$ | 4.81 ± 0.14 | | 5.14 ± 0.14 | |
| $t\bar{t} \rightarrow l + l$ | 6.02 ± 0.07 | | 4.20 ± 0.06 | |
| $t\bar{t}$ total MC | | 121.22 ± 0.43 | | 54.68 ± 0.20 |
| $t\bar{t}$ total fitted | | 133.04 ± 17.09 | | 33.12 ± 15.04 |
| $W$+jets | 17.82 ± 0.33 | | 11.26 ± 0.23 | |
| $Z$+jets | 2.78 ± 0.14 | | 2.39 ± 0.12 | |
| QCD | | 232.35 ± 17.09 | | 412.22 ± 15.04 |
| Signal significance | | 6.77 | | 1.54 |
| S/B ratio | | 0.52 | | 0.08 |

The cross section was measured by minimizing the sum of the negative log-likelihood functions for each bin of both the types 1 and 2 channel and the type 3 $\tau$ channel. These are functions used by MINUIT to perform fits shown in Figs 5 and 6 in Section VIII B. But there $L$ was function of $f(QCD)$ and now we want to use it to measure the cross section, so we must express it in terms of $\sigma(t\bar{t}\,)$:

$$L(\sigma, \tilde{N}_i, N_i^{obs}) \equiv -log(\prod_i \frac{\tilde{N}_i^{N_i^{obs}}}{N_i^{obs}!} e^{-\tilde{N}_i}) \tag{8}$$

where $\tilde{N}_i = \sigma \times BR \times \mathcal{L} \times \epsilon(t\bar{t})_i + N_{bkg}$ is number events predicted in bin i of the data NN distribution and $N_i^{obs}$ is the actual count observed in that bin. The cross-section is then the minimum value of each function. But, as stressed out in Section VII, we have to take into account both signal ($t\bar{t}\,$) and electroweak contamination in the loose-tight sample we use to model QCD in the high NN region used for the measurement. The electroweak component is small and therefore it is kept fixed during the fit and subtracted from the loose-tight sample. However, as dicussed before, the numbers for signal contamination are 5.4% and 3.0% for taus types 1 and 2 and type 3 respectively when we assumed a $t\bar{t}$ cross section of 7.46 pb. This means that 5.4% (12.55 events) of 232.35 QCD events for taus types 1 and 2 are actually $t\bar{t}$ events and 3.0% (12.37 events) of 412.22 QCD events for taus type 3 are actually $t\bar{t}$ events. 12.55 and 12.37 events represent increases of 9.43% and 37.35% on the number of signal events for types 1 and 2 and type 3 respectively. However this is not the final measurement yet since the cross-section measurement only makes sense if the cross-section we measure in the and is the same as the one we have assumed to normalize $t\bar{t}$ MC samples. This means that we had to iterate back by normalizing the signal samples until we found a convergence of the cross-section. Table XXIII summarizes the iteration process.

| Assumed $\sigma(t\bar{t}\,)$ (pb) | signal contamination for types 1 & 2 (%) | signal contamination for type 3 (%) | measured $\sigma(t\bar{t}\,)$ (pb) |
|---|---|---|---|
| 7.46 | 5.4 | 3.0 | 8.37 |
| 8.37 | 6.1 | 3.3 | 8.42 |
| 8.42 | 6.2 | 3.4 | 8.46 |
| 8.46 | 6.2 | 3.4 | 8.46 |

TABLE XXXIII: Cross-section iteration process.

Table above shows that when we assumed a cross-section of 8.46 pb we measured the exact same value, which means that we had to take into account signal contaminations of 6.2% (14.40 events) and 3.4% (14.02 events) for taus types 1 and 2 and 3 respectively. This represents an increase in the number of signal events of 10.82% for types 1 and 2 and 42.33% for type 3. By considering such events as part of the signal $t\bar{t}$ sample we measure for the cross-sections:

$\tau$+jets types 1 and 2 cross section:

$$\sigma(t\bar{t}) = 8.83\ ^{+1.14}_{-1.12}\ (\text{stat})\ ^{+0.89}_{-0.94}\ (\text{syst})\ \pm 0.3\ (\text{lumi})\ \text{pb},$$

$\tau$+jets type 3 cross section:

$$\sigma(t\bar{t}) = 6.06\ ^{+2.77}_{-2.62}\ (\text{stat})\ ^{+0.94}_{-0.99}\ (\text{syst})\ \pm 0.3\ (\text{lumi})\ \text{pb},$$

Combined cross section:

$$\sigma(t\bar{t}) = 8.46\ ^{+1.06}_{-1.04}\ (\text{stat})\ ^{+0.92}_{-0.88}\ (\text{syst})\ \pm 0.3\ (\text{lumi})\ \text{pb}.$$

The correspondent likelihoods of these measurements are shown in Figures 19, 20 and 21. Figures 22, 23 and 24 show zoomed in graphs of the same likelihood functions described above.

All associated systematics concerning this measurement can be seen in Table XXXVI.

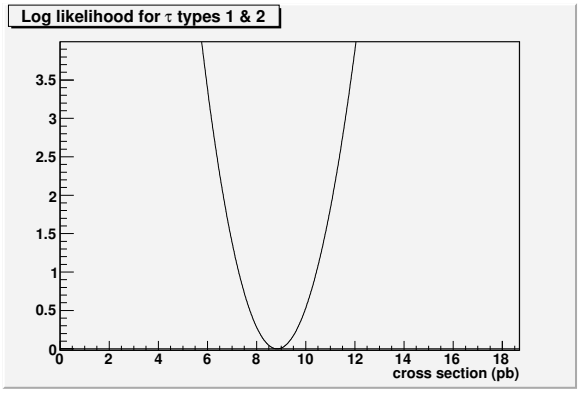


FIG. 19: The log likelihood function for type 1 and 2 $\tau$ channel

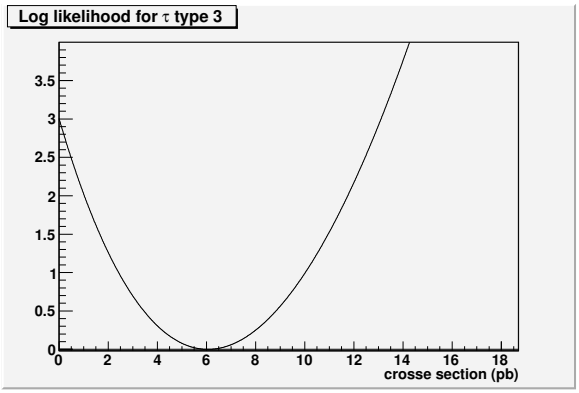


FIG. 20: The log likelihood function for type 3 $\tau$ channel

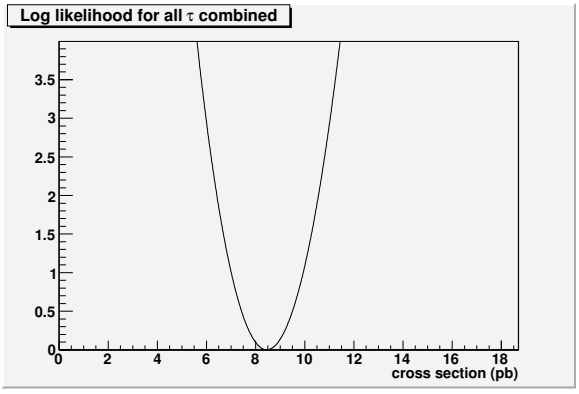


FIG. 21: The log likelihood function for all three types combined

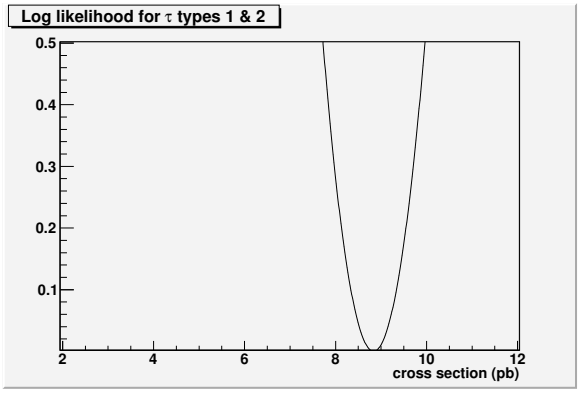


FIG. 22: Zoom in of the log likelihood function for type 1 and 2 $\tau$ channel

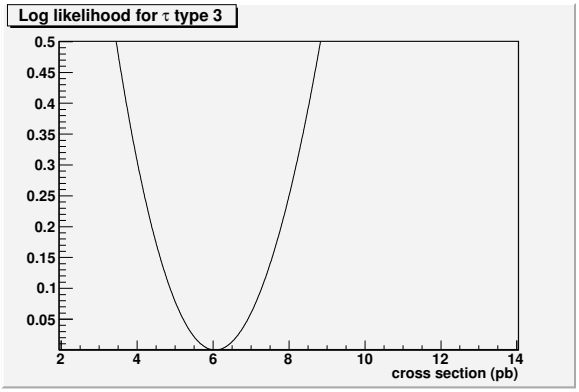


FIG. 23: Zoom in of the log likelihood function for type 3 $\tau$ channel

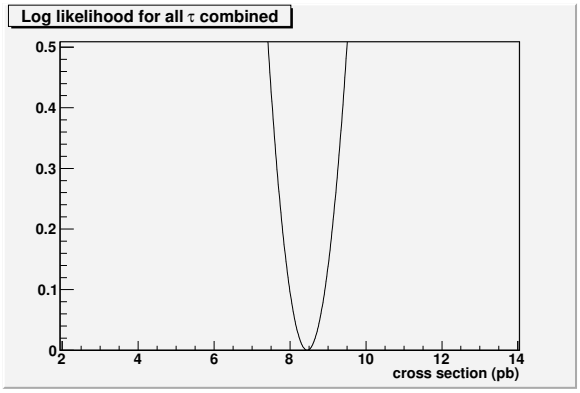


FIG. 24: Zoom in of the log likelihood function for all three types combined

After measuring the combined cross section we observed a significant higher statistical uncertainty value if compared to the one we expected to see based on the fact that we have approximately 5 times more data than in p17, where the signal contamination was not taken into account (see Appendix G). Further investigation showed that the cut NNelec $> 0.9$ applied to taus type 2 only was responsible for such discrepancy. Below we show the same measurement as done above but now with no NNelec cut applied.

Table below summarizes the number of events in each channel after final selection.

TABLE XXXIV: Final number of events in the two analysis channels.

| | $\tau$ type I,II | $\tau$ type I,II (fitted) | $\tau$ type III | $\tau$ type III (fitted) |
|---|---|---|---|---|
| data | 583 | | 459 | |
| $t\bar{t} \to \tau + jets$ | 85.46 ± 0.58 | | 38.82 ± 0.39 | |
| $t\bar{t} \to e + jets$ | 175.23 ± 0.85 | | 6.52 ± 0.16 | |
| $t\bar{t} \to \mu + jets$ | 8.98 ± 0.19 | | 5.14 ± 0.14 | |
| $t\bar{t} \to l + l$ | 12.62 ± 0.10 | | 4.18 ± 0.06 | |
| $t\bar{t}$ total MC | | 282.27 ± 1.05 | | 54.67 ± 0.41 |
| $t\bar{t}$ total fitted | | 260.71 ± 20.74 | | 35.73 ± 15.28 |
| $W$+jets | 39.65 ± 0.50 | | 11.26 ± 0.25 | |
| $Z$+jets | 4.56 ± 0.10 | | 2.38 ± 0.11 | |
| QCD | | 278.04 ± 20.74 | | 409.62 ± 15.28 |
| Signal significance | | 10.80 | | 1.67 |
| S/B ratio | | 0.80 | | 0.08 |

Table below shows the iteration process in this case and and the cross section measurement follows:

| Assumed $\sigma(t\bar{t})$ (pb) | signal contamination for types 1 & 2 (%) | signal contamination for type 3 (%) | measured $\sigma(t\bar{t})$ (pb) |
|---|---|---|---|
| 7.46 | 6.0 | 3.0 | 6.84 |
| 6.84 | 5.4 | 2.7 | 6.91 |
| 6.91 | 5.5 | 2.8 | 6.92 |
| 6.92 | 5.5 | 2.8 | 6.92 |

TABLE XXXV: Cross-section iteration process.

$\tau$+jets types 1 and 2 cross section:

$$\sigma(t\bar{t}) = 7.03\ ^{+0.54}_{-0.56}\ (\text{stat})\ ^{+0.65}_{-0.61}\ (\text{syst})\ \pm 0.3\ (\text{lumi})\ \text{pb},$$

$\tau$+jets type 3 cross section:

$$\sigma(t\bar{t}) = 4.36\ ^{+2.62}_{-2.50}\ (\text{stat})\ ^{+0.62}_{-0.61}\ (\text{syst})\ \pm 0.3\ (\text{lumi})\ \text{pb},$$

Combined cross section:

$$\sigma(t\bar{t}) = 6.92\ ^{+0.54}_{-0.54}\ (\text{stat})\ ^{+0.62}_{-0.60}\ (\text{syst})\ \pm 0.3\ (\text{lumi})\ \text{pb},$$

As we can see the statistical uncertainty decreases to 0.54 pb which is in a good agreement to what we would expect if compared to 1.2 pb measured in p17. Appendix G shows cross sections measurements when signal contamination is not taken into account for both NNelec $> 0.9$ and no NNelec cut applied. Once again we observed a discrepancy when NNelec is applied and the expected value when NNelec is not applied.

## XI. SYSTEMATIC UNCERTAINTIES

Several factors contribute to systematic uncertainties in the measurement. Here we describe such uncertainties.

### A. JES

The jet energy scale (JES) systematic is determined by shifiting the jet energy scale by $\pm 1\sigma$ in all MC samples.

### B. TES

The tau energy scale (TES) systematic is determined by shifiting the tau energy scale by its uncertainty as given in [36].

### C. Jet Energy Resolution and Jet ID

The jet energy resolution (JER) systematic is determined by shifiting the jet energy resolution by $\pm 1\sigma$ in all MC samples.

### D. Trigger

Each event was corrected by the ratio of the actual and predicted trigger result as a function of $H_T$, which was used based on the fact that the agreement varies as function of it.

### E. b-quark fragmentation

This uncertainty is estimated using the standard procedure described in [17] by reweighting $t\bar{t}$ events using different fragmentation functions.

### F. *b*-tagging

b-tagging uncertainty effects are taken into account by varying the systematic and statistical errors on the MC tagging weights.

These errors (which are computed using standard DØ b ID group tools) arise form several independent sources [27]:

- B-jet tagging parameterization.
- C-jet tagging parameterization.
- Light jet tagging parameterization (negative tag rate).
- Semi-leptonic b-tagging efficiency parameterization in MC and in data (System 8).
- Taggability. This includes the statistical error due to finite statistic in the samples from which it had been derived and systematic, reflecting the (neglected) taggability dependence on the jet multiplicity.

### G. $\tau$ ID systematics

Here we include systematics associated to the NN cut (NN $> 0.90$ for taus types 1 and 2 and NN $> 0.95$ for taus type 3) applied to select hadronic taus. As recommended by the $\tau$-ID group these systematics are 9.5%, 3.5% and 5.0% for taus type 1, 2 and 3 respectively. However in this analysis we chose treat taus types 1 and 2 together. This led us to combine their uncertainties in the following way

$$sys_{12} = \sqrt{\epsilon_1^2 * f_1^2 + \epsilon_2^2 * f_2^2} \tag{9}$$

where $\epsilon_1$ and $\epsilon_2$ are the $\tau$ ID efficiencies for taus types 1 and 2 respectively and $f_1$ and $f_2$ are the fractions of taus types 1 (0.16) and 2 (0.84) respectively.

### H. QCD systematics

As explained in the section VIII A we use the control (b-veto) data set to validate our method of modeling the multijet background. Therefore we have to use the same sample to evaluate the associated uncertainties. The way it was done is by reweighting topological event NN for QCD template ("loose-tight" $\tau$), so that it matches the one for "tight" $\tau$ data exactly (electroweak beckgrounds were subtracted).

### I. W and Z scale factors

We apply a ascale factor of 1.47 to both W + bb and W + cc events with an uncertainty of 15%. At the same time a scales factors of 1.52 and 1.67 are applied to Z + bb and Z + cc events, both with an uncertainty of 20%.

### J. Template statistics

When we performed the template fit to data (Section VIII) the QCD template had limited statistics (1132 events for taus types 1 and 2 and 4487 events for taus type 3). We have to take the statistical uncertainty in this histogram as one of the cross section systematics. It was calculated by varying the content of each bin of the QCD template NN distribution within its uncertainty and observing how the cross section result changed.

### K. $t\bar{t}$ contamination in the loose-tight sample

When measuring the cross-section we had to take into account the signal contamination in the loose-tight sample we use to model QCD in the high NN region. The systematic uncertainty in this case is calculated by varying the final assumed cross section by $\pm 1\sigma$, re-estimating the signal contamination and finally measuring the up and down values of the cross section.

### L. PDF

Systematics on Parton Distribution Functions (PDF) are estimated by reweighting signal $t\bar{t}$ MC from CTEQ6L1 to CTEQ6.1m and its twenty error PDF's. The reweighting of the PDF's is done by using `caf_pdfreweight` package tool on Pythia $t\bar{t}$ MC. We then assigned the relative PDF uncertainty obtained with Pythia on the Alpgen $t\bar{t}$ MC.

### M. Luminosity

Here we take the DØ standard measured uncertainty on luminosity of 6.1% .

Tables XXXVI and XXXVII summarize all of these uncertainty sources and shows how the resulting cross section shifts.

TABLE XXXVI: Systematic uncertainties on $\sigma(t\bar{t})$ (in pb) for NNelec $> 0.9$.

| Channel | $\tau$+jets types 1 and 2 | $\tau$+jets type 3 | Combined |
|---|---|---|---|
| Tau Energy Scale | $+0.068,-0.102$ | $+0.340,-0.306$ | $+0.136,-0.136$ |
| Jet Energy Scale | $+0.051,-0.034$ | $+0.051,-0.085$ | $+0.051,-0.000$ |
| Jet Energy Resolution | $+0.102,-0.051$ | $+0.204,-0.034$ | $+0.119,-0.052$ |
| Jet ID | $+0.204,-0.204$ | $+0.153,-0.153$ | $+0.204,-0.204$ |
| b-tag | $+0.562,-0.493$ | $+0.493,-0.426$ | $+0.544,-0.477$ |
| b-fragmentation | $+0.102,-0.102$ | $+0.068,-0.068$ | $+0.085,-0.085$ |
| QCD Modeling | $+0.340,-0.340$ | $+0.221,-0.221$ | $+0.324,-0.305$ |
| $\tau$ ID | $+0.272,-0.272$ | $+0.306,-0.306$ | $+0.290,-0.290$ |
| Trigger | $+0.256,-0.256$ | $+0.238,-0.238$ | $+0.256,-0.256$ |
| W Scale Factor | $+0.034,-0.034$ | $+0.034,-0.034$ | $+0.034,-0.034$ |
| Z Scale Factor | $+0.072,-0.072$ | $+0.072,-0.072$ | $+0.048,-0.048$ |
| Template statistics | $+0.156,-0.156$ | $+0.204,-0.204$ | $+0.168,-0.168$ |
| Signal contamination | $+0.153,-0.153$ | $+0.255,-0.272$ | $+0.188,-0.170$ |
| PDF | $+0.097,-0.084$ | $+0.188,-0.198$ | $+0.092,-0.081$ |

TABLE XXXVII: Systematic uncertainties on $\sigma(t\bar{t})$ (in pb) when no NNelec cut is applied.

| Channel | $\tau$+jets types 1 and 2 | $\tau$+jets type 3 | Combined |
|---|---|---|---|
| Tau Energy Scale | $+0.101,-0.002$ | $+0.238,-0.255$ | $+0.102,-0.017$ |
| Jet Energy Scale | $+0.016,-0.001$ | $+0.017,-0.000$ | $+0.016,-0.000$ |
| Jet Energy Resolution | $+0.084,-0.086$ | $+0.017,-0.034$ | $+0.068,-0.085$ |
| Jet ID | $+0.169,-0.169$ | $+0.017,-0.017$ | $+0.153,-0.153$ |
| b-tag | $+0.424,-0.375$ | $+0.358,-0.306$ | $+0.425,-0.375$ |
| b-fragmentation | $+0.069,-0.069$ | $+0.102,-0.102$ | $+0.068,-0.068$ |
| QCD Modeling | $+0.271,-0.273$ | $+0.153,-0.136$ | $+0.225,-0.256$ |
| $\tau$ ID | $+0.220,-0.220$ | $+0.204,-0.204$ | $+0.221,-0.221$ |
| Trigger | $+0.204,-0.204$ | $+0.170,-0.170$ | $+0.204,-0.204$ |
| W Scale Factor | $+0.034,-0.034$ | $+0.034,-0.034$ | $+0.034,-0.034$ |
| Z Scale Factor | $+0.072,-0.072$ | $+0.072,-0.072$ | $+0.048,-0.048$ |
| Template statistics | $+0.118,-0.118$ | $+0.170,-0.170$ | $+0.102,-0.102$ |
| Signal contamination | $+0.050,-0.052$ | $+0.136,-0.187$ | $+0.051,-0.051$ |
| PDF | $+0.097,-0.084$ | $+0.188,-0.198$ | $+0.092,-0.081$ |

[1] J. A. Coarasa, J. Guasch, and J. Sola, Report No. UAB-FT-451, 1999, hep-ph/9903212
[2] *Measurement of top pair production cross section from the tau + jets channel*, DØ Note 5158.
[3] *Measurement of* $\sigma(p\bar{p} \to t\bar{t}X)$ *in* $\tau + jets$ *channel using 1* $fb^{-1}$ *of data*, DØ Note 5765.
[4] Commom Sample Group, `http://www-d0.fnal.gov/Run2Physics/cs/index.html`
[5] *Search for neutral Higgs bosons in* $\phi b \to b\bar{b}b$ *using RunIIb data*, DØ Note 5709
[6] Commom Sample Group, `http://www-d0.fnal.gov/Run2Physics/cs/MC/MC.html`
[7] M.L. Mangano *et al.*, "ALPGEN: a generator for hard multiparton process in hadronic collisions", JHEP **0307**, 001 (2003);
[8] T. Sjostrand, P. Eden, C. Friberg, L. Lonnblad, G. Miu, S. Mrenna and E. norbin, Computer Phys. Commun. **135**, 238 (2001).
[9] http://charm.physics.ucsb.edu/people/lange/EvtGen/
[10] S. Jadach, Z. Was, R. Decker, J.H. Kuehn, Comp. Phys. Commun. , 361 (1993) (CERN TH-6793 preprint).
[11] `http://www-d0.hef.ru.nl//askArchive.php?base=agenda&categ=a081895&id=a081895s0t3/transparencies`.
[12] S. Muanza, *A compilation of MCFM v5.1 Cross Sections.* DØ Note 5300.
[13] *Systematics Uncertainties in Top Quark Measurements*, DØ Note 6024.
[14] `https://plone4.fnal.gov/P1/D0Wiki/comp/caf/MCreweighting/lumiprofile-reweighting`.
[15] H. Schellman, *The longitudinal shape of the luminous regions at DØ* DØ Note 5885.
[16] D. Price, W. Fisher, and J. Haley, *Studies of Alpgen parameters corrections and uncertainties*, DØ Note 5966.
[17] Y. Peters, M. Begel, K. Hamacher, and D. Wicke, *Reweighting of the fragmentation function for the DØ Monte Carlo*, DØ Note 5325.
[18] N. Makovec and J.F. Grivaz, *Shifiting, smearing, and removing simulated jets*, DØ Note 4914.
[19] *Search For MSSM Higgs Boson Production in the Decay* $h \to \tau_\mu \tau_{had}$ *with the DØ Detector at at* $\sqrt{1.96}$ *TeV*, DØ Note 5708.
[20] *DØ* $\tau$ *ID certification*, DØ Note 4773.
[21] S.Eldelman *et al.* (Particle Data Group), Phys. Lett. B 592, 1(2004) and 2005
[22] G.C. Blazey et al., arXiv.hep-ex/0005012 (2000).
[23] G.Bernardi, E. Busato and J.R. Vlimant, *Improvements from the T42 Algorithm on calorimeter objects reconstruction*, DØ Note 4335.
[24] A. Harel, *Jet ID Optimization*, DØ note 4919.
[25] *Jet Energy Scale Determination at DØ Run II*, DØ Note 5382.
[26] A. Harel, *Capping the JES muon corrections*, DØ Note 5563.
[27] T. Gadfort, A. Haas, D. Johnston, D. Lincoln, T. Scalon and S. Schlobohm *Performance of the DØ NN b-tagging Tool on p20 Data*, DØ Note 5554
[28] M. Anastasoaie, S. Robinson, T. Scalon, *Performance of the NN b-tagging Tool on p17 Data*, DØ Note 5213
[29] T. Scalon and S. Greder, *Measurement of the p20 Fake Rate using Binned Fits do Data*, DØ Note 6046
[30] *Search for Single Top Quark Production with 1.0* $fb^{-1}$, DØ Note 5285
[31] *Measurement of the ttbar cross section in the lepton+jets channel with 5.3* $fb^{-1}$ , DØ Note 6028.
[32] DØ Note 5350 and DØ Note 5360
[33] *Measurement of the* $t\bar{t} \to all - jets$ *production cross section using Secondary Vertex Tagging*, DØ Note 4830
[34] $\not\!\!E_T$ *significance Algorithm in RunII Data*, DØ Note 4254
[35] *Measurement of the top-antitop quark pair production cross section in proton-antiproton collisions at* $\sqrt{1.96}$ *TeV in the lepton + jets final state*, DØ Note 5262
[36] `http://www-d0.hef.kun.nl//fullAgenda.php?ida=a092001&fid=57`.
[37] *DØ Search for Neutral Higgs Bosons at high tan* $\beta$ *in the final state* $\tau_\mu \tau_h b$ *with 4.3* $fb^{-1}$ *of Run2b Data* , DØ Note 6077.
[38] http://schwind.home.cern.ch/schwind/MLPfit.html

# APPENDIX A: TRIGGER EFFICIENCIES

In this appendix we present the trigger weight distributions of all MC samples for different numbers of b-tagged jets. These are the weight distributions we referred to in Sections II A and III.

## 1. Trigger Efficiencies for $\tau + jets$

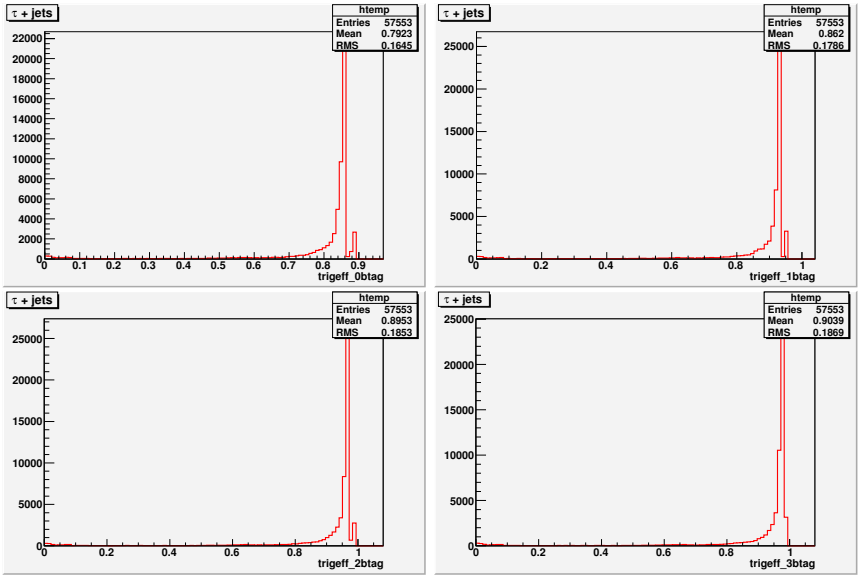


FIG. 25: Trigger Efficiencies for $\tau + jets$.

## 2. Trigger Efficiencies for $e + jets$

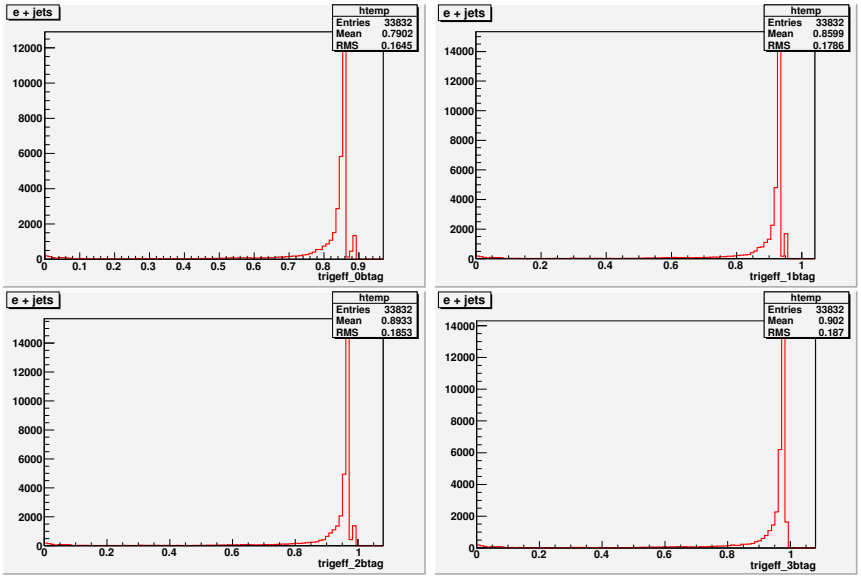


FIG. 26: Trigger Efficiencies for $e + jets$.

670 ### 3. Trigger Efficiencies for $\mu + jets$

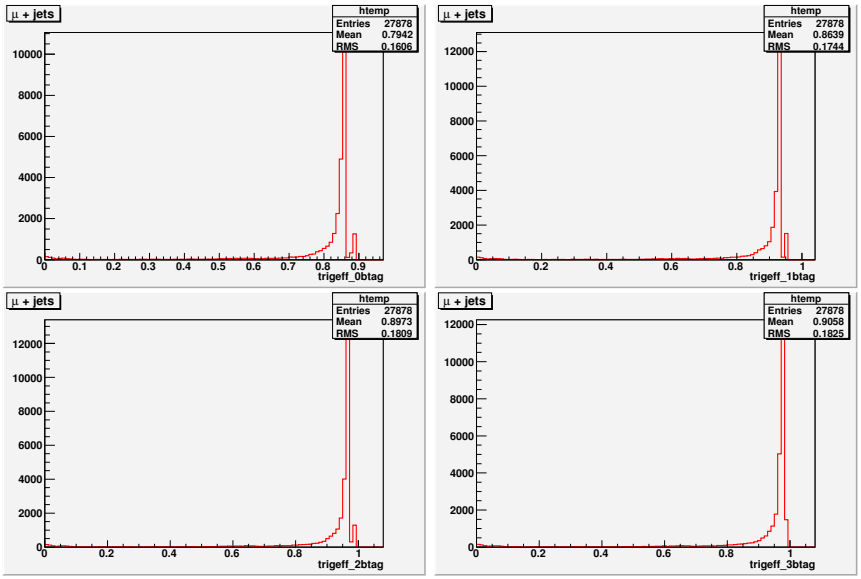


FIG. 27: Trigger Efficiencies for $\mu + jets$.

671 ### 4. Trigger Efficiencies for *dilepton*

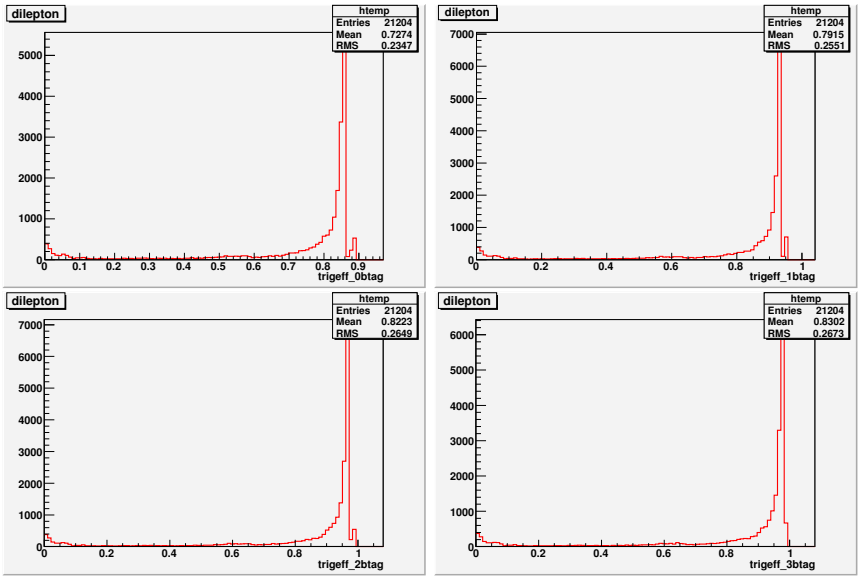


FIG. 28: Trigger Efficiencies for *dilepton*.

672

## 5. Trigger Efficiencies for $alljets$

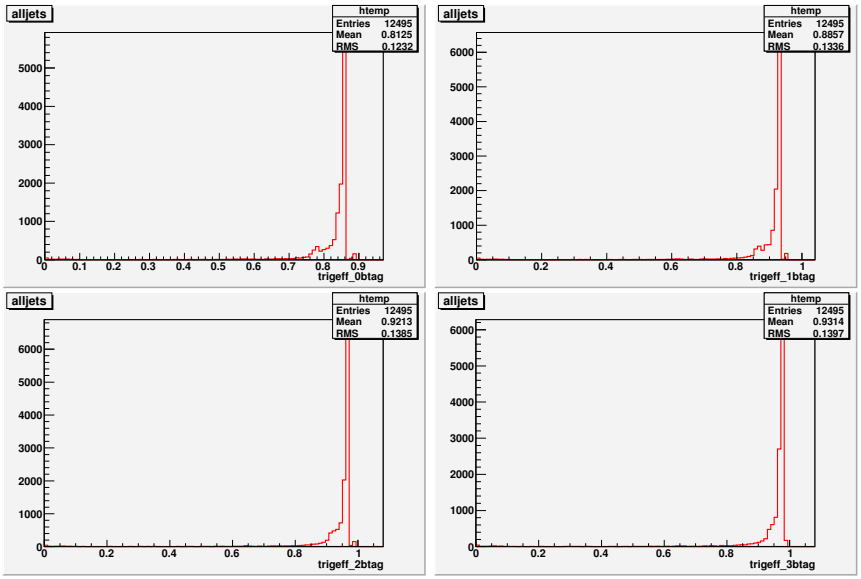


FIG. 29: Trigger Efficiencies for $alljets$.

673

## 6. Trigger Efficiencies for $Wjj + jets$

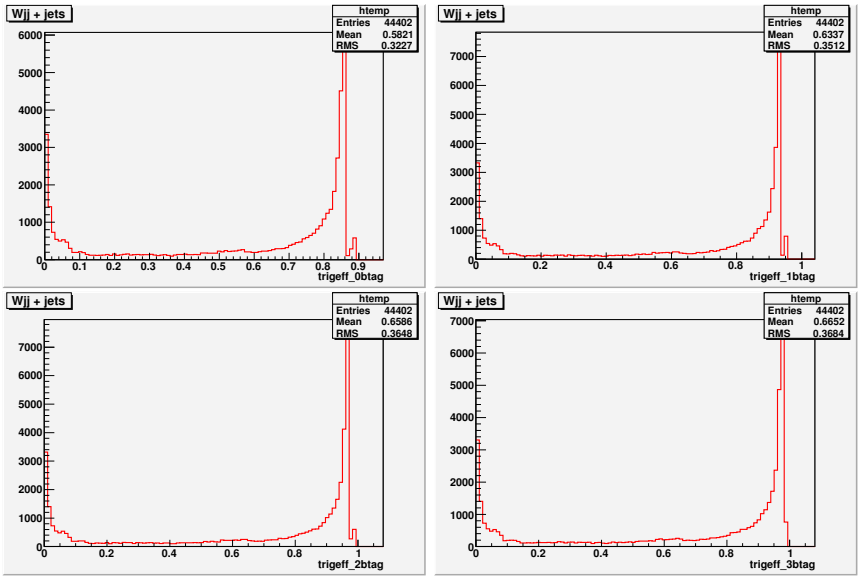


FIG. 30: Trigger Efficiencies for $Wjj + jets$.

674 ## 7. Trigger Efficiencies for $Wbb + jets$

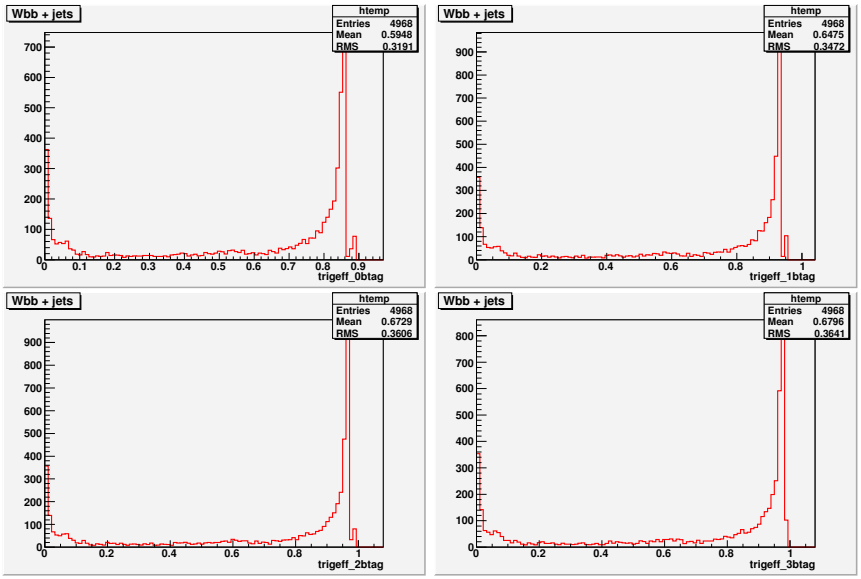


FIG. 31: Trigger Efficiencies for $Wbb + jets$.

675 ## 8. Trigger Efficiencies for $Wcc + jets$

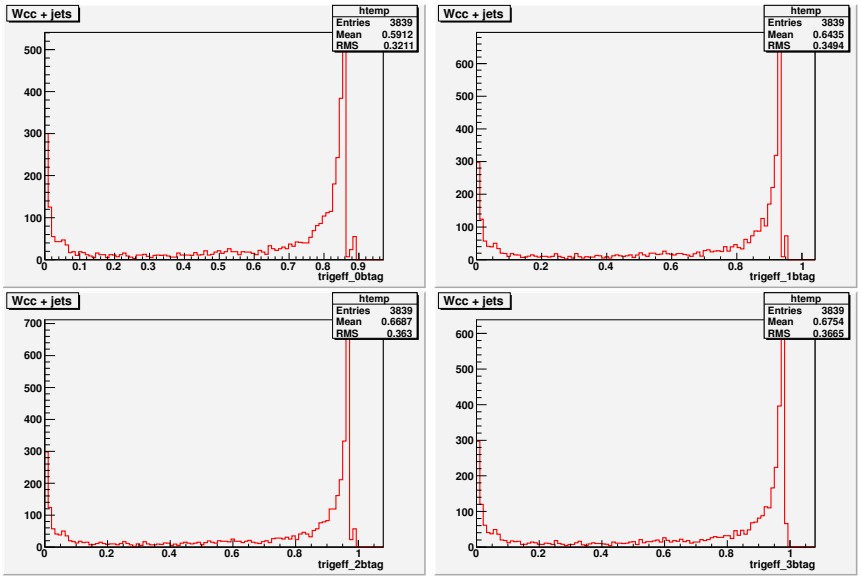


FIG. 32: Trigger Efficiencies for $Wcc + jets$.

676 ## 9. Trigger Efficiencies for $Zjj + jets \rightarrow ee + jj + jets$

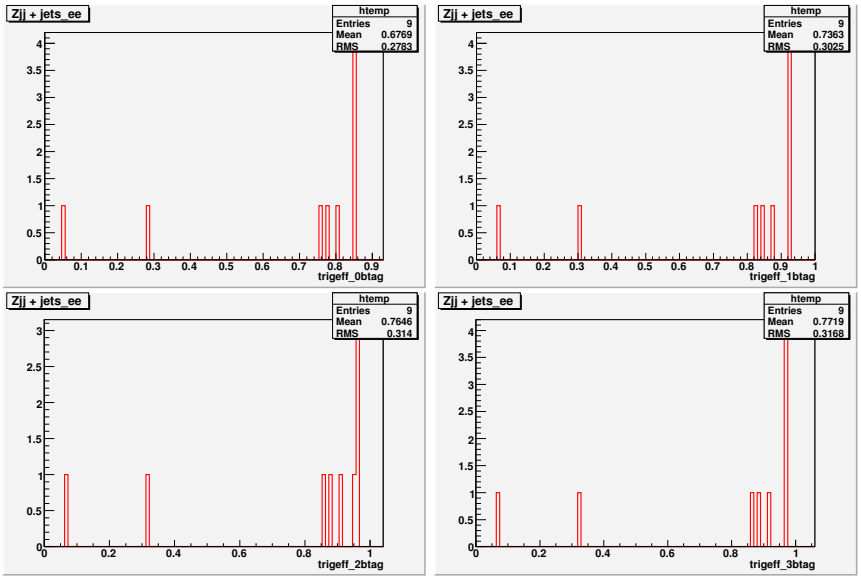


FIG. 33: Trigger Efficiencies for $Zjj + jets \rightarrow ee + jj + jets$.

677 ## 10. Trigger Efficiencies for $Zbb + jets \rightarrow ee + bb + jets$

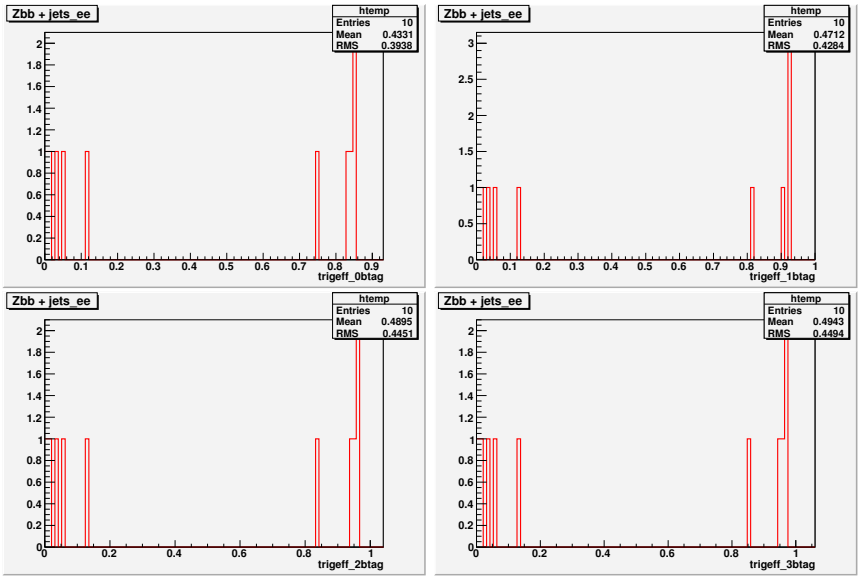


FIG. 34: Trigger Efficiencies for $Zbb + jets \rightarrow ee + bb + jets$.

678

## 11. Trigger Efficiencies for $Zcc + jets \rightarrow ee + cc + jets$

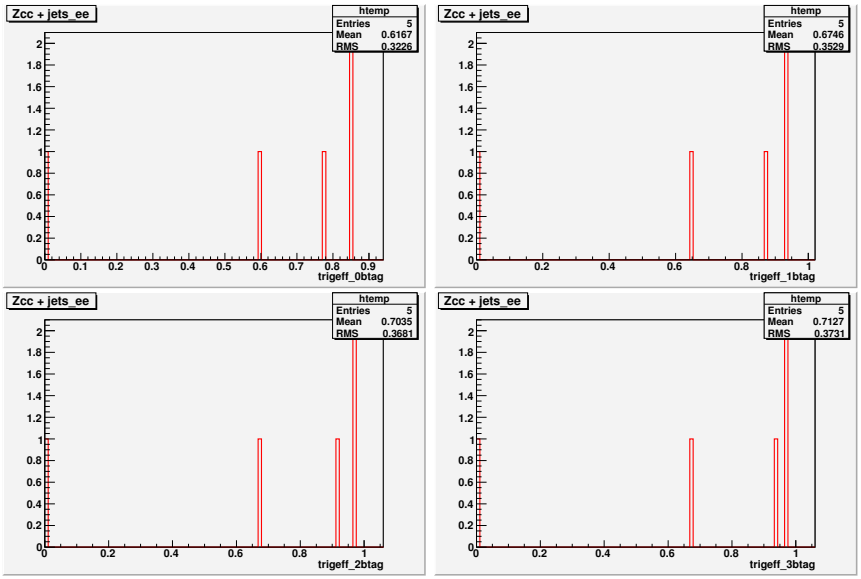


FIG. 35: Trigger Efficiencies for $Zcc + jets \rightarrow ee + cc + jets$.

679

## 12. Trigger Efficiencies for $Zjj + jets \rightarrow \mu\mu + jj + jets$

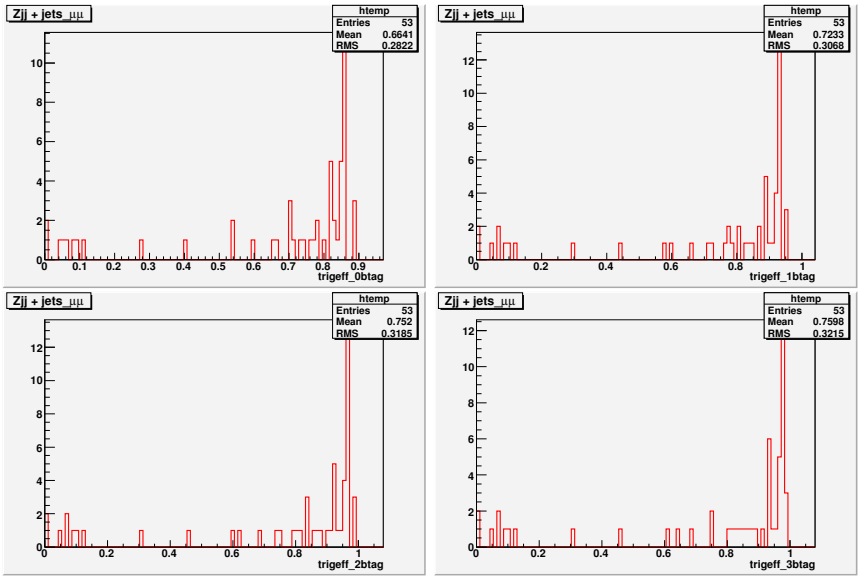


FIG. 36: Trigger Efficiencies for $Zjj + jets \rightarrow \mu\mu + jj + jets$.

680 ## 13. Trigger Efficiencies for $Zbb + jets \rightarrow \mu\mu + bb + jets$

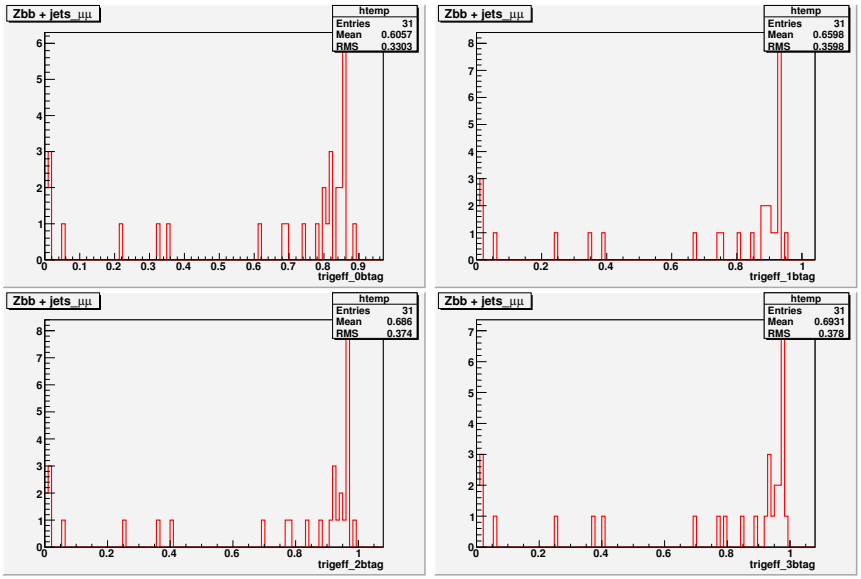


FIG. 37: Trigger Efficiencies for $Zbb + jets \rightarrow \mu\mu + bb + jets$.

681 ## 14. Trigger Efficiencies for $Zcc + jets \rightarrow \mu\mu + cc + jets$

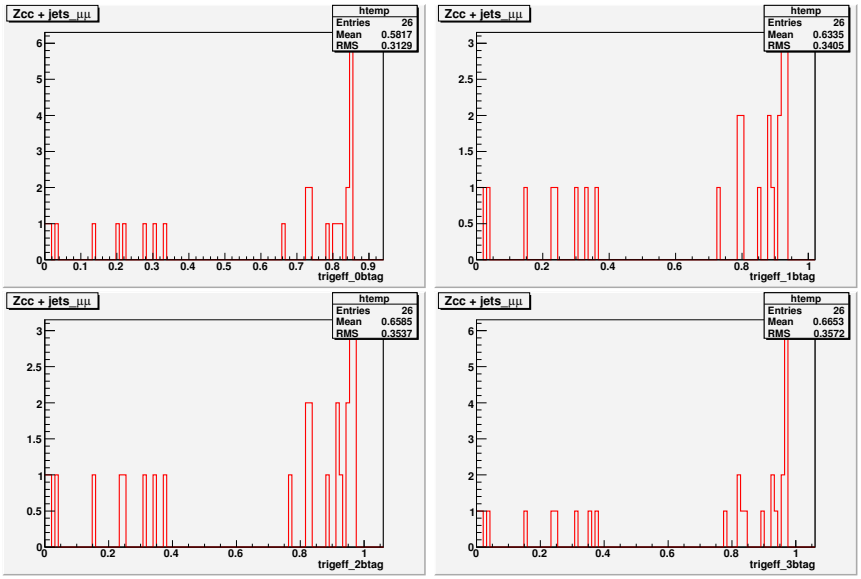


FIG. 38: Trigger Efficiencies for $Zcc + jets \rightarrow \mu\mu + cc + jets$.

682 ## 15. Trigger Efficiencies for $Zjj + jets \rightarrow \tau\tau + jj + jets$

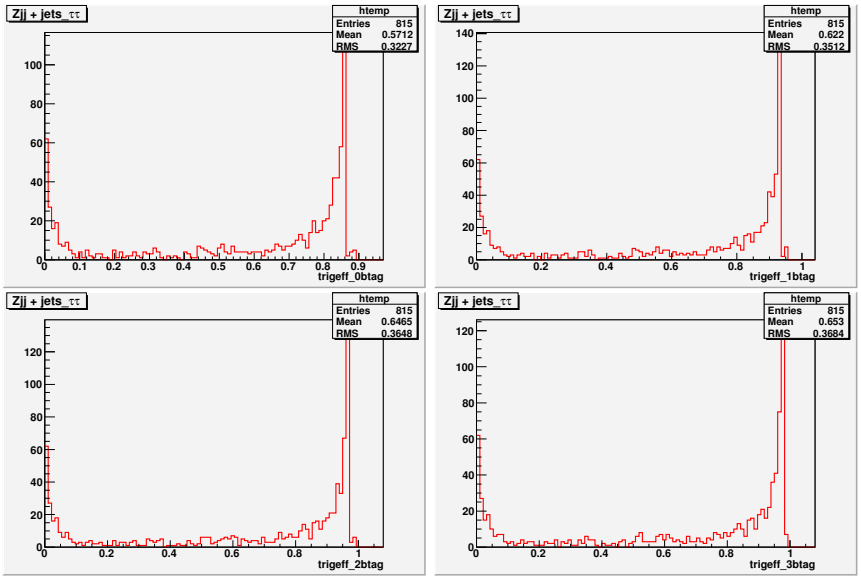


FIG. 39: Trigger Efficiencies for $Zjj + jets \rightarrow \tau\tau + jj + jets$.

683 ## 16. Trigger Efficiencies for $Zbb + jets \rightarrow \tau\tau + bb + jets$

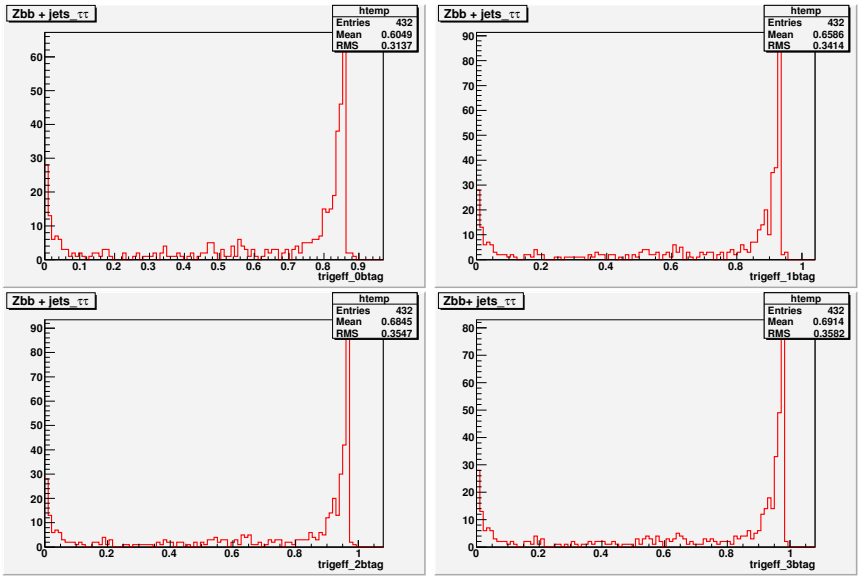


FIG. 40: Trigger Efficiencies for $Zbb + jets \rightarrow \tau\tau + bb + jets$.

684

## 17. Trigger Efficiencies for $Zcc + jets \rightarrow \tau\tau + cc + jets$

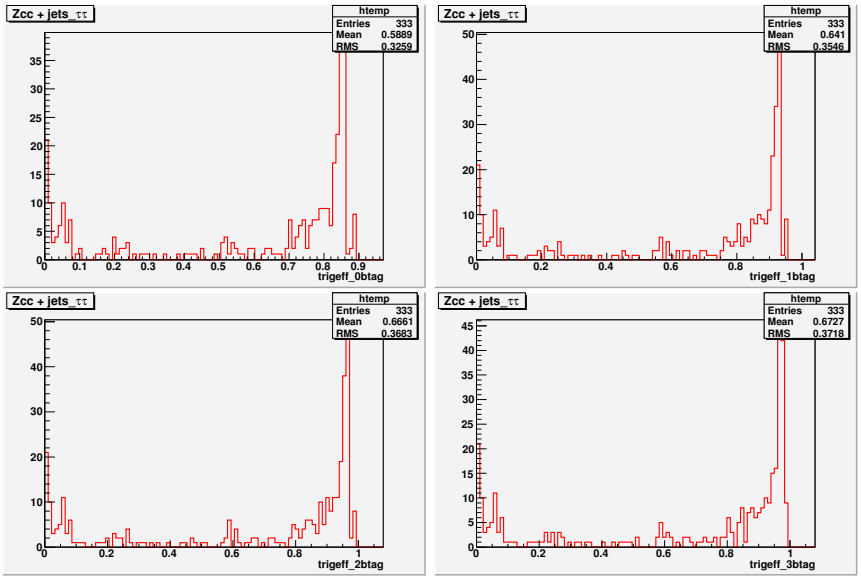


FIG. 41: Trigger Efficiencies for $Zcc + jets \rightarrow \tau\tau + cc + jets$.

685

## 18. Trigger Efficiencies for $Zjj + jets \rightarrow \nu\nu + jj + jets$

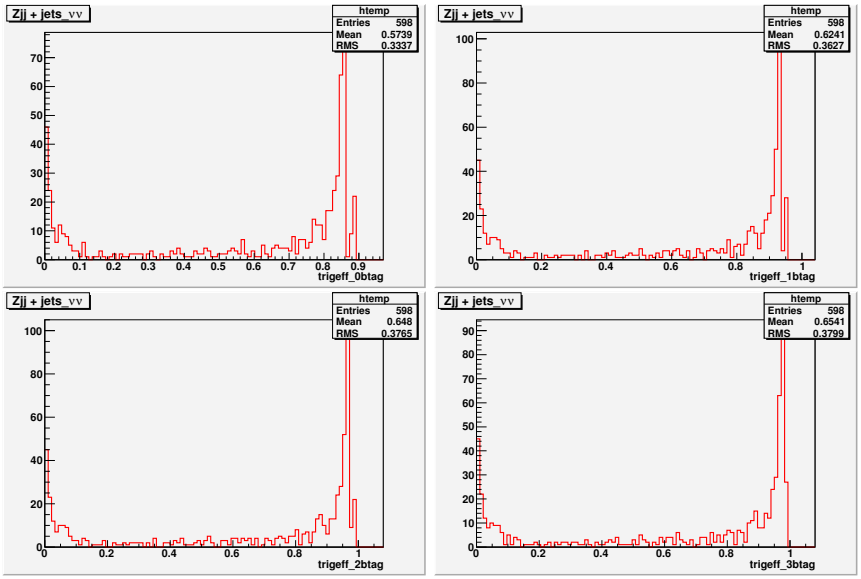


FIG. 42: Trigger Efficiencies for $Zjj + jets \rightarrow \nu\nu + jj + jets$.

686 ### 19. Trigger Efficiencies for $Zbb + jets \rightarrow \nu\nu + bb + jets$

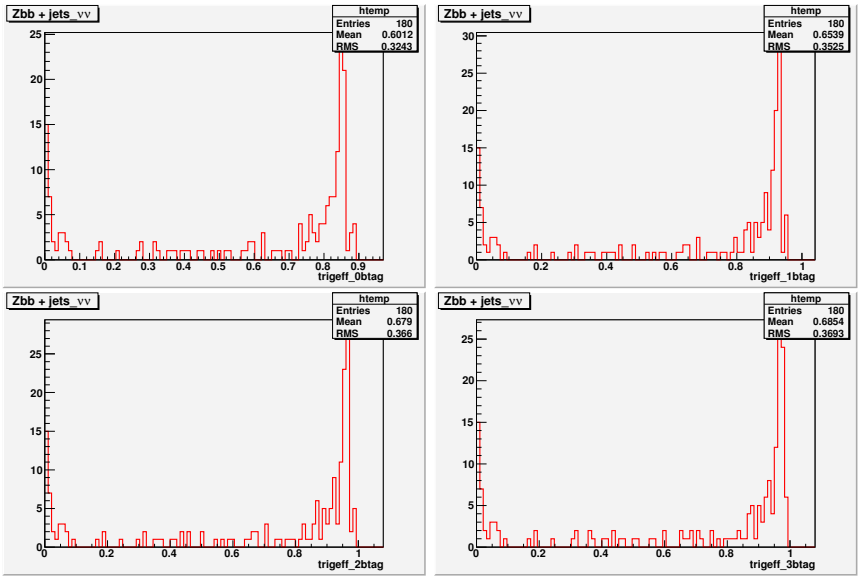


FIG. 43: Trigger Efficiencies for $Zbb + jets \rightarrow \nu\nu + bb + jets$.

687 ### 20. Trigger Efficiencies for $Zcc + jets \rightarrow \nu\nu + cc + jets$

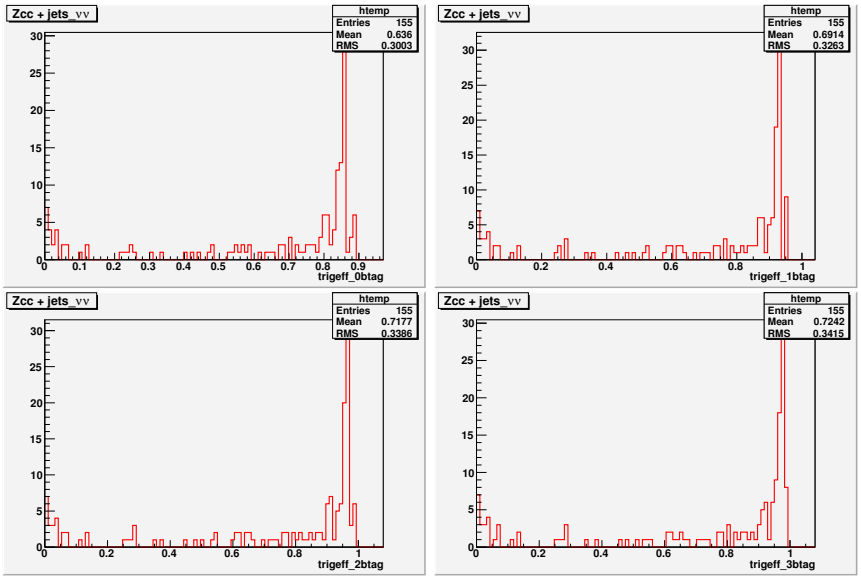


FIG. 44: Trigger Efficiencies for $Zcc + jets \rightarrow \nu\nu + cc + jets$.

688 ## APPENDIX B: TURN ON CURVES FOR TRIGGER JT2_3JT15L_IP_VX

689 Here it is shown all turn-on curves for all three levels of the trigger JT2_3JT15L_IP_VX as described in
690 Section III.

691

### 1. Level 1 jet turn on curves for trigger JT2_3JT15L_IP_VX

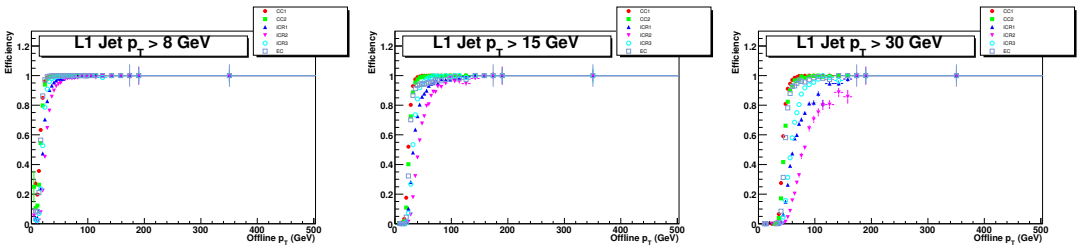


(a) $p_T > 8$ GeV (b) $p_T > 15$ GeV (c) $p_T > 30$ GeV

FIG. 45: Level 1 jet turn-on curves, low luminosity.

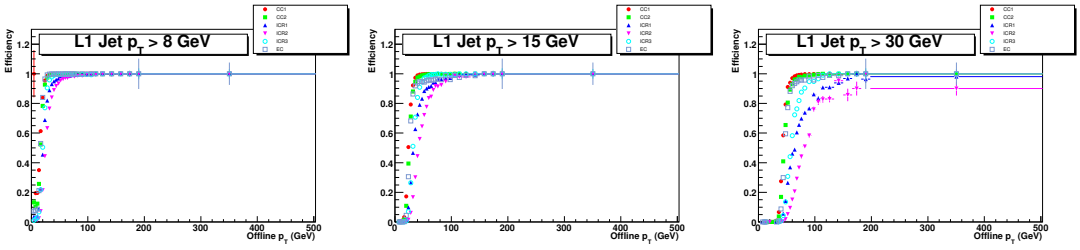


(a) $p_T > 8$ GeV (b) $p_T > 15$ GeV (c) $p_T > 30$ GeV

FIG. 46: Level 1 jet turn-on curves, medium luminosity.

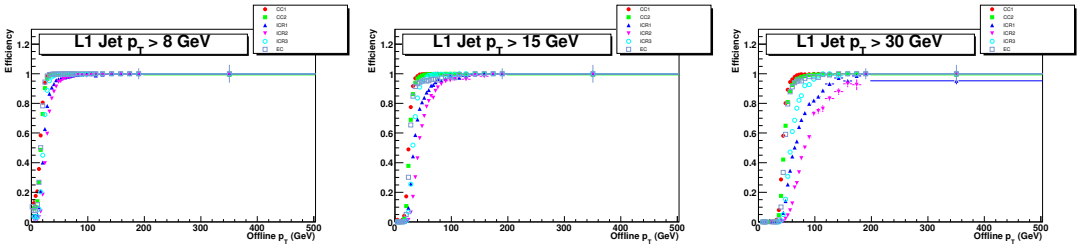


(a) $p_T > 8$ GeV (b) $p_T > 15$ GeV (c) $p_T > 30$ GeV

FIG. 47: Level 1 jet turn-on curves, high luminosity.

692 ### 2. Level 2 jet turn on curves for trigger JT2_3JT15L_IP_VX

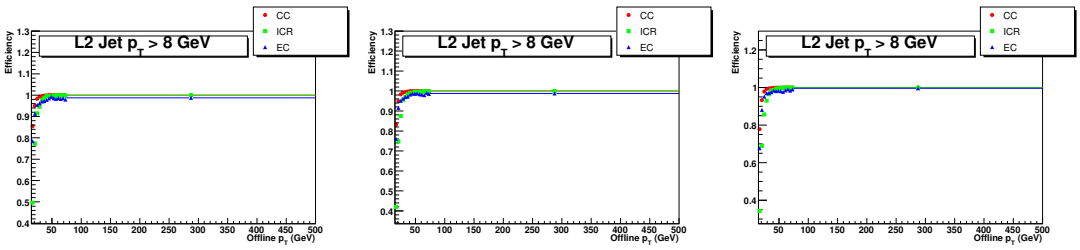


(a) Low luminosity $p_T >$ 8 GeV

(b) Medium luminosity $p_T >$ 8 GeV

(c) high luminosity $p_T >$ 8 GeV

FIG. 48: Level 2 $p_T > 8$ GeV jets turn-on curves.

693 ### 3. Level 2 $H_T$ turn on curves for trigger JT2_3JT15L_IP_VX

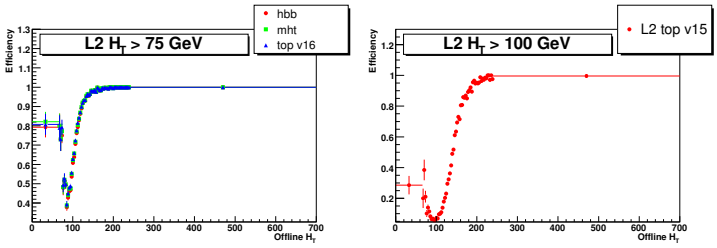


(a) $H_T > 75$ GeV

(b) $H_T > 100$ GeV

FIG. 49: L2 $H_T$ turn-on curves, low luminosity.

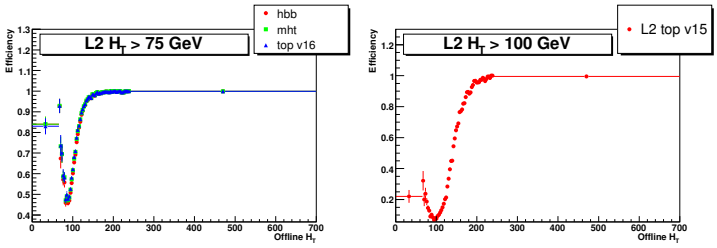


(a) $H_T > 75$ GeV

(b) $H_T > 100$ GeV

FIG. 50: L2 $H_T$ turn-on curves, medium luminosity.

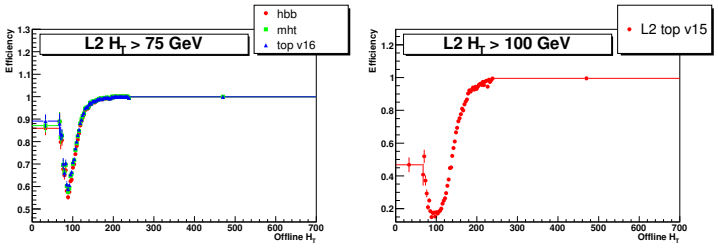


(a) $H_T > 75$ GeV (b) $H_T > 100$ GeV

FIG. 51: L2 $H_T$ turn-on curves, high luminosity.

694 **4. Level 2 $\not\!\!E_T$ turn on curves for trigger JT2_3JT15L_IP_VX**

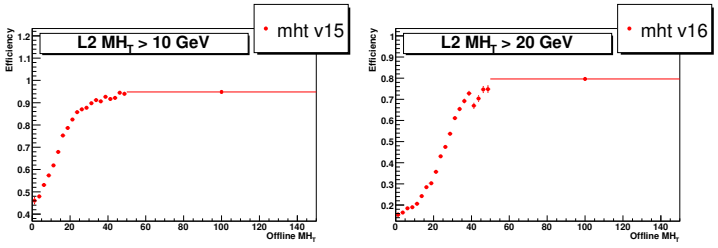


(a) $\not\!\!E_T > 10$ GeV (b) $\not\!\!E_T > 20$ GeV

FIG. 52: L2 $\not\!\!E_T$ turn-on curves, low luminosity.

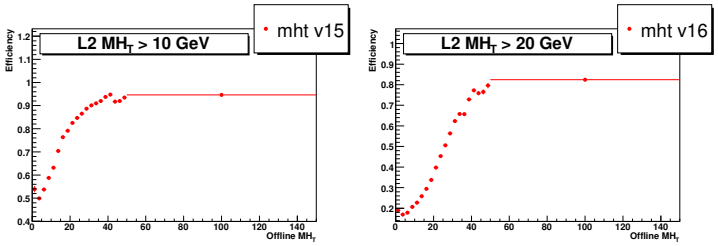


(a) $\not\!\!E_T > 10$ GeV (b) $\not\!\!E_T > 20$ GeV

FIG. 53: L2 $\not\!\!E_T$ turn-on curves, medium luminosity.

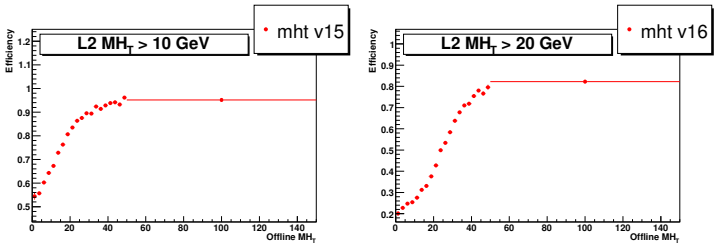


(a) $\not{E}_T > 10$ GeV (b) $\not{E}_T > 20$ GeV

FIG. 54: L2 $\not{E}_T$ turn-on curves, high luminosity.

695 **5. Level 2 Sphericity turn on curves for trigger JT2_3JT15L_IP_VX**

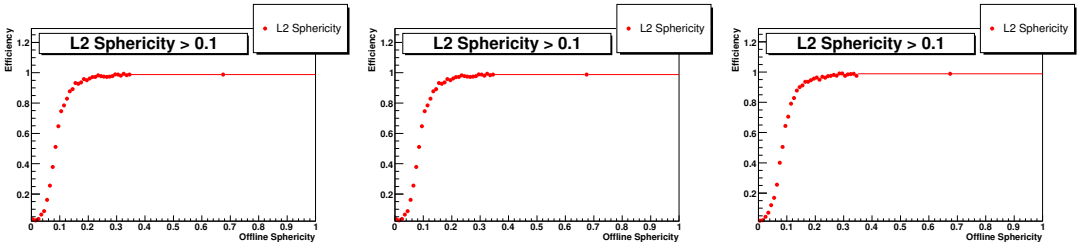


(a) Sphericity > 0.1 turn-on curve, low luminosity

(b) Sphericity > 0.1 turn-on curve, medium luminosity

(c) Sphericity > 0.1 turn-on curve, high luminosity

FIG. 55: L2 Sphericity turn-on curves.

696 **6. Level 2 STTIP turn on curves for trigger JT2_3JT15L_IP_VX**

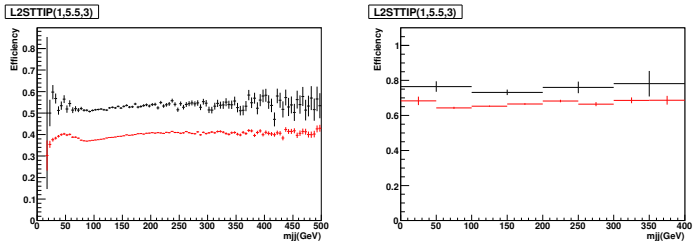


(a) L2STTIP, 0 and 1 tight NN tags

(b) L2STTIP, 2 and 3 tight NN tags

FIG. 56: L2STTIP efficiency in the low luminosity range. Left: events with 0 (red) and 1 (black) tight NN b-tags. Right: events with 2 (red) and 3 (black) tight NN b-tags.

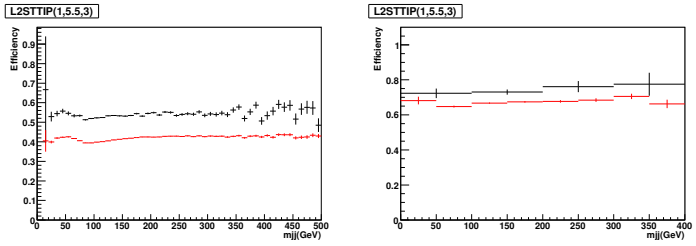


(a) L2STTIP, 0 and 1 tight NN tags

(b) L2STTIP, 2 and 3 tight NN tags

FIG. 57: L2STTIP efficiency in the medium luminosity range. Left: events with 0 (red) and 1 (black) tight NN b-tags. Right: events with 2 (red) and 3 (black) tight NN b-tags.

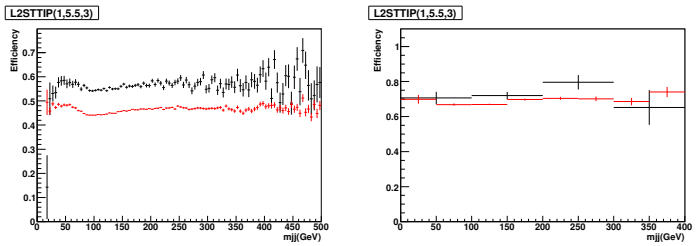


(a) L2STTIP, 0 and 1 tight NN tags

(b) L2STTIP, 2 and 3 tight NN tags

FIG. 58: L2STTIP efficiency in the high luminosity range. Left: events with 0 (red) and 1 (black) tight NN b-tags. Right: events with 2 (red) and 3 (black) tight NN b-tags.

697 **7. Level 3 jet turn on curves for trigger JT2_3JT15L_IP_VX**

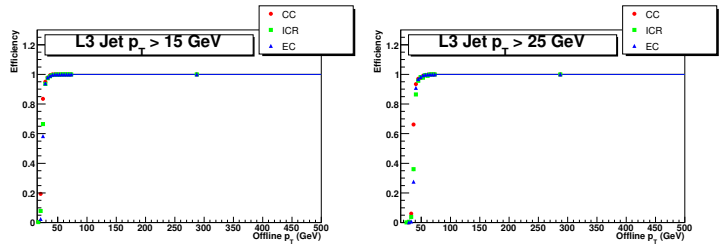


(a) $p_T > 15$ GeV

(b) $p_T > 25$ GeV

FIG. 59: L3 jet turn-on curves, low luminosity.

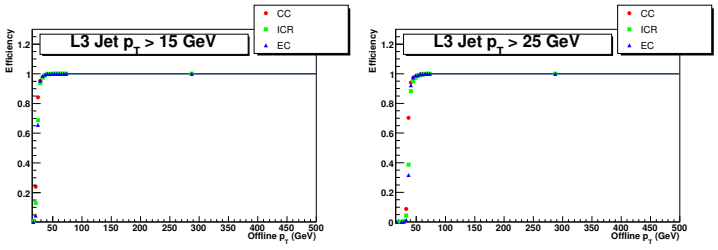


(a) $p_T > 15$ GeV (b) $p_T > 25$ GeV

FIG. 60: L3 jet turn-on curves, medium luminosity.

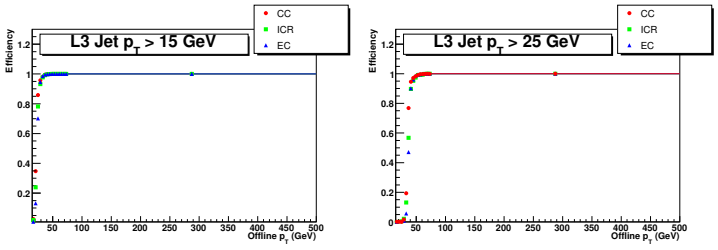


(a) $p_T > 15$ GeV (b) $p_T > 25$ GeV

FIG. 61: L3 jet turn-on curves, high luminosity.

698 **8. Level 3 b-tag on curves for trigger JT2_3JT15L_IP_VX**

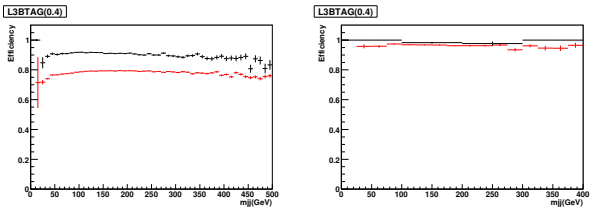


(a) 0 and 1 $b$-tags. (b) 2 and 3 $b$-tags.

FIG. 62: (a) Efficiency of the L3 $b$-tag (Level3 Event $b$-tag$<$ 0.4) for the low luminosity range in triggerlist v15. The selected events passed the rest of the trigger and offline event selection and had zero (red) or one (black) offline NN (TIGHT) $b$-tags. (b) Same for events with 2(red) and 3(black) offline NN (TIGHT) $b$-tags.

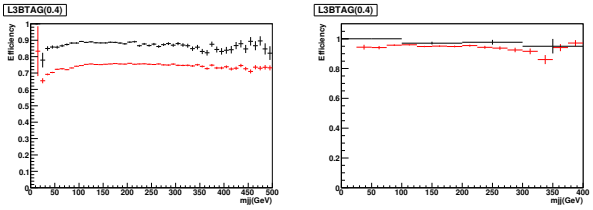


(a) 0 and 1 $b$-tags. (b) 2 and 3 $b$-tags.

FIG. 63: (a) Efficiency of the L3 $b$-tag (Level3 Event $b$-tag$<$ 0.4) for the medium luminosity range in triggerlist v15. The selected events passed the rest of the trigger and offline event selection and had zero (red) or one (black) offline NN (TIGHT) $b$-tags. (b) Same for events with 2(red) and 3(black) offline NN (TIGHT) $b$-tags.

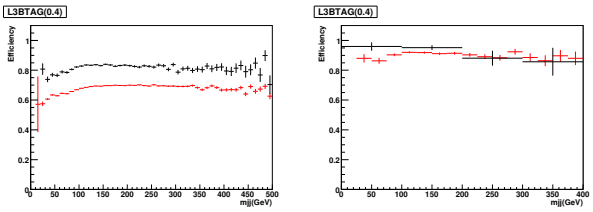


(a) 0 and 1 $b$-tags. (b) 2 and 3 $b$-tags.

FIG. 64: (a) Efficiency of the L3 $b$-tag (Level3 Event $b$-tag$<$ 0.4) for the high luminosity range in triggerlist v15. The selected events passed the rest of the trigger and offline event selection and had zero (red) or one (black) offline NN (TIGHT) $b$-tags. (b) Same for events with 2(red) and 3(black) offline NN (TIGHT) $b$-tags.

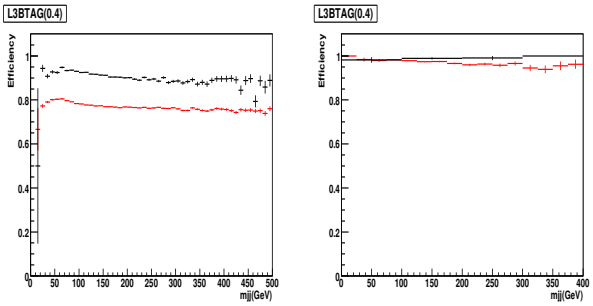


(a) 0 and 1 $b$-tags. (b) 2 and 3 $b$-tags.

FIG. 65: (a) Efficiency of the L3 $b$-tag (Level3 Event $b$-tag$<$ 0.4) for the low luminosity range in triggerlist v16. The selected events passed the rest of the trigger and offline event selection and had zero (red) or one (black) offline NN (TIGHT) $b$-tags. (b) Same for events with 2(red) and 3(black) offline NN (TIGHT) $b$-tags.

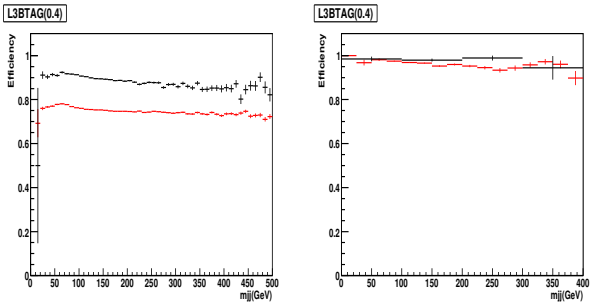


(a) 0 and 1 $b$-tags. (b) 2 and 3 $b$-tags.

FIG. 66: (a) Efficiency of the L3 $b$-tag (Level3 Event $b$-tag$<$ 0.4) for the medium luminosity range in triggerlist v16. The selected events passed the rest of the trigger and offline event selection and had zero (red) or one (black) offline NN (TIGHT) $b$-tags. (b) Same for events with 2(red) and 3(black) offline NN (TIGHT) $b$-tags.

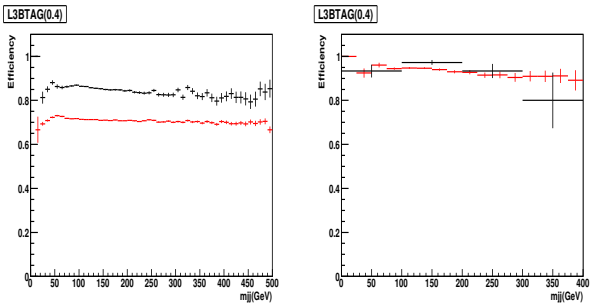


(a) 0 and 1 $b$-tags. (b) 2 and 3 $b$-tags.

FIG. 67: (a) Efficiency of the L3 $b$-tag (Level3 Event $b$-tag$<$ 0.4) for the high luminosity range in triggerlist v16. The selected events passed the rest of the trigger and offline event selection and had zero (red) or one (black) offline NN (TIGHT) $b$-tags. (b) Same for events with 2(red) and 3(black) offline NN (TIGHT) $b$-tags.

## APPENDIX C: DISCRIMINANT VARIABLES

This appendix shows normalized plots of signal and background samples for all discriminant variables tested for this analysis.

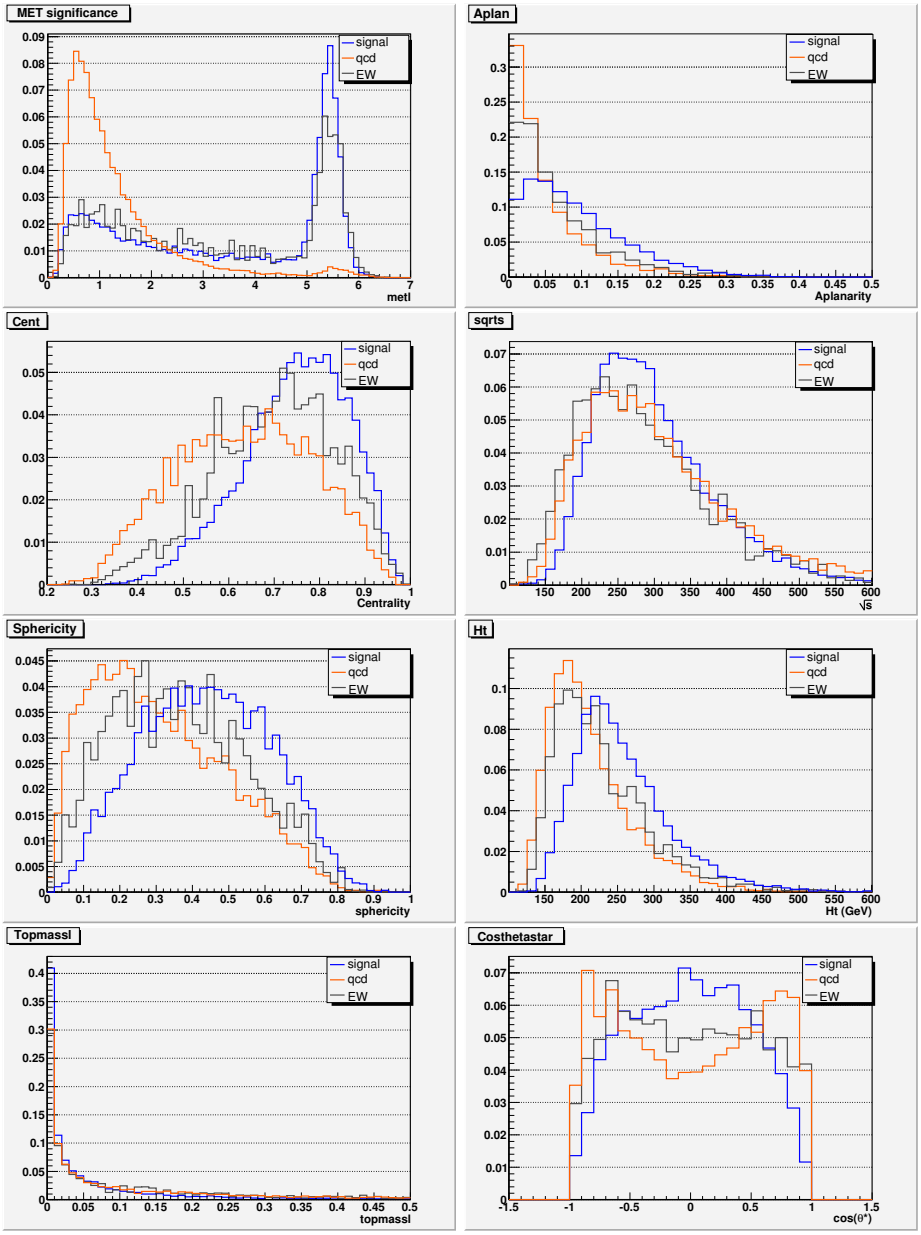


FIG. 68: Discriminant variables.

## APPENDIX D: SET OPTIMIZATION

In this appendix it is shown plots of the figure of merit (Equation 6) used to perform the NN variables set optimization as described in Section VIII C.

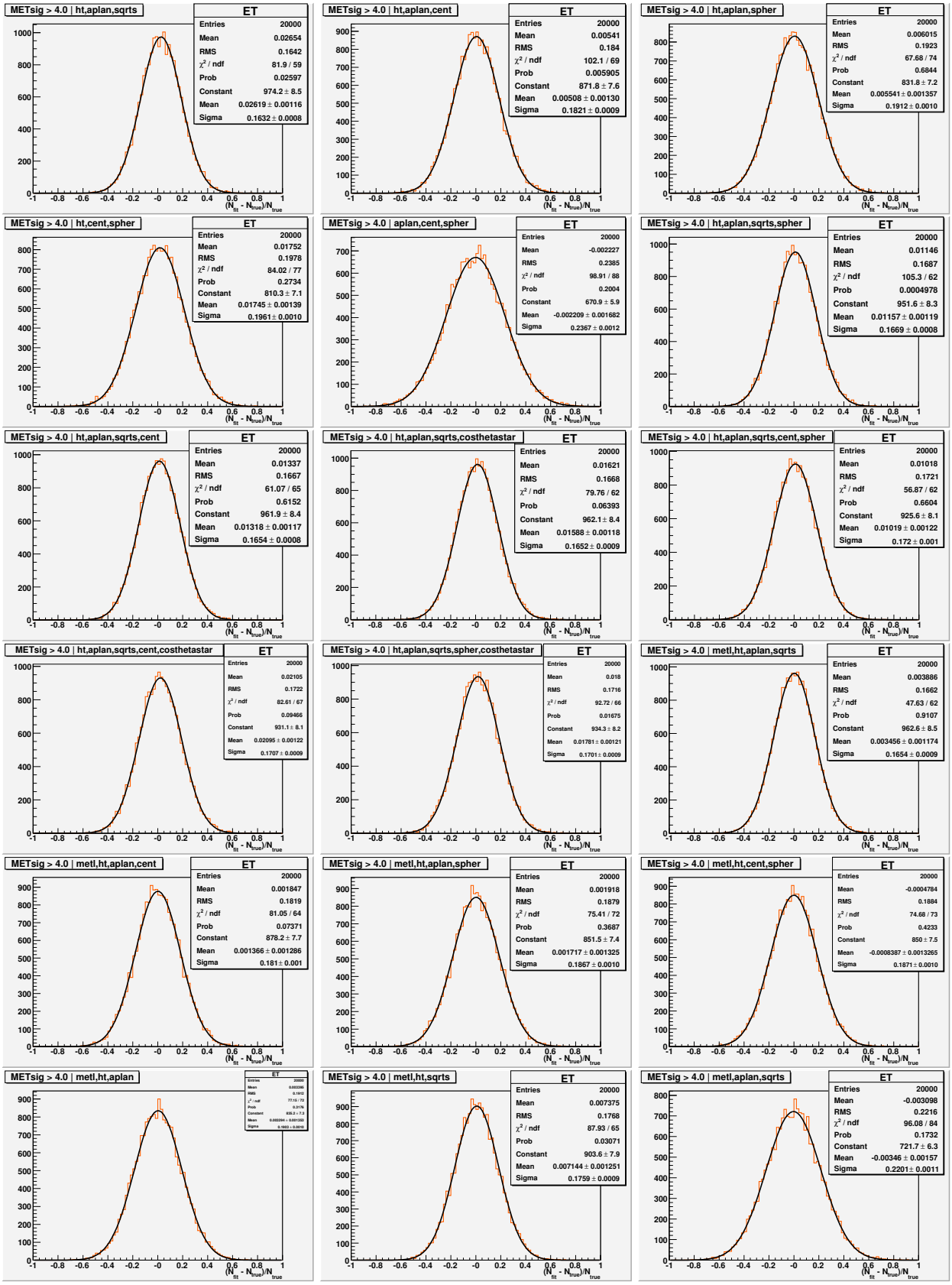


FIG. 69: Sets of NN inputs variables with $\not\!\!E_T$ significance > 4.0 for set optimization.

## APPENDIX E: SET OPTIMIZATION CONTINUED

In this appendix it is shown plots of the figure of merit (Equation 6) used to perform the NN variables set optimization as described in Section VIII C.

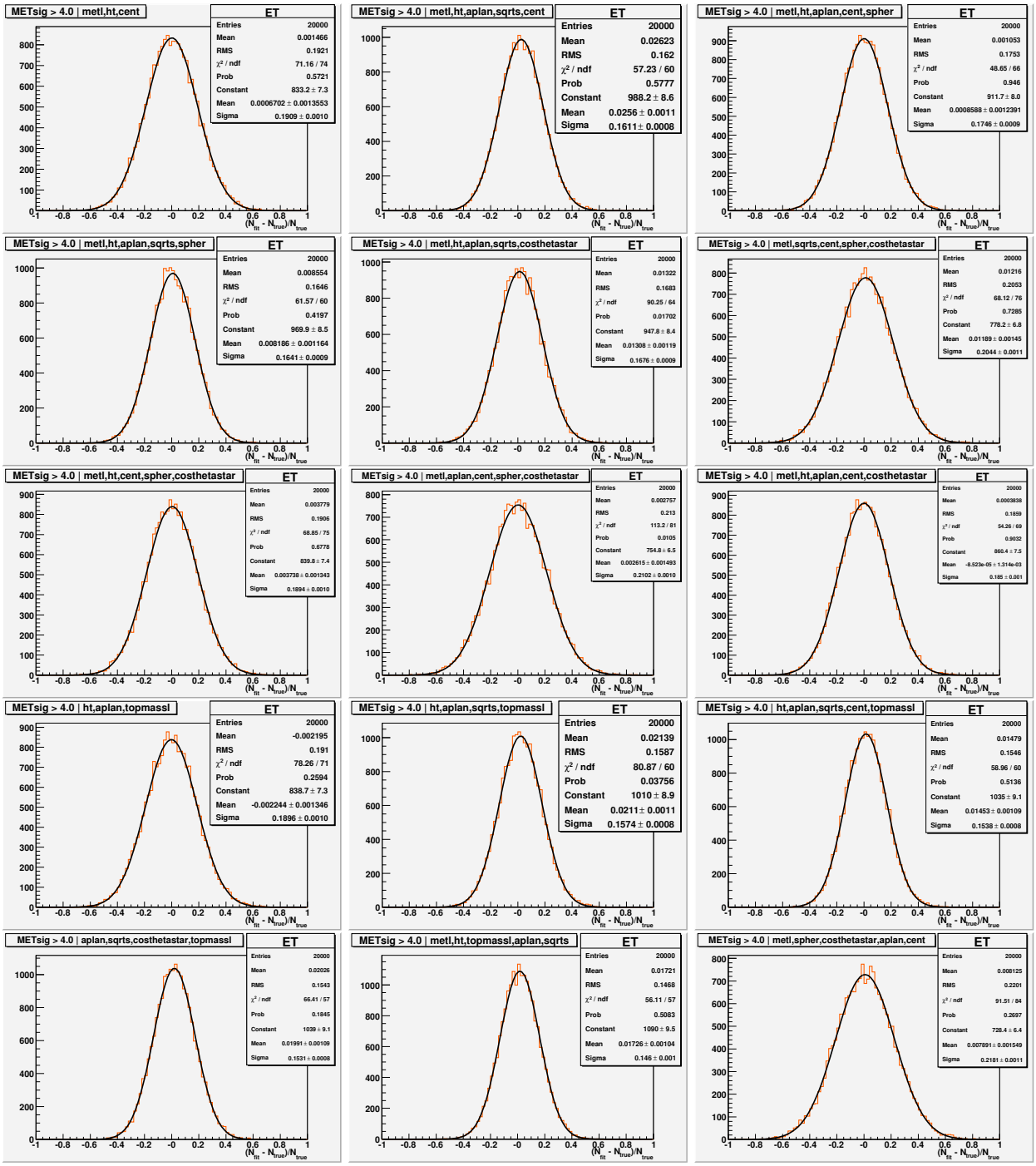


FIG. 70: Sets of NN inputs variables with $\not\!\!E_T$ significance > 4.0 for set optimization.

708

# APPENDIX F: $\not\!\!E_T$ SIGNIFICANCE OPTIMIZATION

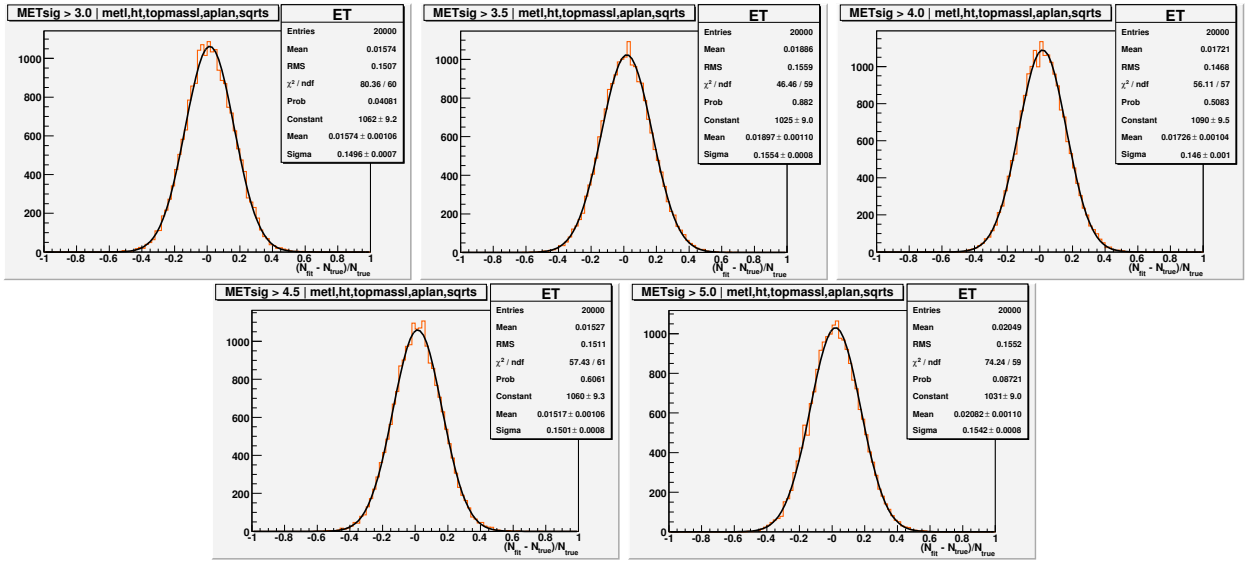


FIG. 71: Variation of $\not\!\!E_T$ significance cut for Set XXXII = metl, $H_T$, topmassl, aplan, sqrts.

## APPENDIX G: CROSS SECTION MEASUREMENTS WHEN SIGNAL CONTAMINATION IS IGNORED

In this appendix it is shown plots of the figure of merit (Equation 6) used to perform the NN variables set optimization as described in Section VIII C.

### 1. Results for Set = metl, $H_T$, topmassl, aplan, sqrts, metl > 4.0, lumi = 4951.86/pb, VC jets and NNelec > 0.9

Table below summarizes the number of events in each channel after final selection.

TABLE XXXVIII: Final number of events in the two analysis channels.

| | $\tau$ type I,II | $\tau$ type I,II (fitted) | $\tau$ type III | $\tau$ type III (fitted) |
|---|---|---|---|---|
| data | 386 | | 459 | |
| $t\bar{t} \to \tau + jets$ | 72.04 ± 0.53 | | 38.82 ± 0.39 | |
| $t\bar{t} \to e + jets$ | 38.35 ± 0.36 | | 6.52 ± 0.16 | |
| $t\bar{t} \to \mu + jets$ | 4.81 ± 0.14 | | 5.14 ± 0.14 | |
| $t\bar{t} \to l + l$ | 6.02 ± 0.07 | | 4.20 ± 0.06 | |
| $t\bar{t}$ total MC | | 121.22 ± 0.43 | | 54.68 ± 0.20 |
| $t\bar{t}$ total fitted | | 133.04 ± 17.09 | | 33.12 ± 15.04 |
| $W$+jets | 17.82 ± 0.33 | | 11.26 ± 0.23 | |
| $Z$+jets | 2.78 ± 0.14 | | 2.39 ± 0.12 | |
| QCD | | 232.35 ± 17.09 | | 412.22 ± 15.04 |
| Signal significance | | 6.77 | | 1.54 |
| S/B ratio | | 0.52 | | 0.08 |

Without taking into account the signal contamination the result is (only statistical uncertainties are shown)

$\tau$+jets types 1 and 2 cross section:

$$\sigma(t\bar{t}) = 8.05\ ^{+1.04}_{-1.02}\ (\text{stat})\ \pm 0.3\ (\text{lumi})\ \text{pb},$$

$\tau$+jets type 3 cross section:

$$\sigma(t\bar{t}) = 4.24\ ^{+1.94}_{-1.80}\ (\text{stat})\ \pm 0.3\ (\text{lumi})\ \text{pb},$$

Combined cross section:

$$\sigma(t\bar{t}) = 7.26\ ^{+0.92}_{-0.92}\ (\text{stat})\ \pm 0.3\ (\text{lumi})\ \text{pb},$$

### 2. Results for Set = metl, $H_T$, topmassl, aplan, sqrts, metl > 4.0, lumi = 4951.86/pb, VC jets and no NNelec cut

Table below summarizes the number of events in each channel after final selection.

TABLE XXXIX: Final number of events in the two analysis channels.

| | $\tau$ type I,II | $\tau$ type I,II (fitted) | $\tau$ type III | $\tau$ type III (fitted) |
|---|---|---|---|---|
| data | 583 | | 459 | |
| $t\bar{t} \to \tau + jets$ | 85.46 ± 0.58 | | 38.82 ± 0.39 | |
| $t\bar{t} \to e + jets$ | 175.23 ± 0.85 | | 6.52 ± 0.16 | |
| $t\bar{t} \to \mu + jets$ | 8.98 ± 0.19 | | 5.14 ± 0.14 | |
| $t\bar{t} \to l + l$ | 12.62 ± 0.10 | | 4.18 ± 0.06 | |
| $t\bar{t}$ total MC | | 282.27 ± 1.05 | | 54.67 ± 0.41 |
| $t\bar{t}$ total fitted | | 260.71 ± 20.74 | | 35.73 ± 15.28 |
| $W$+jets | 39.65 ± 0.50 | | 11.26 ± 0.25 | |
| $Z$+jets | 4.56 ± 0.10 | | 2.38 ± 0.11 | |
| QCD | | 278.04 ± 20.74 | | 409.62 ± 15.28 |
| Signal significance | | 10.80 | | 1.67 |
| S/B ratio | | 0.80 | | 0.08 |

Without taking into account the signal contamination the result is (only statistical uncertainties are shown)

$\tau$+jets types 1 and 2 cross section:

$$\sigma(t\bar{t}) = 6.47\ ^{+0.53}_{-0.53}\ (\text{stat})\ \pm 0.3\ (\text{lumi})\ \text{pb},$$

$\tau$+jets type 3 cross section:

$$\sigma(t\bar{t}) = 4.58\ ^{+1.96}_{-1.85}\ (\text{stat})\ \pm 0.3\ (\text{lumi})\ \text{pb},$$

Combined cross section:

$$\sigma(t\bar{t}) = 6.35\ ^{+0.51}_{-0.51}\ (\text{stat})\ \pm 0.3\ (\text{lumi})\ \text{pb},$$